الجمهورية الجزائرية الديمقراطية الشعبية

POPULAR & DEMOCRATIC REPUBLIC OF ALGERIA

وزارة التعليم العالي و البحث العلمي

MINISTRY OF HIGHER EDUCATION & SCIENTIFIC RESEARCH

جامعة أبي بكر بلقايد – تلمسان –

Aboubakr Belkaïd University – Tlemcen –
Faculty of TECHNOLOGY

THESIS

Submitted in candidacy for the **Degree** of **3rd cycle Doctorate**

In: Mechanical Engineering

Specialty: Mechanical Construction

By: Ahmed MEZRAG

Subject

Dynamics of Rotors Made by Porous Materials

(Dynamique des rotors en matériaux poreux)

Publicly defended on 04 / 10 / 2025, head on the following board of examiners:

BENACHOUR Mustapha	Professor	Tlemcen University	Chairman
BOUKHALFA Abdelkrim	Professor	Tlemcen University	Supervisor
BENSAID Ismail	MC-A	Tlemcen University	Examiner 1
SAIMI Ahmed	MC-A	Ain Temouchent university	Examiner 2

University Year: 2024/2025

بِسْمِ اللَّهِ الرَّحْمَٰنِ الرَّحِيمِ

DEDICATIONS

I dedicate this modest work

To my dear parents Mohammed and Fatima Zohra for their big support, their encouragement, their sacrifices and their patience throughout my studies.

To my dear brother Hamza and my dear sisters.

To the families: MEZRAG and CHEKKAF.

To all professors in my school carrier and in university cycles, especially Pr. BOUKHALFA Abdelkrim

To my colleagues in Abou Bekr Balkaid university, and all my friends.

To all those I have known from near or far.

Ahmed MEZRAG

THANKS

Praise be to Allah for guiding me to the right path of light and knowledge.

I would like to thank my thesis supervisor, Professor Abdelkrim BOUKHALFA, for having directed this work and for his very enriching teachings.

I express my gratitude to all the members of the jury for having agreed to read this work, for their exacts evaluations, and to provide the necessary criticisms for the final formatting of this thesis.

My thanks also go to all my friends and colleagues at the MECACOPM laboratory, especially Dr Ahmed GUENANOU for his big help and guideline's.

I thank all those who have helped in any way to carry out this work.

Ahmed MEZRAG

Abstract

This thesis presents a comprehensive investigation into the dynamic vibration behavior of rotating shafts fabricated from advanced porous materials, including Porous Functionally Graded Materials (PFGM) and Functionally Graded Porous (FGP) structures. The primary objective is to develop a robust computational framework to accurately predict how engineered porosity influences critical rotor characteristics such as natural frequencies, mode shapes, and critical speeds. The methodology is founded on a modified Timoshenko Beam Theory (TBT), which accounts for shear deformation and rotary inertia, implemented within a hierarchical p-version Finite Element Method (p-FEM) to ensure high accuracy and convergence. Extensive parametric studies were conducted to analyze the effects of material gradation, porosity distribution models (even, uneven, symmetric, and non-symmetric), geometric parameters, and boundary conditions. Key findings reveal that while increasing porosity generally reduces stiffness and lowers natural frequencies, its effect is highly dependent on the spatial distribution. Notably, symmetric porosity distributions in FGP shafts can enhance dynamic performance by optimizing the stiffness-to-mass ratio, leading to an increase in critical speed. Conversely, non-symmetric and uneven distributions can introduce complex, non-monotonic behaviors and degrade stability, particularly when interacting with bearing stiffness and disk mass. The results underscore that porosity can be a deliberate design feature for creating lightweight, high-performance rotors, but its architecture must be precisely controlled. This research contributes valuable design guidelines for engineering advanced rotor systems with tailored dynamic properties, which is significant for applications in the aerospace, automotive, and energy industries where operational reliability is critical.

Keywords: Rotor Dynamics, Vibration Analysis, Porous Materials, Porous Functionally Graded Materials (PFGM), Functionally Graded Porous (FGP) Structures, Timoshenko Beam Theory (TBT), p-Finite Element Method (FEM), Critical Speed, Natural Frequency, Campbell Diagram, Porosity Distribution, Gyroscopic Effect.

ملخص

تقدم هذه الأطروحة تحقيقًا شاملاً في السلوك الديناميكي للاهتزازات في الأعمدة الدوّارة المصنوعة من المواد المسامية المتقدمة، بما في ذلك المواد المسامية المتدرجة وظيفيًا (PFGM) والهياكل المسامية المتدرجة وظيفيًا(FGP) . يتمثل الهدف الأساسي في تطوير إطار حسابي متين للتنبؤ بدقة لكيفية تأثير المسامية المُهندسة على الخصائص الحرجة للدوّارات مثل الترددات الطبيعية، وأشكال الأنماط، والسرعات الحرجة. تستند المنهجية إلى نظرية تيموشينكو للعارضة المعدلة (TBT)، التي تأخذ في الاعتبار تشوه القص والقصور الذاتي الدوراني، والمُنفذة ضمن طريقة العناصر المحدودة ذات النسخة p (p-FEM) لضمان دقة عالية وتقارب عددي. أجريت دراسات واسعة النطاق للمعاملات لتحليل تأثير التدرج المادي، ونماذج توزيع المسامية (متجانس، غير متجانس، متماثل، وغير متماثل)، والمعلمات الهندسية، وظروف التثبيت. تكشف النتائج الرئيسية أنه رغم أن زيادة المسامية تقلل عادةً من الصلابة وتخفض الترددات الطبيعية، فإن تأثيرها يعتمد بشكل كبير على التوزيع المكاني. ومن اللافت أن التوزيعات المتماثلة للمسامية في الأعمدة FGP يمكن أن تحسن الأداء الديناميكي من خلال تحسين نسبة الصلابة إلى الكتلة، مما يؤدي إلى زيادة السرعة الحرجة. وعلى العكس، يمكن أن تؤدي التوزيعات غير المتماثلة وغير المتجانسة إلى سلوكيات معقدة وغير خطية وتدهور الاستقرار، خاصة عند التفاعل مع صلابة المحمل وكتلة القرص. تؤكد النتائج أن المسامية يمكن أن تكون سمة تصميمية مقصودة لإنشاء دوارات خفيفة الوزن وعالية الأداء، ولكن يجب التحكم بدقة في بنيتها. تسهم هذه الدراسة في توفير إرشادات تصميم قيّمة لهندسة أنظمة دوارة متقدمة بخصائص ديناميكية مُصممة خصيصًا، وهو أمر بالغ الأهمية لتطبيقات في صناعات الطيران والسيارات والطاقة حيث تكون الموثوقية التشغيلية ضرورية.

الكلمات المفتاحية: ديناميكا الدوارات، تحليل الاهتزازات، المواد المسامية، المواد المسامية المتدرجة وظيفيًا (PFGM)، الهياكل المسامية المتدرجة وظيفيًا (FGP) ، نظرية تيموشينكو للعارضة (TBT) ، طريقة العناصر المحدودة (p-FEM)، السرعة الحرجة، التردد الطبيعي، مخطط كامبل، توزيع المسامية، التأثير الجيروسكوبي.

Résumé

Cette thèse présente une étude approfondie du comportement dynamique vibratoire des arbres tournants fabriqués à partir de matériaux poreux avancés, y compris les matériaux fonctionnellement gradués poreux (PFGM) et les structures poreuses fonctionnellement graduées (FGP). L'objectif principal est de développer un cadre computationnel robuste permettant de prédire avec précision l'influence de la porosité conçue sur les caractéristiques critiques du rotor, telles que les fréquences propres, les formes modales et les vitesses critiques. La méthodologie repose sur une théorie des poutres de Timoshenko modifiée (TBT), tenant compte de la déformation en cisaillement et de l'inertie de rotation, implémentée dans une méthode des éléments finis hiérarchique p-version (p-FEM), afin d'assurer une grande précision et une bonne convergence. Des études paramétriques étendues ont été réalisées pour analyser les effets du gradient de matériau, des modèles de distribution de porosité (uniforme, non uniforme, symétrique et non symétrique), des paramètres géométriques et des conditions aux limites. Les résultats principaux montrent que, bien qu'une augmentation de la porosité réduise généralement la rigidité et abaisse les fréquences propres, son effet dépend fortement de la distribution spatiale. Notamment, les distributions symétriques de porosité dans les arbres FGP peuvent améliorer la performance dynamique en optimisant le rapport rigidité/masse, ce qui conduit à une augmentation de la vitesse critique. À l'inverse, les distributions non symétriques et non uniformes peuvent induire des comportements complexes et non monotones et dégrader la stabilité, en particulier lors des interactions avec la rigidité des paliers et la masse du disque. Les résultats soulignent que la porosité peut être une caractéristique de conception intentionnelle pour créer des rotors légers et performants, mais que son architecture doit être précisément contrôlée. Cette recherche apporte des lignes directrices de conception précieuses pour l'ingénierie des systèmes rotatifs avancés avec des propriétés dynamiques adaptées, ce qui est crucial pour les applications dans les secteurs aéronautique, automobile et énergétique où la fiabilité opérationnelle est essentielle.

Mots-clés : Dynamique des rotors, Analyse vibratoire, Matériaux poreux, Matériaux fonctionnellement gradués poreux (PFGM), Structures poreuses fonctionnellement graduées (FGP), Théorie des poutres de Timoshenko (TBT), Méthode des éléments finis p-version (p-FEM), Vitesse critique, Fréquence propre, Diagramme de Campbell, Distribution de porosité, Effet gyroscopique.

Zusammenfassung

Diese Dissertation präsentiert eine umfassende Untersuchung des dynamischen Schwingungsverhaltens von rotierenden Wellen, die aus fortschrittlichen porösen Materialien hergestellt wurden, darunter porös funktional gradierte Materialien (PFGM) und funktional gradierte poröse Strukturen (FGP). Das Hauptziel besteht darin, ein robustes Rechenmodell zu entwickeln, das präzise vorhersagen kann, wie die konstruierte Porosität kritische Rotoreigenschaften wie Eigenfrequenzen, Eigenschwingungsformen und kritische Drehzahlen beeinflusst. Die Methodik basiert auf einer modifizierten Timoshenko-Balkentheorie (TBT), die Schubverformung und Rotationsinertie berücksichtigt, und wird innerhalb der hierarchischen p-Version der Finite-Elemente-Methode (p-FEM) implementiert, um hohe Genauigkeit und Konvergenz zu gewährleisten. Umfangreiche Parameterstudien wurden durchgeführt, um die Auswirkungen der Materialgraduierung, der Porositätsverteilungsmodelle (gleichmäßig, ungleichmäßig, symmetrisch und unsymmetrisch), geometrischer Parameter und Randbedingungen zu analysieren. Wichtige Ergebnisse zeigen, dass eine Erhöhung der Porosität zwar im Allgemeinen die Steifigkeit verringert und die Eigenfrequenzen absenkt, ihre Wirkung jedoch stark von der räumlichen Verteilung abhängt. Besonders symmetrische Porositätsverteilungen in FGP-Wellen können die dynamische Leistung verbessern, indem sie das Steifigkeits-Masse-Verhältnis optimieren, was zu einer Erhöhung der kritischen Drehzahl führt. Im Gegensatz dazu können unsymmetrische und ungleichmäßige Verteilungen komplexe, nicht-monotone Verhaltensweisen hervorrufen und die Stabilität beeinträchtigen, insbesondere bei Wechselwirkungen mit der Lagersteifigkeit und der Scheibenmasse. Die Ergebnisse unterstreichen, dass Porosität als bewusstes Designelement zur Herstellung leichter, leistungsstarker Rotoren genutzt werden kann, ihre Architektur jedoch präzise kontrolliert werden muss. Diese Forschung liefert wertvolle Gestaltungshinweise für die Entwicklung fortschrittlicher Rotorsysteme mit maßgeschneiderten dynamischen Eigenschaften, was für Anwendungen in der Luft- und Raumfahrt, im Automobilbau und in der Energietechnik, bei denen die Betriebssicherheit entscheidend ist, von großer Bedeutung ist.

Schlüsselwörter: Rotordynamik, Schwingungsanalyse, Poröse Materialien, Porös funktional gradierte Materialien (PFGM), Funktional gradierte poröse Strukturen (FGP), Timoshenko-Balkentheorie (TBT), p-Finite-Elemente-Methode (p-FEM), Kritische Drehzahl, Eigenfrequenz, Campbell-Diagramm, Porositätsverteilung, Gyroskopeffekt.

Resumen

Esta tesis presenta una investigación integral sobre el comportamiento vibratorio dinámico de ejes rotatorios fabricados con materiales porosos avanzados, incluyendo materiales gradados funcionalmente porosos (PFGM) y estructuras porosas gradadas funcionalmente (FGP). El objetivo principal es desarrollar un marco computacional robusto que permita predecir con precisión cómo la porosidad diseñada influye en características críticas del rotor como las frecuencias naturales, las formas modales y las velocidades críticas. La metodología se basa en una teoría de vigas de Timoshenko modificada (TBT), que considera la deformación por cortante y la inercia rotacional, implementada dentro de un método de elementos finitos jerárquico en su versión p (p-FEM), para garantizar alta precisión y convergencia. Se realizaron amplios estudios paramétricos para analizar los efectos de la gradación del material, los modelos de distribución de porosidad (uniforme, no uniforme, simétrica y no simétrica), los parámetros geométricos y las condiciones de contorno. Los resultados clave revelan que, si bien el aumento de la porosidad generalmente reduce la rigidez y disminuye las frecuencias naturales, su efecto depende en gran medida de la distribución espacial. En particular, las distribuciones simétricas de porosidad en ejes FGP pueden mejorar el rendimiento dinámico optimizando la relación rigidez-masa, lo que conduce a un aumento de la velocidad crítica. Por el contrario, las distribuciones no simétricas y no uniformes pueden introducir comportamientos complejos y no monótonos y degradar la estabilidad, especialmente al interactuar con la rigidez de los cojinetes y la masa del disco. Los resultados destacan que la porosidad puede ser una característica de diseño intencional para crear rotores livianos y de alto rendimiento, pero su arquitectura debe controlarse con precisión. Esta investigación aporta valiosas pautas de diseño para la ingeniería de sistemas de rotor avanzados con propiedades dinámicas adaptadas, lo cual es significativo para aplicaciones en las industrias aeroespacial, automotriz y energética donde la confiabilidad operativa es crítica.

Palabras clave: Dinámica de rotores, Análisis de vibraciones, Materiales porosos, Materiales gradados funcionalmente porosos (PFGM), Estructuras porosas gradadas funcionalmente (FGP), Teoría de vigas de Timoshenko (TBT), Método de elementos finitos p (p-FEM), Velocidad crítica, Frecuencia natural, Diagrama de Campbell, Distribución de porosidad, Efecto giroscópico.

Sommario

Questa tesi presenta un'indagine completa sul comportamento dinamico delle vibrazioni di alberi rotanti realizzati con materiali porosi avanzati, tra cui materiali a gradiente funzionale porosi (PFGM) e strutture porose a gradiente funzionale (FGP). L'obiettivo principale è sviluppare un quadro computazionale robusto per prevedere con precisione come la porosità ingegnerizzata influisca su caratteristiche critiche del rotore quali frequenze naturali, forme modali e velocità critiche. La metodologia si basa su una teoria della trave di Timoshenko modificata (TBT), che tiene conto della deformazione da taglio e dell'inerzia rotazionale, implementata all'interno di un metodo degli elementi finiti p-versione (p-FEM) per garantire elevata precisione e convergenza. Sono stati condotti ampi studi parametrici per analizzare gli effetti della gradazione del materiale, dei modelli di distribuzione della porosità (uniforme, non uniforme, simmetrica e non simmetrica), dei parametri geometrici e delle condizioni al contorno. I principali risultati rivelano che, sebbene l'aumento della porosità riduca generalmente la rigidità e abbassi le frequenze naturali, il suo effetto dipende fortemente dalla distribuzione spaziale. In particolare, distribuzioni simmetriche di porosità negli alberi FGP possono migliorare le prestazioni dinamiche ottimizzando il rapporto rigidità/massa, portando a un incremento della velocità critica. Al contrario, distribuzioni non simmetriche e non uniformi possono introdurre comportamenti complessi e non monotoni e ridurre la stabilità, in particolare quando interagiscono con la rigidità dei cuscinetti e la massa del disco. I risultati sottolineano che la porosità può essere una caratteristica di progettazione intenzionale per creare rotori leggeri e ad alte prestazioni, ma la sua architettura deve essere controllata con precisione. Questa ricerca contribuisce a fornire preziose linee guida progettuali per l'ingegneria di sistemi rotanti avanzati con proprietà dinamiche personalizzate, rilevanti per applicazioni nei settori aerospaziale, automobilistico ed energetico, dove l'affidabilità operativa è fondamentale.

Parole chiave: Dinamica dei rotori, Analisi delle vibrazioni, Materiali porosi, Materiali a gradiente funzionale porosi (PFGM), Strutture porose a gradiente funzionale (FGP), Teoria della trave di Timoshenko (TBT), Metodo degli elementi finiti p (p-FEM), Velocità critica, Frequenza naturale, Diagramma di Campbell, Distribuzione della porosità, Effetto giroscopico.

Resumo

Esta tese apresenta uma investigação abrangente sobre o comportamento dinâmico vibratório de eixos rotativos fabricados a partir de materiais porosos avançados, incluindo Materiais Funcionalmente Graduados Porosos (PFGM) e Estruturas Porosas Funcionalmente Graduadas (FGP). O principal objetivo é desenvolver uma estrutura computacional robusta para prever com precisão como a porosidade projetada influencia características críticas do rotor, tais como frequências naturais, formas modais e velocidades críticas. A metodologia baseia-se em uma Teoria da Viga de Timoshenko (TBT) modificada, que considera a deformação por cisalhamento e a inércia rotacional, implementada dentro de um Método dos Elementos Finitos de versão p (p-FEM) hierárquico, a fim de garantir alta precisão e convergência. Estudos paramétricos extensivos foram conduzidos para analisar os efeitos da gradação do material, dos modelos de distribuição da porosidade (uniforme, não uniforme, simétrica e não simétrica), dos parâmetros geométricos e das condições de contorno. Os principais resultados revelam que, embora o aumento da porosidade geralmente reduza a rigidez e diminua as frequências naturais, seu efeito depende fortemente da distribuição espacial. Notavelmente, distribuições simétricas de porosidade em eixos FGP podem melhorar o desempenho dinâmico, otimizando a relação rigidez/massa, o que leva a um aumento da velocidade crítica. Por outro lado, distribuições não simétricas e não uniformes podem introduzir comportamentos complexos e não monotônicos e degradar a estabilidade, particularmente quando interagem com a rigidez dos mancais e a massa do disco. Os resultados ressaltam que a porosidade pode ser uma característica de projeto intencional para criar rotores leves e de alto desempenho, mas sua arquitetura deve ser precisamente controlada. Esta pesquisa contribui com diretrizes de projeto valiosas para a engenharia de sistemas rotativos avançados com propriedades dinâmicas personalizadas, o que é significativo para aplicações nas indústrias aeroespacial, automotiva e de energia, onde a confiabilidade operacional é crítica.

Palavras-chave: Dinâmica de rotores, Análise de vibrações, Materiais porosos, Materiais Funcionalmente Graduados Porosos (PFGM), Estruturas Porosas Funcionalmente Graduadas (FGP), Teoria da Viga de Timoshenko (TBT), Método dos Elementos Finitos p (p-FEM), Velocidade crítica, Frequência natural, Diagrama de Campbell, Distribuição da porosidade, Efeito giroscópico.

Сводка

В данной диссертации представлено комплексное исследование динамического вибрационного поведения вращающихся валов, изготовленных из современных пористых материалов, включая пористые функционально-градиентные материалы (PFGM) и функционально-градиентные пористые структуры (FGP). Основная цель заключается в разработке надежной вычислительной методики для точного прогнозирования того, как искусственно созданная пористость влияет на критические характеристики ротора, такие как собственные частоты, формы колебаний и критические скорости. Методология основана на модифицированной теории балки Тимошенко (TBT), учитывающей сдвиговую деформацию и вращательную инерцию, реализованной в иерархическом p-варианте метода конечных элементов (p-FEM), что обеспечивает высокую точность и сходимость. Проведены обширные параметрические исследования для анализа влияния градиента материала, моделей распределения пористости (равномерного, неравномерного, симметричного и несимметричного), геометрических параметров и граничных условий. Основные результаты показывают, что, хотя увеличение пористости, как правило, снижает жесткость и уменьшает собственные частоты, её эффект в значительной степени зависит от пространственного распределения. Особенно следует отметить, что симметричные распределения пористости в валах FGP могут повысить динамические характеристики за счет оптимизации соотношения жесткость/масса, что приводит к увеличению критической скорости. Напротив, несимметричные и неравномерные распределения могут вызывать сложные немонотонные процессы и снижать устойчивость, особенно при взаимодействии с жесткостью подшипников и массой диска. Полученные результаты подчеркивают, что пористость может быть преднамеренным элементом проектирования для создания легких и высокоэффективных роторов, однако её архитектура должна быть строго контролируема. Данное исследование вносит ценные рекомендации в проектирование передовых роторов с индивидуально подобранными динамическими свойствами, что имеет большое значение для применения в аэрокосмической, автомобильной и энергетической промышленности, где критична эксплуатационная надежность.

Ключевые слова: Динамика роторов, Вибрационный анализ, Пористые материалы, Пористые функционально-градиентные материалы (PFGM), Функционально-градиентные пористые структуры (FGP), Теория балки Тимошенко (TBT), p-метод конечных элементов (p-FEM), Критическая скорость, Собственная частота, Диаграмма Кэмпбелла, Распределение пористости, Гироскопический эффект.

Özet

Bu tez, gelişmiş gözenekli malzemelerden üretilmiş döner millerin dinamik titreşim davranışına ilişkin kapsamlı bir araştırma sunmaktadır. Bu malzemeler arasında Gözenekli Fonksiyonel Derecelendirilmiş Malzemeler (PFGM) ve Fonksiyonel Derecelendirilmiş Gözenekli (FGP) yapılar yer almaktadır. Temel amaç, tasarlanmış gözenekliliğin doğal frekanslar, mod şekilleri ve kritik hızlar gibi kritik rotor özelliklerini nasıl etkilediğini doğru bir şekilde öngörebilecek sağlam bir hesaplama çerçevesi geliştirmektir. Metodoloji, kayma deformasyonunu ve dönme ataletini dikkate alan ve hiyerarşik p-sürüm Sonlu Elemanlar Yöntemi (p-FEM) ile uygulanan değiştirilmiş Timoshenko Kiriş Teorisine (TBT) dayanmaktadır. Yüksek doğruluk ve yakınsama sağlamak için kapsamlı parametre çalışmaları gerçekleştirilmiştir. Bu çalışmalar, malzeme derecelendirmesinin, gözeneklilik dağılımı modellerinin (düzgün, düzensiz, simetrik ve asimetrik), geometrik parametrelerin ve sınır koşullarının etkilerini incelemektedir. Temel bulgular, gözenekliliğin artmasının genellikle rijitliği azalttığını ve doğal frekansları düşürdüğünü, ancak etkisinin büyük ölçüde mekânsal dağılıma bağlı olduğunu ortaya koymaktadır. Özellikle, FGP millerde simetrik gözeneklilik dağılımları, rijitlik/kütle oranını optimize ederek dinamik performansı artırabilir ve kritik hızda artışa yol açabilir. Buna karşılık, asimetrik ve düzensiz dağılımlar karmaşık, monoton olmayan davranışlara yol açabilir ve özellikle yatak rijitliği ve disk kütlesi ile etkileşim halinde kararlılığı bozabilir. Sonuçlar, gözenekliliğin hafif, yüksek performanslı rotorlar yaratmak için bilinçli bir tasarım özelliği olabileceğini, ancak mimarisinin kesinlikle kontrol edilmesi gerektiğini vurgulamaktadır. Bu araştırma, havacılık, otomotiv ve enerji endüstrilerinde operasyonel güvenilirliğin kritik olduğu durumlarda, özel dinamik özelliklere sahip gelişmiş rotor sistemlerinin mühendisliği için değerli tasarım yönergeleri sunmaktadır.

Anahtar kelimeler: Rotor Dinamiği, Titreşim Analizi, Gözenekli Malzemeler, Gözenekli Fonksiyonel Derecelendirilmiş Malzemeler (PFGM), Fonksiyonel Derecelendirilmiş Gözenekli Yapılar (FGP), Timoshenko Kiriş Teorisi (TBT), p-Sonlu Elemanlar Yöntemi (p-FEM), Kritik Hız, Doğal Frekans, Campbell Diyagramı, Gözeneklilik Dağılımı, Jiroskopik Etki.

总结

本论文对由先进多孔材料制成的旋转轴的动态振动行为进行了全面研究，其中包括多孔功能梯度材料 (PFGM) 和功能梯度多孔 (FGP) 结构。主要目标是开发一个稳健的计算框架，能够准确预测设计孔隙度如何影响转子关键特性，例如固有频率、模态形状和临界转速。方法基于修正的Timoshenko梁理论 (TBT)，该理论考虑了剪切变形和旋转惯性，并在分层的 p-版本有限元方法 (p-FEM) 中实现，以确保高精度和收敛性。进行了广泛的参数研究，以分析材料梯度、孔隙分布模型（均匀、不均匀、对称和非对称）、几何参数和边界条件的影响。主要结果表明，虽然增加孔隙度通常会降低刚度并降低固有频率，但其效果在很大程度上取决于空间分布。值得注意的是，FGP轴中的对称孔隙分布可以通过优化刚度与质量比来提高动态性能，从而导致临界转速的增加。相反，非对称和不均匀的分布可能引入复杂的、非单调的行为并降低稳定性，尤其是在与轴承刚度和盘质量相互作用时。结果强调，孔隙度可以作为一种有意的设计特征，用于制造轻量化、高性能的转子，但其结构必须得到精确控制。本研究为工程设计具有定制动态特性的先进转子系统提供了宝贵的设计指南，这对航空航天、汽车和能源工业等对运行可靠性要求极高的应用具有重要意义。

关键词：转子动力学，振动分析，多孔材料，多孔功能梯度材料 (PFGM)，功能梯度多孔结构 (FGP)，Timoshenko梁理论 (TBT)，p-有限元方法 (p-FEM)，临界转速，固有频率，Campbell图，孔隙分布，陀螺效应。

概要

本論文は、先進的な多孔質材料から製作された回転軸の動的振動挙動について包括的に調査したものである。対象とする材料には、多孔質機能傾斜材料 (PFGM) および機能傾斜多孔質構造 (FGP) が含まれる。主な目的は、設計された多孔性が固有振動数、モード形状、臨界回転速度といったローターの重要特性にどのように影響するかを正確に予測できる堅牢な計算枠組みを構築することである。本研究の方法論は、せん断変形および回転慣性を考慮した修正ティモシェンコ梁理論 (TBT) に基づき、階層的 p-版有限要素法 (p-FEM) に実装することで、高精度かつ収束性を確保している。材料の傾斜、孔隙分布モデル（均一、不均一、対称、非対称）、幾何学的パラメータ、境界条件の影響を分析するために、広範なパラメトリック研究を実施した。主要な結果として、多孔性の増加は一般的に剛性を低下させ、固有振動数を下げるが、その効果は空間分布に大きく依存することが明らかになった。特に、FGP 軸における対称的な孔隙分布は、剛性と質量比を最適化することで動的性能を向上させ、臨界速度を上昇させる。一方、非対称および不均一な分布は、複雑で非単調な挙動を引き起こし、安定性を低下させる可能性があり、とりわけ軸受剛性やディスク質量との相互作用において顕著である。これらの結果は、多孔性が軽量で高性能なローターを設計するための意図的な設計要素となり得ることを強調しているが、その構造は精密に制御されなければならない。本研究は、特注の動的特性を備えた先進的なローターシステムの工学設計に有益な指針を提供しており、運用信頼性が不可欠な航空宇宙、自動車、エネルギー産業における応用にとって重要である。

キーワード: ローター動力学、振動解析、多孔質材料、多孔質機能傾斜材料 (PFGM)、機能傾斜多孔質構造 (FGP)、ティモシェンコ梁理論 (TBT)、p-有限要素法 (p-FEM)、臨界速度、固有振動数、キャンベル線図、孔隙分布、ジャイロスコープ効果。

CONTENTS

Abstract I

ملخص II

Résumé III

Zusammenfassung IV

Resumen V

Sommario VI

Özet IX

总结 X

概要 XI

CONTENTS XII

Figures captions XVIII

Tables captions XXIII

List of abbreviations XXIV

List of symbols XXV

Introduction 1

Background and Context 1

Research Motivation and Objectives 2

Research Questions 3

Significance and Contributions 3

Methodology Overview 3

Thesis Structure 4

I. Literature Review 5

I.1. Introduction 5

I.2. Theoretical Background and Methodologies 5

I.3. Vibration Behavior of FGM Rotors 6

I.4. Modeling approaches and dynamic behavior of FGP structures 6

I.5. Parametric Studies in FGP Structures 7

I.6. Porous Rotor Dynamics and Stability Analysis 7

I.7. Advanced Modeling Techniques and Multiphysics Approaches 8

II. State-of-The-Art 9

II.1. Introduction 9

II.2. Definition and history of FGMs 10

II.2.1. Definition 10

II.2.2. History 10

II.3. Definition and history of porosity 12

II.3.1. Definition 12

II.3.2. History 12

II.4. Porous materials in literature 13

II.4.1. Porosity as a defect in FGM fabrication: 14
II.4.2. Porosity as a design feature in FGMs 16
II.4.3. Comparison of porosity as a defect vs. Foam design 18
II.4.4. Types of porous materials 18
II.5. Dynamic vibration behavior of rotor systems 22
II.5.1. Fundamental concepts in rotor dynamics 22
II.5.2. Impact of material properties – FGMs – 23
II.5.3. Role of porosity in FGMs for rotor applications 23
II.5.4. Role of porosity for rotor applications 24
II.6. Recent advances and trends 24
II.6.1. Latest research and emerging trends 24
II.6.2. Gaps and challenges in the literature 25
II.6.3. Applications and case studies of porous rotor systems 26
II.6.4. Practical applications of porous rotor systems 26
II.6.5. Performance analysis and engineering benefits 27
II.7. The Hi-tech in materials selected 28
II.7.1. Functionally Graded Materials (FGMs) 28
II.7.2. Functionally Graded Porous (FGP) Structures (Foams) 32
III. Modelization of porous rotors structure 36
III.1. Beam theories in rotor vibration analysis: 36

III.2. General assumptions of beam theories 36
III.3. Euler–Bernoulli beam theory 36
III.3.1. Assumptions of EBBT 36
III.3.2. Displacement field of EBBT 37
III.4. Timoshenko beam theory 37
III.4.1. Assumptions of TBT 37
III.4.2. Comparison of Beam Theories 37
III.4.3. Justification for using TBT in this study 38
III.5. Application of TBT in rotor vibration analysis 38
III.5.1. Displacement field of TBT 39
III.5.2. Stress tensor 40
III.6. Hierarchical beam element formulation 41
III.7. Modelization of shaft 42
III.7.1. Strain energy 42
III.7.2. Kinetic energy 42
III.7.3. Matrices of shaft 43
III.8. Modelization of disc 44
III.8.1. Kinetic energy 44
III.8.2. Matrices of disc 44
III.9. Modelization of bearing and damping 45

III.10. Global matrices of the rotors system 46
III.10.1. Global mass matrix 46
III.10.2. Global gyroscopic matrix 46
III.10.3. Global stiffness matrix 46
III.10.4. Solving the equation of motion system 47
III.11. Algorithmic framework of calculation program 47
III.12. Mechanical properties of PFGM 51
III.13. Mechanical properties of FGP 52
IV. Results and discussions 54
IV.1. Convergence and comparison studies 54
IV.2. Parametric study of PFGM shaft 58
IV.2.1. Effect of $\boldsymbol{n}, \boldsymbol{\alpha}$, boundary conditions, and modes 58
IV.2.2. Effect of $\boldsymbol{n}, \boldsymbol{\alpha}$, boundary conditions, and situation motion 61
IV.2.2. Geometric effect in Campbell's diagram 68
IV.3. Critical Speed of PFGM shaft 73
IV.3.1. Effect of geometric parameters and boundary conditions 73
IV.3.2. The influence of the FGM types in critical speed of PFGM shaft 75
IV.3.3. The influence of the bearing in critical speed of PFGM shaft 77
IV.3.4. The influence of the damping in critical speed of PFGM shaft 79
IV.3.5. The influence of the disk in critical speed of PFGM shaft 81

IV.4. Parametric study of FGP shaft 83

IV.4.1. Porosity Influence of FGP shaft under varying boundary conditions 83

IV.4.3. Material influence in critical speed of FGP shaft 93

IV.4.4. Bearing influence in critical speed of FGP shaft 95

IV.4.5. Damping influence in critical speed of FGP shaft 97

IV.4.6. Disk influence in critical speed of FGP shaft 99

Conclusion 101

References 104

Figures captions

Figure 1 Alternator that changes mechanical energy into electrical energy driven by steam turbine (Taked in science center museum in Kocaeli, Turkey). 1

Figure III-1: Evolution of functionally graded materials 11

Figure III-2 Evolution of porosity understanding 13

Figure III-3 Impact of porosity in FGM fabrication 15

Figure III-4 Specification of Porous FGMs 17

Figure III-5 Microscopic appearance of IN625-SUS304L (Ni-SS) PFGM [41] 29

Figure III-7 Cross-sectional microstructure of ZrO2–NiCr FGM fabricated by (a) pressureless sintering at 1400C; (b) hot pressing at 1250C, 5MPa [43] 30

Figure III-6 formation of porosity in Ni coating and Ni/ZrO2 gradient coating depend of temperature Fabricated by Double Pulses Electrodeposition 30

Figure III-8 Micrograph of a representative Ni-Al2O3 FGM showing made by Electrophoretic Deposition 31

Figure III-9 FGP classification by gradient type [49] 32

Figure III-10 Schematic diagram of powder metallurgy technique for metallic foams [49] 33

Figure III-11 Zirconia Ceramic Foam Filters [55] 34

Figure III-12 Alumina Ceramic Foam Filters [57] 35

Figure IV-1 Displacements of a cross-section of the shaft 39

Figure IV-2 Beam element with two nodes 41

Figure IV-3 Shaft with disc structure under clamped end 44

Figure IV-4 Shaft under bearing and damping condition 45

Figure IV-5 flowchart represent the calculation program algorithm. 50
Figure IV-6 Structure characterization, inner and outer radius of Even Porous FGM shaft. 51
Figure IV-7 Different porosity distribution for an PFGM structure [22] 52
Figure IV-8 Cross-section for an FGP cylindrical shaft with different porosity distribution [70]. 53
Figure V-1 Convergence study for three first modes of natural frequencies in function in the number of shape functions with different boundary conditions. 54
Figure V-2 first steady-state natural frequencies of Even PFGM for different BC. a) S-BC; b) C-BC; c) SC-BC. 62
Figure V-3 first rotational natural frequencies of Even PFGM for different BC. a) S-BC; b) C-BC; c) SC-BC. 63
Figure V-4 first steady-state natural frequencies of Uneven PFGM for different BC. a) S-BC; b) C-BC; c) SC-BC. 65
Figure V-5 first rotational natural frequencies of Uneven PFGM for different BC. a) S-BC; b) C-BC; c) SC-BC. 66
Figure V-6 Three first modes of steady natural frequencies for various porosity with S-BC, C-BC, and SC-BC. 67
Figure V-7 Campbell's diagrams for different thickness ratios of even PFGM. a) $\alpha = 0$; b) $\alpha = 0.2$; c) $\alpha = 0.5$ 69
Figure V-8 Campbell's diagrams for different thickness ratios of uneven PFGM. a) $\alpha = 0$; b) $\alpha = 0.2$; c) $\alpha = 0.5$ 70
Figure V-9 Campbell's diagrams for different slenderness ratios of even PFGM. a) $\alpha = 0$; b) $\alpha = 0.2$; c) $\alpha = 0.5$. 71

Figure V-10 Campbell's diagrams for different slenderness ratios of uneven PFGM. a) $\alpha = 0$; b) $\alpha = 0.2$; c) $\alpha = 0.5$. 72
Figure V-11 First critical speeds in function in porosity of Even PFGM under various boundary conditions (S-BC, C-BC, and SC-BC) in function in porosity α. a) $L/D = 5$; b) $L/D = 10$; c) $L/D = 20$. 74
Figure V-13 First critical speeds in function in porosity for deferent uneven Porous FGMs types (SS-Ni, Ni-ZrO2, and Ni-Al2O3) in function in porosity α. 76
Figure V-12 First critical speeds in function in porosity for deferent even Porous FGMs types (SS-Ni, Ni-ZrO2, and Ni-Al2O3) in function in porosity α. 76
Figure V-14 First critical speeds in function in porosity of even PFGM shaft, for deferent symmetric Bearing values 78
Figure V-15 First critical speeds in function in porosity of uneven PFGM shaft, for deferent symmetric Bearing values 78
Figure V-17 First critical speeds in function in porosity of even PFGM shaft, for deferent symmetric Damping values 80
Figure V-16 First critical speeds in function in porosity of uneven PFGM shaft, for deferent symmetric Damping values 80
Figure V-18 First critical speeds in function in porosity of even PFGM shaft, for deferent configurations of the disk 82
Figure V-19 First critical speeds in function in porosity of uneven PFGM shaft, for deferent configurations of the disk 82
Figure V-20 First three modes natural frequencies of various non-symmetric FGP shaft under different BCs, a) S-BC, b) C-BC, and c) SC-BC 85

Figure V-21 First three modes natural frequencies of symmetric FGP shaft under different BCs, a) S-BC, b) C-BC, and c) SC-BC 86
Figure V-22 Campbell's diagrams for different thickness ratios of symmetric FGP. a) $e0 = 0$; b) $e0 = 0.2$; c) $e0 = 0.8$ 88
Figure V-23 Campbell's diagrams for different thickness ratios of non-symmetric FGP. a) $e0 = 0$; b) $e0 = 0.2$; c) $e0 = 0.8$ 89
Figure V-24 Campbell's diagrams for different slenderness ratios of symmetric FGP. a) $e0 = 0$; b) $e0 = 0.2$; c) $e0 = 0.8$ 91
Figure V-25 Campbell's diagrams for different slenderness ratios of non-symmetric FGP. a) $e0 = 0$; b) $e0 = 0.2$; c) $e0 = 0.8$ 92
Figure V-26 First critical speed for deferent symmetric FGP types (SS, ZrO2, and Al2O3) in function in porosity $e0$ 94
Figure V-27 First critical speed for deferent non-symmetric FGP types (SS, ZrO2, and Al2O3) in function in porosity $e0$ 94
Figure V-29 First critical speeds in function in porosity for non-symmetric porosity of FGP shaft, for different symmetric damping values 96
Figure V-28 First critical speeds in function in porosity for symmetric porosity of FGP shaft, for different symmetric damping values 96
Figure V-30 First critical speeds in function in porosity for symmetric porosity of FGP shaft, for different symmetric damping values 98
Figure V-31 First critical speeds in function in porosity for non-symmetric porosity of FGP shaft, for different symmetric damping values 98

Figure V-32 First critical speeds in function in porosity for symmetric porosity of FGP shaft, for deferent configurations of the disk 100
Figure V-33 First critical speeds in function in porosity for non-symmetric porosity of FGP shaft, for deferent configurations of the disk 100

Tables captions

Table IV-1 Comparison of Beam Theories 38

Table V-1 FEM-p values and exact values of the four first modes of the homogenous beam. 55

Table V-2 Three first modes for FGM (SS-Ni) beam 55

Table V-3 Geometric parameter e/R influence in natural frequency for FGM beam 56

Table V-4 Graded index influence in first natural frequency for FGM cylindrical shaft. 56

Table V-5 Dimensionless natural frequencies of Porous FGM cylindrical shaft 56

Table V-6 Dimensionless natural frequencies of FGP cylindrical shaft 57

Table V-7 Materials properties at $T = 300$ °K [5] 58

Table V-8 First three modes natural frequencies of various Even PFGM with different BC 59

Table V-9 First three modes natural frequencies of various Uneven PFGM with different BC 60

List of abbreviations

PFGM	Porous Functionally Graded Material
FGP	Functionally Graded Porous
FGM	Functionally Graded Material
TBT	Timoshenko Beam Theory
p-FEM	Finite Element Method *p*-version
HIP	Hot Isostatic Pressing
CNTs	Carbon Nanotubes
AM	Additive Manufacturing
SLM	Selective Laser Melting
EBM	Electron Beam Melting
PM	Powder Metallurgy
EPD	Electrophoretic Deposition
SS	Stainless Steel
Ni	Nickel
ZrO_2	Zirconia
Al_2O_3	Alumina
EBBT	Euler – Bernoulli Beam Theory
S-BC	Simply supported boundary condition
C-BC	Clamped– Clamped boundary condition
CS-BC	Simply supported– Clamped boundary condition
FW	Forward mode
BW	Backward mode

List of symbols

$\vec{U}_{EBT}$	Displacement field of EBBT
$\vec{U}_{TBT}$	Displacement field of TBT
$U_0(x,t)$	Longitudinal displacement
$V_0(x,t)$	Transversal horizontal displacement
$W_0(x,t)$	Transversal vertical displacement
ϕ	Angular displacement
β_x	Rotation angles about y
β_y	Rotation angles about z
t	Time
σ, τ	Stress
ε, γ	Strain
k_s	Shear correction factor
$E[N/m^2]$	Young's modular
$\rho[kg/m^3]$	Density
ν	Poisson's ratio
Q_{ii}	Elasticity constant
x, r, θ	Cylindrical coordinate system
x	Longitudinal axe
r	Radius coordinate
θ	Angle coordinate
$[N]$	Shape function matrix
ξ	Non-dimensional coordinates

f_i	Shape functions
p	Number of shape functions for displacements
E_{sS}	Strain energy of the shaft
$\vec{R}_{P/O}$	Displacement vector
E_{kS}	Kinetic energy of the shaft
E_{kD}	Kinetic energy of the disk
$L[m]$	Length of the shaft
$R_o[m]$	Outer radius of the shaft
$R_i[m]$	Inner radius of the shaft
$e[m]$	Thickness of the shaft
$D[m]$	medium diameter of shaft
δA	Virtual work
F_{V_0}, F_{W_0}	Generalized forces
$\{q_U\}$	Generalized coordinates
$[M^S]$	Mass matrix of the shaft
$[K^S]$	Rigidity matrix of the shaft
$[G^S]$	Gyroscope matrix of the shaft
$[M^D]$	Mass matrix of the disk
$[G^D]$	Gyroscope matrix of the disk
$[K^B]$	Rigidity matrix of the bearing
$[C^D]$	Clamping matrix of the damping
$[M]$	Global mass matrix
$[G]$	Global gyroscopic matrix
$[K]$	Global stiffness matrix

$P(r)$	Expression of material properties
P_o	Outer material properties
P_i	Inner material properties
n	Power low index
α	Coefficient of porosity (PFGM)
e_0	Coefficient of porosity (FGP)
E_0	Minimum values of elasticity module
E_1	Maximum values of elasticity module
G	Shear modulus
ω $[Hz]$	Natural frequencies
A	Aire of cross-section
λ	Frequency parameter
$T[°K]$	Temperature
Ω $[RPM]$	Rotational speed

Introduction

Background and Context

Rotating machinery is fundamental to a vast array of engineering fields, from aerospace propulsion and energy generation to industrial manufacturing (Figure 1). The dynamic behavior of these systems, particularly their rotors, is a critical factor influencing performance, operational safety, and reliability. For decades, research in rotor dynamics has primarily focused on components made from isotropic and homogeneous materials, assuming uniform mass distribution and structural integrity. However, recent advancements in material science have introduced innovative materials like porous materials. These materials are gaining significant interest for their unique ability to combine lightweight structures with tunable mechanical properties, offering enhanced vibration damping and thermal resistance.

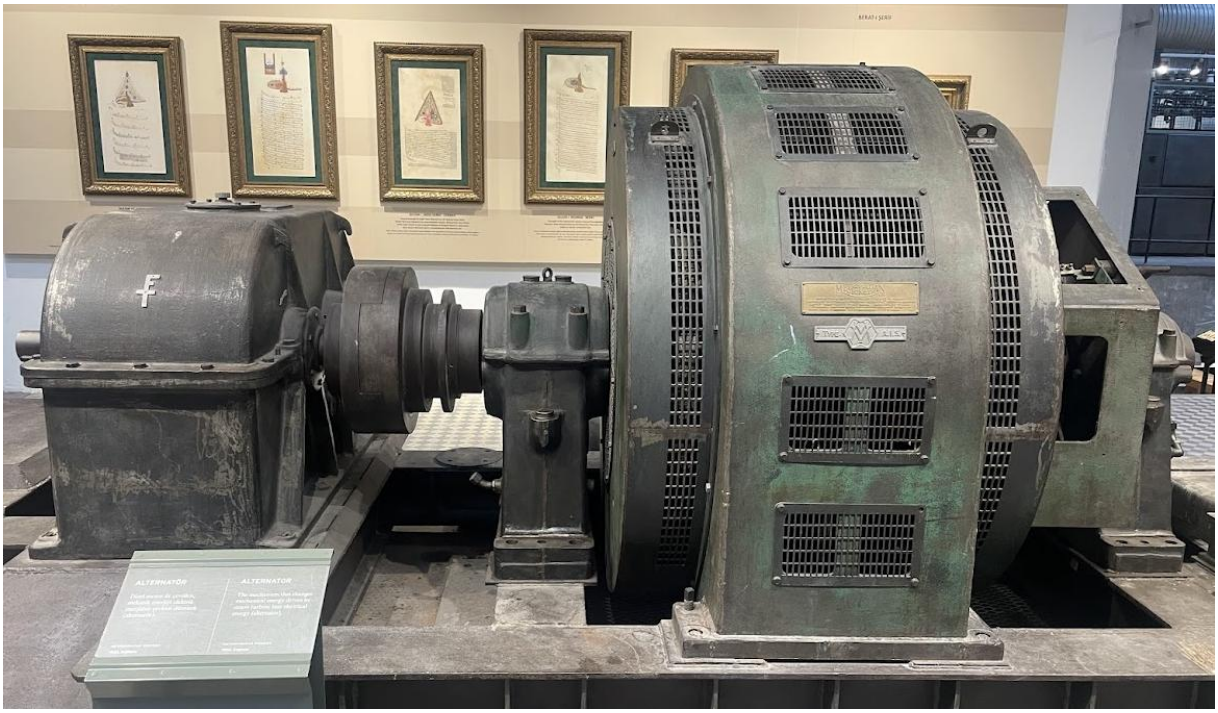

Figure 1 Alternator that changes mechanical energy into electrical energy driven by steam turbine (Taked in science center museum in Kocaeli, Turkey).

The introduction of porosity, characterized by a network of voids within a solid matrix, brings new complexities to the dynamic analysis of rotating systems. The pores directly alter the rotor's mass distribution, stiffness, and damping capacity, causing its behavior to deviate significantly

from classical dynamic models. Despite the increasing use of porous materials in engineering, a significant gap exists in the literature regarding their dynamic behavior. Most existing studies have either overlooked the effect of porosity or have confined their analysis to static or thermomechanical contexts, leaving the dynamic modeling of porous rotors under rotational motion largely unexplored. Consequently, a comprehensive framework that accurately captures the coupled effects of rotational motion and porous heterogeneity on the dynamic response of such systems is currently lacking. Critical questions concerning the influence of porosity on modal characteristics, gyroscopic effects, and stability thresholds in rotor-bearing systems remain largely unanswered.

Research Motivation and Objectives

The primary motivation for this research stems from the urgent need to understand and predict the dynamic behavior of rotors made from porous materials, especially in high-speed applications where vibration and instability can lead to catastrophic failure. Traditional design methodologies and computational tools are often inadequate when applied to porous structures, necessitating the development of new models that explicitly incorporate porosity distribution and its impact on dynamic properties.

The main objectives of this study are:

- To enhances a comprehensive mathematical and computational framework for analyzing the dynamic behavior of porous rotors, accounting for material heterogeneity and porosity distribution.
- To investigate the influence of key porosity parameters on the rotor's critical speed, natural frequencies, mode shapes, and dynamic stability.
- To conduct a thorough parametric study to identify the critical material and geometric variables that affect the vibration characteristics of porous rotors.
- To provide valuable insights and guidelines for the design of lightweight, high-performance rotating systems utilizing porous materials.

Research Questions

This study aims to answer the following fundamental research questions:

1. How does the presence and distribution of porosity influence the natural frequencies and mode shapes of a rotating shaft system?
2. What is the quantitative effect of porosity on the critical speed and stability margin of a rotor?
3. How can the spatial grading of material composition and porosity be optimized to enhance the dynamic performance and stability of rotors?

Significance and Contributions

This thesis makes a significant contribution to the field of rotor dynamics by bridging the existing gap between porous material modeling and dynamic vibration analysis. It introduces a novel analytical and numerical framework that integrates the effects of porosity directly into the governing equations of rotor dynamics. The findings will provide invaluable guidance for engineers and researchers in designing advanced rotors with tailored dynamic properties, particularly in applications where weight reduction, vibration control, and material efficiency are paramount. Furthermore, this research enriches the fundamental understanding of how microstructural features, such as porosity, influence system-level dynamics, thereby expanding the applicability of rotor dynamic theories to a new class of advanced engineering materials.

Methodology Overview

The research methodology employs a combination of theoretical modeling and numerical simulation. A Timoshenko beam theory is adopted to construct a rotor model that accurately incorporates the effects of shear deformation and rotary inertia, which are pronounced in porous structures. The material properties are defined as functions of spatial coordinates and porosity, allowing for the analysis of both uniform and graded porosity distributions. The governing equations of motion are derived using the Euler-Lagrange principle, and the dynamic frequency is computed using numerical techniques, including the finite element method p version (p-FEM) and

modal analysis. The model's accuracy and reliability are rigorously verified through convergence studies and by comparing results with established benchmarks from the literature.

Thesis Structure

The remainder of this thesis is organized as follows:

- **Chapter 1** provides a comprehensive review of the relevant literature on rotor dynamics, porous materials, and related modeling techniques.
- **Chapter 2** provides a state-of-the-art review of the literature on the dynamic vibration behavior of PFGM and FGP rotor systems.
- **Chapter 3** presents the detailed mathematical formulation of the porous rotor model, including the underlying assumptions, governing equations, and boundary conditions. describes the numerical methods used for solving the equations and outlines the procedures for model validation.
- **Chapter 4** discusses the results of the parametric studies, detailing the influence of key parameters on the porous rotor's dynamic behavior (boundary conditions, mode shape, distribution types of porosity, geometric parameters, types of materials, bearing, damping, and the disk).
- **Chapter 5** concludes the study with a summary of the findings, provides design recommendations, and suggests directions for future research.

I. Literature Review

I.1. Introduction

The study of porous materials in structural dynamics has gained significant momentum in recent years due to their potential applications in lightweight and high-performance mechanical systems. These materials, which include engineered porosity to reduce mass and tailor mechanical properties, are increasingly used in rotating machinery such as turbine rotors, aerospace shafts, and biomedical devices. Depending on design requirements, porous materials can be implemented with or without a FGM composition, allowing for either homogenous or spatially varying material characteristics. Researchers have been particularly interested in understanding how porosity — independently or in combination with FGMs — affects the dynamic performance of rotating structures. This has led to a range of studies focusing on natural frequencies, critical speeds, mode shapes, and dynamic stability of rotors manufactured from such materials. This review aims to consolidate the existing body of literature that investigates the vibration behavior of porous rotating shafts, emphasizing both FGM and non-FGM configurations, to provide a comprehensive understanding of current advancements and identify future research directions.

I.2. Theoretical Background and Methodologies

Several foundational theories have shaped rotor dynamics. Nelson and McVaugh [1] introduced a finite element method (FEM) framework for rotor-bearing systems, which laid the groundwork for subsequent complex analyses. Nelson [2] expanded this by incorporating Timoshenko beam theory into rotating shaft elements, accounting for shear deformation effects. These works remain critical for modeling rotors with non-uniform properties.

Building on these fundamentals, Szeidl and Kiss [3] offered a modern take on mechanical vibrations, emphasizing the mathematical modeling of dynamic systems. Ling [4] provided a comprehensive overview of the dynamic analysis of rotating systems, bridging theoretical modeling with practical engineering applications.

I.3. Vibration Behavior of FGM Rotors

Early work by Loy et al. [5] demonstrated the potential of FGMs in cylindrical shells, noting their impact on natural frequencies and mode shapes. Reddy and Chin [6] further analyzed the thermomechanical behavior of FGM cylinders and plates, showing temperature-dependent vibration characteristics.

Recent studies have shifted focus to porous structures. Ebrahimi and Jafari [7] explored higher-order thermomechanical vibration in temperature-dependent FGM beams with porosity, showing that porosity significantly reduces stiffness and thus alters the natural frequency. Forooghi et al. [8] highlighted the impact of thermal instability on nanoscale porous FGM plates under fluid flow, introducing the role of foundation stiffness and fluid-structure interaction. Dang et al. [9] analyzed free vibrations of rotating porous FGM cylindrical shells with different boundary conditions, finding that both geometry and support conditions significantly influence natural frequencies.

I.4. Modeling approaches and dynamic behavior of FGP structures

In recent years, the study of functionally graded porous (FGP) structures has attracted significant interest due to their enhanced mechanical performance and lightweight nature. These structures, which combine material gradation and porosity, offer great potential in advanced engineering applications. Analytical, numerical, and semi-analytical models have been extensively developed to investigate their vibrational and stability characteristics under various conditions. For instance, Salehi et al. [10] developed an analytical approach to study nonlinear vibrations of FG porous cylindrical shells reinforced with graphene platelets, revealing the sensitivity of nonlinear frequency responses to porosity distributions and material gradation. Similarly, Gao et al. [11] employed the method of multiple scales to explore primary resonance in FG porous cylindrical shells under harmonic excitation, highlighting the influence of damping and porosity on hardening-type nonlinear behavior. Wang and Wu [12] used sinusoidal shear deformation theory to analyze free vibration of FG porous cylindrical shells, showing that porosity distribution and boundary conditions significantly affect the dynamic characteristics. These works underscore the effectiveness of advanced shear deformation theories and asymptotic methods in predicting the complex behavior of FGP systems.

I.5. Parametric Studies in FGP Structures

Other studies have focused on a broader spectrum of FGP structures including rotating, laminated, and shallow shell configurations. Ghasemi and Meskini [13] analyzed the free vibration behavior of porous laminated rotating cylindrical shells, showing that increasing porosity reduces both backward and forward natural frequencies. Chen et al. [14] presented a Timoshenko beam-based model for elastic buckling and bending of FG porous beams and emphasized how different porosity distributions and boundary conditions alter the mechanical response. Zhao et al. [15] extended the modeling of FGP shallow shells by incorporating a modified Fourier series and general boundary conditions using a virtual spring technique, thereby enhancing solution accuracy and boundary flexibility. Similarly, Li et al. [16] introduced Jacobi polynomial-based displacement functions to evaluate free vibration in FG porous spherical shells, achieving high computational efficiency and accuracy. Li et al. [17] similarly demonstrated that boundary restraints and shell geometry dictate the dynamic response, suggesting semi-analytical methods as efficient alternatives to full numerical simulations. Finally, Wu et al. [18] provided a comprehensive review of the mechanical behavior of FGP structures, covering material modeling, micromechanics, and structural response. Together, these contributions illustrate the importance of accurate geometric modeling and boundary condition treatment in capturing the rich dynamic behavior of FGP systems under various operational scenarios.

I.6. Porous Rotor Dynamics and Stability Analysis

Sathujoda et al. [19] conducted a finite element analysis of a thermally loaded porous FGM rotor-bearing system, showing that increasing porosity and thermal gradients reduce system stability. Bose and Sathujoda [20] analyzed natural frequencies of porous FGM shafts, demonstrating that porosity distribution critically influences dynamic response.

In follow-up studies, Jaiman and Sathujoda [21] examined a porous FGM Jeffcott rotor, incorporating thermal gradients, and confirmed the adverse effects of porosity on system stiffness and frequency response. Vaka et al. [22] provided a thorough review of porous FGM rotor dynamics, identifying key parameters such as gradient index, porosity profile, and thermal effects.

Batchu et al. [23] modeled porous FGM rotor-bearing systems using FEM, emphasizing the importance of accurate material property gradation and porosity modeling. The authors pointed out that while FEM is widely used, mesh refinement and higher-order elements are crucial for accurate vibration analysis.

I.7. Advanced Modeling Techniques and Multiphysics Approaches

Recent approaches integrate multi-physics models. Behar et al. [24] used nonlocal strain gradient theory to assess electromechanical vibrations in nanotubes, indicating that scale effects become prominent at micro and nano levels. Similarly, Aouinat et al. [25] applied state-space methods to FGM nanotubes, providing analytical solutions that balance computational efficiency and accuracy.

Assem et al. [26] and [27] utilized h-p finite element methods for FGM rotors in thermal environments, demonstrating enhanced accuracy in capturing localized stress and displacement fields. These methods are particularly valuable for porous structures where material property gradients are nonlinear.

II. State-of-The-Art

II.1. Introduction

The application of rotor systems includes a number of engineering fields: aerospace and automotive industries, and energy production. The performance and reliability of this equipment are greatly influenced by the dynamic behavior of these systems. In view of the various operating conditions rotor systems are faced with, knowledge of their dynamic characteristics is relevant to their safety, efficiency, and life expectation.

Within advanced engineering applications, functionally graded materials (FGM) have been invented as innovative solutions for their property variations, which are gradual to meet the intended specifications. Compared to conventional homogeneous materials, these materials create a lot of functionalities by showing improved thermal resistance and mechanical performance. The introduction of Porosity within FGMs or without it further tailors the properties so that it is applicable for weight reduction with improved damping characteristics. However, porosity also tends to complicate this area mainly in making proper predictions for dynamic response of the material under operational conditions.

This chapter is intended to bring forth a state-of-the-art review of literature available on the dynamic vibration behavior of Porous FGM rotor systems. In the chapter to come, we will be covering some of the important topics associated with FGM and porosity, their adopted analytical and numerical methods applied for dynamic analysis, experimental techniques, and latest development in this regard. Deficiencies in available literature and areas that need further exploration are also identified.

This review details studies on modelling and analysis of FGMs with porosity, theoretical and experimental methods, and practical applications in relevant industries. Although the primary focus will be on recent developments, seminal works that really laid the basis for this research area shall not be skipped. The structure of the chapter is as follows: first of all, we introduce the background related to FGMs and the role of porosity; secondly, methods for dynamic analysis are presented; thirdly, experimental findings are shown; lastly, recent trends and future research directions will be concluded.

This chapter provides a general understanding of the state of the art in laying the framework for the subsequent research that is presented to further advance the current understanding of the dynamic behavior of FGMs with porosity in rotor systems.

II.2. Definition and history of FGMs

II.2.1. Definition

Functionally graded materials (FGMs) are typical advanced composite materials wherein composition and structure vary smoothly over their volume, leading to corresponding property variations. In contrast to more traditional composite materials with interfaces between different distinct materials, this variation of properties in FGMs is continuous, thus having the effect of reducing stress concentrations and generally improving performance. This gradual transition can improve many properties, like thermal resistance, mechanical strength, and corrosion resistance, making FGM appropriate for use in a large number of applications in aerospace, biomedical implants, and thermal barrier coatings.

II.2.2. History

The concept of functionally graded materials dates back to the late 1980s as seen in Figure II-1 from [28], triggered by a high demand for materials that could withstand extreme thermal gradients. The pioneering work was conducted in Japan, especially in regard to aerospace applications. It aimed at designing materials capable of resisting high thermal stresses encountered in space vehicles and other high-temperature environments without the drawbacks of traditional composites.

1. Early developments (1980s):
   a. The concept was first proposed by a team of Japanese researchers in 1984. Their idea was to create a material that would graduate smoothly from metal to ceramic without undergoing the stresses caused by the temperature changes [29].
   b. Earlier research focused on theoretical modelling and experimental methods for producing these gradients for thermal barrier applications mainly in aerospace [30].
2. Advancements in the 1990s:
   a. In the 1990s, dramatic improvements in fabrication techniques of FGMs were realized. Different methods such as powder metallurgy, centrifugal casting, and

chemical vapor deposition were developed in order to produce the materials with required gradients [28].

b. Researchers began applying this new class of materials in other fields of engineering, like in electronics, where graded electrical properties of the materials were of essence [31].

3. Modern era (2000s - Present):

a. In the 2000s, computational methods and techniques from material science have been put together to design and optimize FGMs for certain applications. Computational models could predict behavior under different working conditions, thus enabling more efficient designs [32].

b. Biomedicine has turned out to be another huge field of application, where the use of FGMs in implants and prosthetics better harmonizes with the mechanical properties of human tissues [28].

c. Today, FGMs are applied in many industries—from automotive and defense to energy—where materials with tailored properties are required for improved performance and life [28].

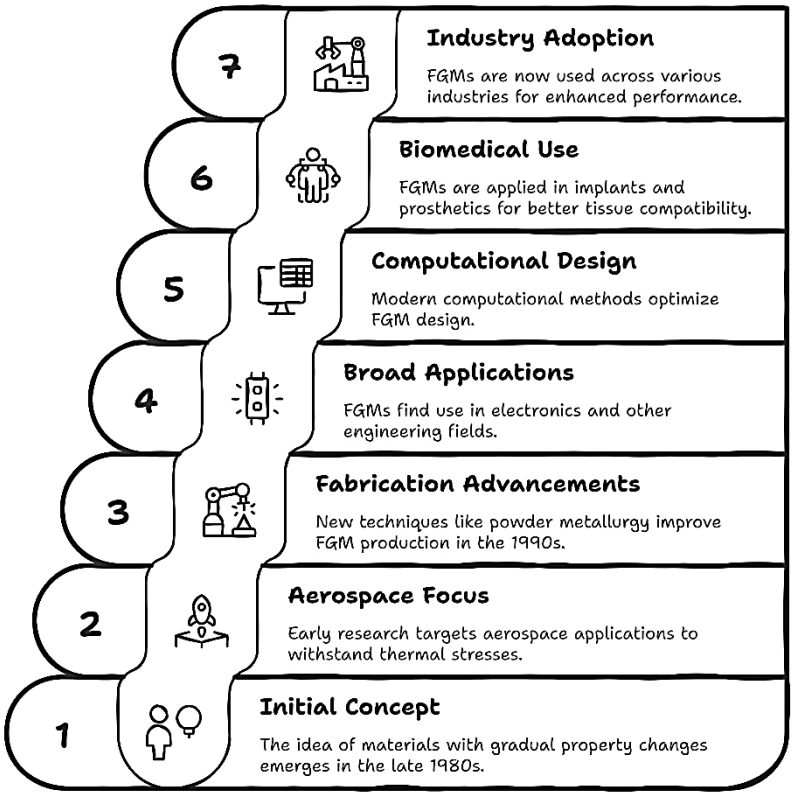

Figure II-1: Evolution of functionally graded materials

II.3. Definition and history of porosity

II.3.1. Definition

Porosity is a measure of the volume of voids (pores) existing in a material and is expressed as a fraction of the total volume. This is one of the primary physical properties in a wide scope of materials, which affects mechanical strength, permeability, and density. Porosity is of concern in geology, material science, and engineering, as this property has effects on the performance and applicability of a material for any specific purpose. For example, if a rock has a high porosity, then in petroleum engineering, it may indicate good quality of the reservoir. Also in construction materials, porosity can be adapted to affect insulation.

II.3.2. History

The research in and knowledge of porosity progressed a great deal with time (summarized in Figure II-2). This development was in line with technological changes and increasing demand by different industries.

1. Early Observations (Ancient Times – 19th Century)

Early human civilizations, such as the Romans and Greeks, used porous materials like pumice for building and water purification, realizing practical advantages where porosity existed without a scientific understanding of it.

In the 19th century, the Industrial Revolution resulted in interest in material properties—including porosity—by engineers who wanted to develop better construction materials and delve more deeply into natural resources' properties.

2. Theoretical Developments: Late 19th Century - Early 20th Century

It is in the work of Henry Darcy on fluid flow through porous media in the middle of the 19th century that roots for current hydrogeology and petroleum engineering can be traced. His now famous Darcy's Law, which describes flow of fluid through a porous medium, is still a keystone in these fields.

At the beginning of the 20th century, scientists were finally able to view and study the porosity of different materials more closely due to the development of microscopy and material science. Better control over porosity in synthetic materials grew out of that understanding.

3. Contemporary Period (Mid-20th Century to Date):

The emergence of new characterization techniques such as mercury intrusion porosimeter, gas adsorption, and nuclear magnetic resonance imaging gave more precise and detailed measurements of porosity.

In the second half of the 20th century, under pressure from needs to accurately estimate oil and gas reservoirs' quality, understanding about porosity was greatly pushed forward. It led to an integration between petrophysics, geology, and modern computational methods applied in modelling and prediction of porosity.

Today, the study of porosity has become critical to a diverse range of fields that stretch from environmental engineering to materials science in pursuit of the enhancement, through engineered porosity, in the performance of catalysts, filters, and biomaterials.

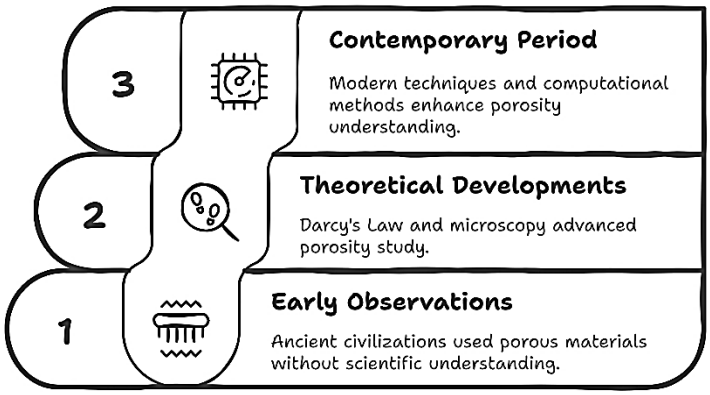

Figure II-2 Evolution of porosity understanding

II.4. Porous materials in literature

In the literature we can find the porosity as a defect or in the design feature; in FGM also in foam structural

Porosity in FGMs can be approached from two distinct perspectives in the literature: as a defect in the fabrication process and as a designed feature in foam materials.

Porosity as a designed feature in foam structural involves the intentional incorporation of voids or pores into a material's structure to achieve specific, enhanced properties. These porous materials are commonly engineered in the form of foams, lattices, or networks of interconnected pores, and their use spans various industries, such as aerospace, biomedical engineering, energy, and environmental technology.

Both perspectives offer important insights into how porosity impacts the material properties and performance, particularly in dynamic vibration analysis of rotor systems.

II.4.1. Porosity as a defect in FGM fabrication:

In traditional FGM fabrication processes, such as powder metallurgy, sintering, or additive manufacturing, porosity is often viewed as a defect. The presence of unintended voids or pores within the material structure can occur due to improper processing parameters, insufficient compaction, or incomplete sintering. These fabrication defects can lead to a range of negative effects on the material's mechanical and thermal properties (as it’s illustrating in the Figure II-3):

a. Impact on mechanical properties:

- Reduced strength and stiffness: Unintended porosity introduces weaknesses in the material's microstructure, reducing its overall strength and stiffness. These defects can act as stress concentrators, leading to crack initiation and propagation, ultimately reducing the material's load-bearing capacity.
- Increased fatigue sensitivity: Porosity defects can increase the material's sensitivity to fatigue, especially in cyclic loading conditions. In rotor systems, which are subject to continuous rotational forces, this can lead to premature failure due to the growth of micro-cracks around the pores.
- Damping and vibrational characteristics: In dynamic vibration behavior analysis, the presence of unintended porosity can affect the natural frequencies of the material and alter its damping properties. This can result in undesirable resonances or changes in the vibration response of the rotor system.

b. Challenges in quality control:

- Ensuring uniform material properties across the gradient in FGMs is difficult when porosity is considered a defect. Quality control measures, such as non-destructive testing (e.g.,

ultrasonic inspection, X-ray tomography), are often employed to detect and quantify porosity levels.

- Remediation techniques: Various post-processing techniques, such as hot isostatic pressing (HIP) or re-sintering, can be used to reduce porosity and improve material homogeneity. However, these techniques add complexity and cost to the manufacturing process.

c. Thermal Conductivity and Heat Resistance:

- Unintended porosity can negatively impact the thermal conductivity of FGMs, especially in applications where thermal gradients are critical. The voids disrupt the heat flow within the material, reducing its ability to withstand high temperatures, which is essential in aerospace and energy applications.

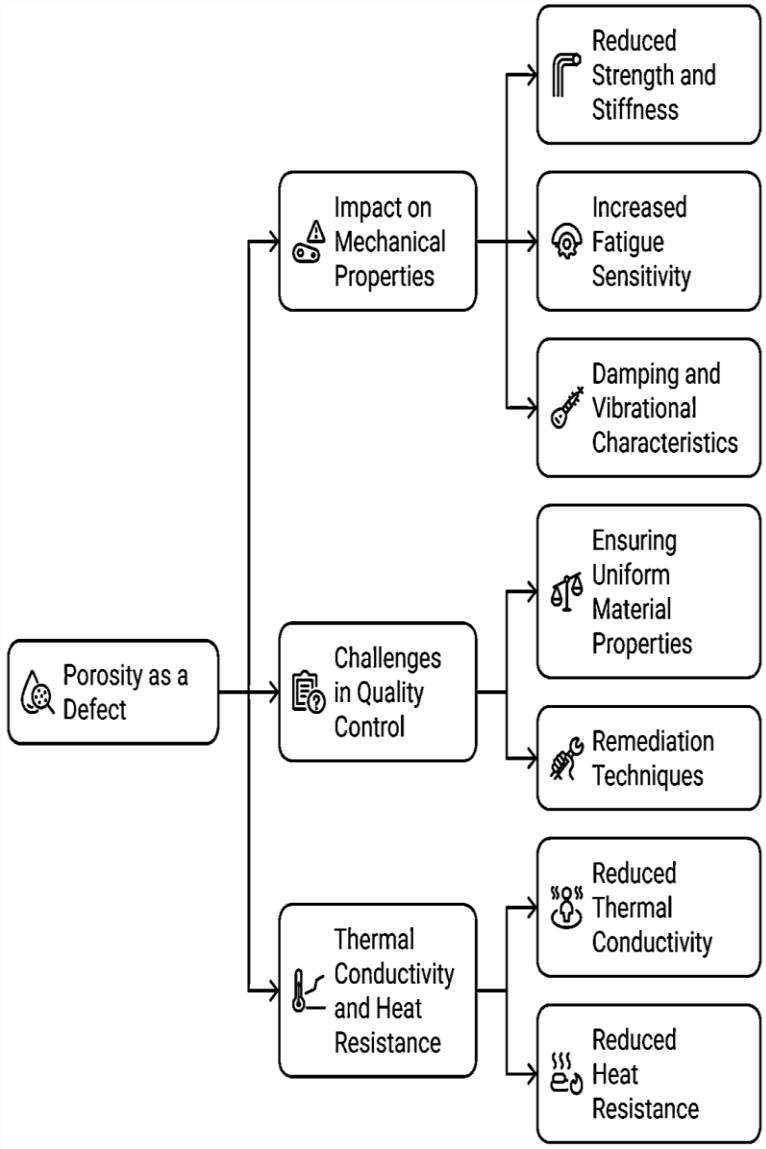

Figure II-3 Impact of porosity in FGM fabrication

II.4.2. Porosity as a design feature in FGMs

Conversely, porosity can be intentionally introduced as a designed feature in FGM. In this approach, porosity is strategically incorporated to achieve desired functional properties. Foam FGMs are developed to take advantage of the beneficial characteristics of porosity, such as lightweight structure, enhanced thermal insulation, and improved damping capabilities.

1. Tailored Mechanical Properties:
    - Weight reduction: One of the primary advantages of foam FGMs is the significant reduction in weight. This is especially important in applications like aerospace, automotive, and biomedical devices, where lightweight materials are essential for performance and fuel efficiency.
    - Enhanced damping and vibration control: Porosity in foam FGMs can enhance the damping properties of the material, reducing vibration amplitudes in dynamic systems. This makes foam FGMs ideal for rotor systems, where controlling vibration is critical to avoiding resonance and ensuring stability during operation.
    - Energy absorption: The porous structure of foam FGMs allows them to absorb energy more effectively than dense materials. This makes them suitable for applications requiring impact resistance or where energy dissipation is crucial.
2. Thermal Insulation and Heat Resistance:
    - Thermal management: Foam FGMs with tailored porosity are often used in applications that require effective thermal insulation. The air pockets within the foam structure act as barriers to heat transfer, making these materials ideal for high-temperature environments, such as turbine blades or thermal barrier coatings.
    - High-temperature stability: In addition to insulation, foam FGMs can be engineered to maintain their structural integrity at high temperatures. This is particularly beneficial in aerospace applications, where materials must withstand extreme thermal gradients.
3. Fabrication Techniques for Foam FGMs:
    - Additive manufacturing**:** Modern techniques like additive manufacturing allow for precise control over the porosity distribution in foam FGMs. This level of control enables the creation of materials with specific gradients in porosity, optimizing their mechanical and thermal properties for particular applications.

- Powder metallurgy and space holders**:** In some cases, space holder materials are used during the fabrication process to create a foam-like structure. These materials are later removed, leaving behind a controlled porous network.

  a. Applications in Rotor Systems:

- Lightweight rotors: In rotor systems, where mass reduction is essential for efficiency, foam FGMs offer a way to reduce the rotor's weight without sacrificing strength or performance. These materials can be used also in turbine blades, fans, and other rotating components.
- Vibration control: The enhanced damping characteristics of foam FGMs can improve the vibrational performance of rotor systems, reduce the likelihood of resonance and extend the operational life of the system.

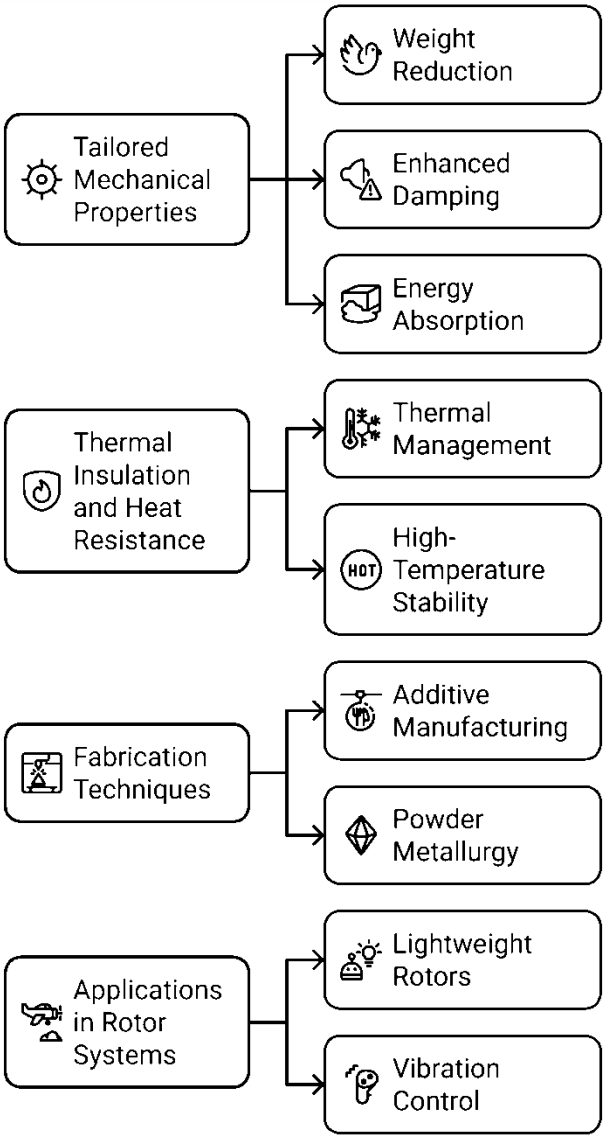

Figure II-4 Specification of Porous FGMs

II.4.3. Comparison of porosity as a defect vs. Foam design

The key distinction between porosity as a defect and as a design feature lies in intentionality and control. When porosity is a defect, it introduces unpredictability and weakens the material's performance. Quality control becomes essential to minimize its negative impact. However, when porosity is engineered as part of the material design, as in foam FGMs, it is carefully controlled and can enhance the material's performance in specific applications.

a. Impact on mechanical and dynamic properties:

- In defective porosity, the material's mechanical properties (e.g., strength, stiffness) are compromised, potentially reducing its effectiveness in load-bearing applications.
- In foam FGMs, the material's properties are optimized for specific purposes, such as reducing weight and enhancing damping, making them more suited to applications like lightweight rotor systems or energy-absorbing components.

b. Thermal and vibration behavior:

- Defective porosity can disrupt thermal conductivity and vibration behavior, leading to poor heat resistance and unpredictable dynamic responses in rotor systems.
- Engineered foam FGMs, on the other hand, can improve thermal insulation and damping while maintaining sufficient structural integrity, enhancing the material's performance in dynamic environments.

II.4.4. Types of porous materials

Porous materials are classified based on their pore size and structure, which determines their mechanical and functional behavior. The two primary types are open-cell and closed-cell porous materials [33].

- **Open-cell materials:** These have interconnected pores, allowing fluid, gas, or energy to pass through. They are commonly used in filtration, energy absorption, and biomedical scaffolding.
- **Closed-cell materials:** These have isolated pores, often filled with gas, providing excellent insulation properties and lightweight construction.

II.4.4.1. Advantages of porous materials as a designed feature

The intentional design of porosity in materials provides several key advantages over solid materials:

a. Enhanced damping and energy absorption:

Porous materials can absorb and dissipate energy effectively, providing enhanced damping properties. This makes them useful in dynamic environments where vibration reduction is crucial, such as in mechanical systems, civil engineering structures, and shock absorbers. The porous structure of materials, particularly those with open-cell networks, can absorb significant amounts of mechanical energy. This feature is especially beneficial in applications like crash protection in vehicles, protective gear, and packaging materials for delicate electronics [33].

b. Weight reduction and structural efficiency:

The primary benefit of porous materials is their significantly reduced density compared to their solid counterparts. The pores introduce empty spaces, dramatically lowering the material's weight while still maintaining a degree of structural integrity. Even with reduced weight, porous materials can be designed to have a high strength-to-weight ratio, making them ideal for load-bearing applications where mass is a critical factor, such as in aerospace and automotive components [34].

c. Thermal insulation and acoustic absorption:

Closed-cell porous materials, such as foams, are excellent insulators due to the air or gas trapped within the cells. This property is highly valuable in applications requiring heat resistance, such as thermal insulation panels in buildings, aerospace, and refrigeration systems. Porous materials can also act as sound absorbers, with open-cell materials being particularly effective in dampening sound waves. This property makes them suitable for use in noise control, such as in soundproofing walls, floors, and industrial noise-reduction applications [35].

d. Permeability and filtration capabilities:

Open-cell porous materials are permeable, allowing fluids or gases to pass through the material. This makes them ideal for applications such as filters (water and air), membranes for

separation technologies, and fuel cells in energy systems. Porous materials with high surface areas can act as catalysts or supports for chemical reactions. They are widely used in environmental applications, such as catalytic converters for pollution control, or in industrial processes, such as fuel processing and oil refining [35].

II.4.4.2. Applications of designed porous materials

Porous materials, designed without functionally graded properties, are tailored for specific applications where their unique mechanical, thermal, or chemical properties are beneficial. Below are some key areas where porous materials play a crucial role:

a. Biomedical Engineering:

Porous materials, particularly biocompatible metals (e.g., titanium) and polymers, are used in the development of bone scaffolds. These materials mimic the porous structure of natural bone, allowing cell infiltration and vascularization, which are essential for bone growth and tissue regeneration in implants and prosthetics. Porous materials are designed to act as carriers for controlled drug release. The pores in these materials can hold drugs and release them slowly over time, improving the efficiency of treatments for various diseases. Porous materials with interconnected networks provide platforms for tissue growth. These scaffolds can be tailored to have the correct mechanical properties and pore size to support the growth of specific tissues.

b. Aerospace and Automotive:

In aerospace and automotive industries, where weight reduction is critical for performance and fuel efficiency, porous materials are used to develop lightweight structural components without compromising strength or stiffness. Aluminum and titanium foams are examples of materials designed for this purpose. Porous materials are highly effective at absorbing energy during impacts, making them suitable for crash zones in vehicles, protective gear like helmets, and even in packaging sensitive electronics.

c. Thermal Management Systems:

Closed-cell porous materials, such as polymer and ceramic foams, are widely used as thermal insulation barriers in industries that involve high temperatures, such as in spacecraft, industrial

ovens, and power generation turbines. These materials prevent heat transfer while maintaining structural stability. Porous metals, such as metal foams, are used in heat exchangers. Their high surface area allows for efficient heat transfer between fluids while maintaining low pressure drops.

d. Environmental and Energy Applications:

Porous materials are commonly used in air and water filtration systems. Their open-cell structure allows them to trap contaminants while allowing the passage of air or water, making them essential for air purification, desalination, and wastewater treatment. Porous materials with high surface areas are used in fuel cells and batteries as electrodes or catalysts. In these applications, the porosity enhances the efficiency of electrochemical reactions, allowing for better energy conversion and storage.

e. Construction and Civil Engineering:

Porous materials are employed in the construction industry for soundproofing applications. The open-cell structure of foams and other porous materials absorbs sound waves, reducing noise levels in buildings and industrial environments. Porous concrete is used in pavements and roads to allow water to permeate through the surface, reducing runoff and preventing flooding. This type of concrete also helps in reducing the urban heat island effect by allowing water evaporation.

II.4.4.3. Manufacturing techniques for porous materials:

Porous materials are manufactured using various techniques, each offering different levels of control over pore size, distribution, and connectivity. Key techniques include:

a. Space holder methods: In the space holder method, sacrificial particles are mixed with the material during its formation. Once the material solidifies, the space holder particles are removed (e.g., by heat or dissolution), leaving behind a porous structure. This technique is used in creating metal foams and ceramics with tailored porosity [35].
b. Foaming processes: Foaming is a common technique for creating porous materials, where gas bubbles are introduced into a molten or liquid material, which is then solidified. The resulting material has a foam-like structure, with either open or closed pores depending on the foaming process used. Examples include polyurethane foams for insulation or aluminum foams for lightweight structures [35].

c. Sintering and powder metallurgy: In powder metallurgy, metal or ceramic powders are pressed into a desired shape and then heated to sinter the articles together, leaving controlled pores within the structure. This method is used to create porous metals and ceramics with high strength and controlled porosity [35].

In summary, porosity plays a dual role in FGMs, either as an unintended defect that needs to be minimized or as a deliberate feature that enhances material performance. The impact of porosity on the dynamic vibration behavior of rotor systems depends on whether it is controlled and designed or an accidental outcome of the fabrication process. For your thesis, examining both perspectives will provide a more comprehensive understanding of how porosity influences FGM rotor systems and inform the development of materials with optimized performance.

Porosity, when used as a designed feature in materials, opens up a wide range of possibilities for creating lightweight, efficient, and functional materials in various industries. Unlike defects that occur during manufacturing, intentional porosity enhances the material's properties, offering tailored solutions for applications that require specific mechanical, thermal, or chemical behavior. By designing materials with engineered porosity, engineers and researchers can develop advanced materials for next-generation technologies, from energy-efficient systems to medical devices and beyond.

II.5. Dynamic vibration behavior of rotor systems

II.5.1. Fundamental concepts in rotor dynamics

Rotor dynamics is a crucial sub-discipline of mechanical engineering that focuses on the behavior of rotating shafts and systems under dynamic conditions. Rotating machinery, such as turbines, compressors, jet engines, and electrical generators, inherently experiences vibrations due to imbalance, gyroscopic effects, shaft flexibility, misalignment, and bearing dynamics. Understanding the dynamic behavior of rotor systems is vital for predicting critical speeds, avoiding resonance, minimizing noise, and ensuring long-term reliability and performance.

Classical rotor dynamic models, such as the Jeffcott rotor, laid the groundwork for analyzing lateral vibrations. Over the decades, researchers have expanded upon these basic models to include effects such as damping, non-linear stiffness, and unbalance response. The emergence of advanced

materials has further prompted investigation into how the material constitution of the shaft influences vibration characteristics, particularly when moving beyond homogeneous materials [36].

Rotor systems are typically modeled using beam theory (e.g., Euler–Bernoulli or Timoshenko beams), and modal analysis is used to investigate the natural frequencies and mode shapes. In modern systems, finite element methods (FEM) are also employed for more complex geometries and material behavior. The integration of smart materials, composites, and FGMs into rotors has brought new challenges and opportunities to rotor dynamic analysis [37].

II.5.2. Impact of material properties – FGMs –

The FGMs are engineered materials characterized by a gradual variation in composition and structure, leading to a corresponding gradient in mechanical properties (e.g., stiffness, density, thermal conductivity). In rotor systems, using FGMs can significantly influence the vibration characteristics due to their spatially varying stiffness and mass properties [38].

The gradient in material properties allows FGMs to better manage thermal stresses, reduce stress concentrations, and improve dynamic performance. For rotors, this means the possibility of tailoring the material distribution to shift natural frequencies away from operating speeds, thereby enhancing stability and reducing the risk of resonance. Researchers have shown that FGMs can effectively increase the first critical speed of a shaft and improve the vibration attenuation performance under harmonic and transient loads [39].

Furthermore, FGMs can help reduce the weight of rotating components while maintaining structural integrity, an important factor in high-speed rotating machinery.

II.5.3. Role of porosity in FGMs for rotor applications

Porosity in FGMs can occur either unintentionally during the manufacturing process (e.g., powder metallurgy, sintering) or intentionally, to create functionally graded porous materials (FGPMs)**.** In dynamic applications such as rotor systems, the presence of porosity adds a layer of complexity to the vibration analysis.

Porosity affects both mass density and elastic modulus, often reducing stiffness and increasing damping. These changes can significantly influence the natural frequencies, mode shapes, and dynamic stability of rotor systems. Depending on the porosity distribution (e.g., symmetric, asymmetric, exponential), the rotor can exhibit different dynamic responses. Some studies have shown that tailored porosity can help in damping out vibrations, while in other cases, it leads to premature failure due to reduced strength [40].

FGPMs are also investigated for their bio-inspired design, mimicking structures like bones or natural foams that are optimized for vibration absorption and weight minimization.

II.5.4. Role of porosity for rotor applications

Porosity has emerged as a critical design variable in modern rotor systems, offering both opportunities and challenges in the context of dynamic performance. The incorporation of porosity—whether intentional or resulting from manufacturing processes—can significantly alter the mass distribution, stiffness, and damping characteristics of rotating components. This study reviews the role of porosity in influencing the dynamic behavior of rotor systems, emphasizing its effects on natural frequencies, critical speeds.

II.6. Recent advances and trends

The field of rotor dynamics involving FGMs and porous structures is evolving rapidly, driven by the growing demand for lightweight, high-performance, and tailored materials in rotating machinery. This section reviews the most recent advances in materials, fabrication methods, modeling approaches, and analysis tools, followed by an overview of current research gaps and unresolved challenges.

II.6.1. Latest research and emerging trends

Recent studies show a clear shift toward integrated, multi-functional rotor systems that not only reduce weight but also enhance damping, thermal resistance, and reliability under harsh operating conditions.

a. Advanced material systems

- Researchers have started exploring hybrid FGMs, combining metal-ceramic systems with carbon nanotubes (CNTs), graphene reinforcements, or shape memory alloys, to enhance stiffness and vibration resistance.
- Smart materials such as piezoelectric FGMs are being embedded into rotors for active vibration control and real-time structural health monitoring.

b. Additive Manufacturing (AM) of FGMs and Porous Structures

- Additive manufacturing has enabled the fabrication of complex porosity distributions and graded compositions with high precision. Techniques such as Selective Laser Melting (SLM) and Electron Beam Melting (EBM) allow layer-by-layer control over porosity and material gradient.
- These methods support the development of bio-inspired, lattice-based, or topology-optimized rotor structures that balance weight and dynamic performance.

c. Innovative modeling and analysis approaches

- The integration of multi-scale modeling and machine learning-based surrogate models has gained traction for fast prediction of vibration characteristics in graded and porous systems.
- Nonlocal elasticity and strain gradient theories are increasingly used to study micro/nano-scale rotors where classical models fail to capture size-dependent behavior.

II.6.2. Gaps and challenges in the literature

Despite these advancements, several critical issues remain open in the current body of research:

a. Limited experimental validation

- While many studies are heavily focused on theoretical and numerical analysis, experimental validation of vibration behavior in porous FGM rotors is still scarce.
- There's a lack of standardized testing methods and reliable fabrication techniques to create repeatable porous FGM structures.

b. Simplified modeling assumptions

- Most analytical and numerical models assume ideal porosity distributions, perfect bonding, and linear elastic behavior, which may not hold in real-world applications.
- Modeling rotor–bearing interactions, gyroscopic effects, and nonlinear vibration in porous FGMs remains a complex challenge.

c. Lack of application-specific design guidelines

- Current research tends to focus on general modeling rather than providing application-oriented solutions for aerospace, energy, or biomedical rotor systems.
- More work is needed on design optimization, lifecycle analysis, and fatigue modelling under dynamic loading

d. Thermo-mechanical and multi-physics coupling

- Few studies address thermal effects, fluid–structure interaction, or electro-mechanical coupling in porous FGM rotors, which are essential in many advanced applications.

II.6.3. Applications and case studies of porous rotor systems

Porous materials have found increasing relevance in rotor system design due to their potential to reduce weight**,** enhance damping, and customize dynamic performance. Unlike traditional homogeneous materials, porous structures offer a controllable internal architecture that can be engineered to meet specific functional requirements in high-speed rotating machinery. This section highlights key industrial applications of porous rotor systems, accompanied by performance analysis and case studies that demonstrate their effectiveness.

II.6.4. Practical applications of porous rotor systems

Porous materials are being incorporated in various rotor-based systems across industries such as aerospace, automotive, energy generation, and biomedical engineering.

a. Aerospace sector

- In aircraft turbine rotors and jet engines, porous metals and ceramics are used to reduce mass while maintaining adequate stiffness and mechanical integrity. This contributes to improved fuel efficiency and dynamic stability at high speeds.
- Porous rotors are also explored for noise reduction and vibration isolation in aerospace auxiliary systems.

b. Energy and power systems

- High-speed rotors in gas turbines and micro-generators benefit from porous designs that offer thermal dissipation and vibration damping.
- Advanced porous designs are used in cooling rotors for electrical generators, enhancing heat transfer while minimizing mechanical stress.

c. Automotive engineering

- In high-performance engine components (e.g., turbochargers, crankshafts), engineered porosity enables mass optimization and energy absorption, which leads to smoother operation and extended part life.
- Some brake systems also use porous rotors to manage thermal shock and reduce vibration-induced noise.

d. Biomedical devices

- Micro-scale porous rotors are implemented in blood pumps, dental tools, and surgical drills. The porous architecture helps minimize vibration transmission to surrounding tissue while maintaining rotational performance.
- In some devices, porous rotors also facilitate fluid flow control, enhancing operational precision.

II.6.5. Performance analysis and engineering benefits

Several studies and experimental validations have demonstrated the benefits of incorporating porosity into rotor systems:

a. Weight reduction and inertia control

- Porous materials can be designed with targeted density distributions, allowing precise control over the mass moment of inertia, which directly affects rotor acceleration and deceleration behavior.
- This is critical in aerospace and automotive applications, where agility and response time are paramount.

b. Improved damping characteristics

- Introducing porosity enhances internal friction, resulting in increased material damping capacity. This helps in suppressing excessive vibration amplitudes during transient or resonant conditions.
- Porous rotors can attenuate vibrations without requiring external damping systems, contributing to a lighter and more integrated design.

c. Thermal management

- Open-cell and graded porosity structures enhance heat dissipation in high-temperature rotor environments. This contributes to better thermal stability, especially in continuous-operation systems such as turbines and motors.

d. Tailored Dynamic Behavior

- By adjusting pore size, distribution, and volume fraction, engineers can tune the natural frequencies and mode shapes of the rotor to avoid resonance within operating ranges.

II.7. The Hi-tech in materials selected

This section reviews various types of functionally graded materials (FGMs) and functionally graded porous (FGP) structures suitable for engineering applications that center around Ni-based FGMs and porous metal/ceramic foams.

II.7.1. Functionally Graded Materials (FGMs)

II.7.1.1. Nickel–Stainless Steel (Ni–SS) FGMs

Ni–SS FGMs integrate corrosion resistance and ductility of nickel with tensile strength and cost-effectiveness of stainless steel; the graded structure minimizes thermal and residual stresses across interfaces, thus performing better under any complex loading.

a. Manufacturing Processes:

It is advanced by manufacturing technologies including additive manufacturing (AM) and powder metallurgy (PM). AM could, nevertheless, incur surface roughness and defects [41]. The advantage of PM lies in the microstructural refining of the part; however, for intricate geometries, the process is commercially unviable.

b. Application:

- Aerospace: turbine blades, engine components, thermal insulation systems
- Automotive: cylinder liners, combustion chambers, and brake discs
- Defense: lightweight impact- and crack-resistant armor [42]

c. Justification:

Ni–SS FGMs, due to their graded characteristic, develop optimum distribution of mechanical, thermal, and chemical properties, making them far superior to homogeneous materials for sustaining structural integrity in extreme environments.

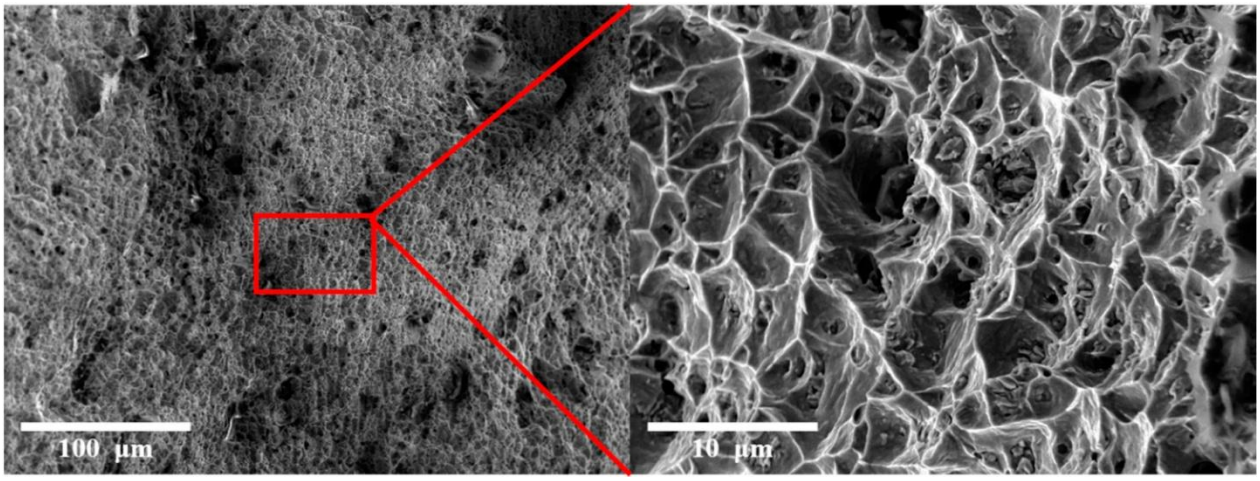

Figure II-5 Microscopic appearance of IN625-SUS304L (Ni-SS) PFGM [41]

II.7.1.2. Nickel-Zirconia (Ni-ZrO_2) FGMs

Ni-ZrO_2 FGMs combine the hardness and thermal stability of zirconia with the ductility and corrosion resistance of nickel, making them suited for situations involved in electrochemical and high-temperature applications.

a. Production Techniques:

Powder metallurgy (PM): Provides microstructural control, the porosity introduced due to solidification mismatches [43].

Electrodeposition techniques (e.g., double pulse): Allow for production of dense, defect-free coatings with enhanced corrosion and wear resistance [44].

b. Applications:

- Aeronautical and automotive sectors where thermal resistance is required
- Electrochemical components and coatings
- Wear-resistant structures

c. Justification:

Ni-ZrO_2 FGMs exhibit superior oxidation resistance, lesser friction, and more charge-transfer resistance than pure Ni coatings [44], [45].

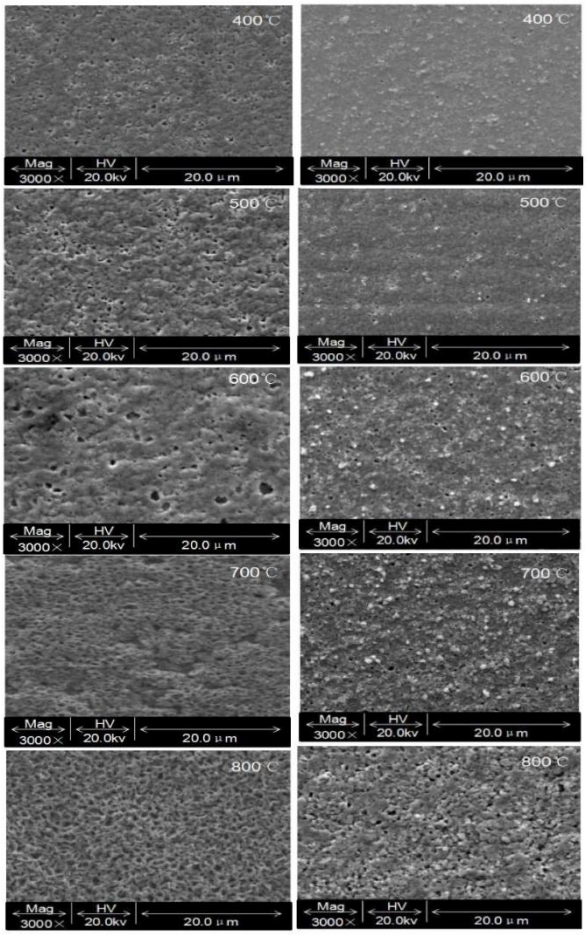

Figure II-6 formation of porosity in Ni coating and Ni/ZrO_2 gradient coating depend of temperature Fabricated by Double Pulses Electrodeposition [44]

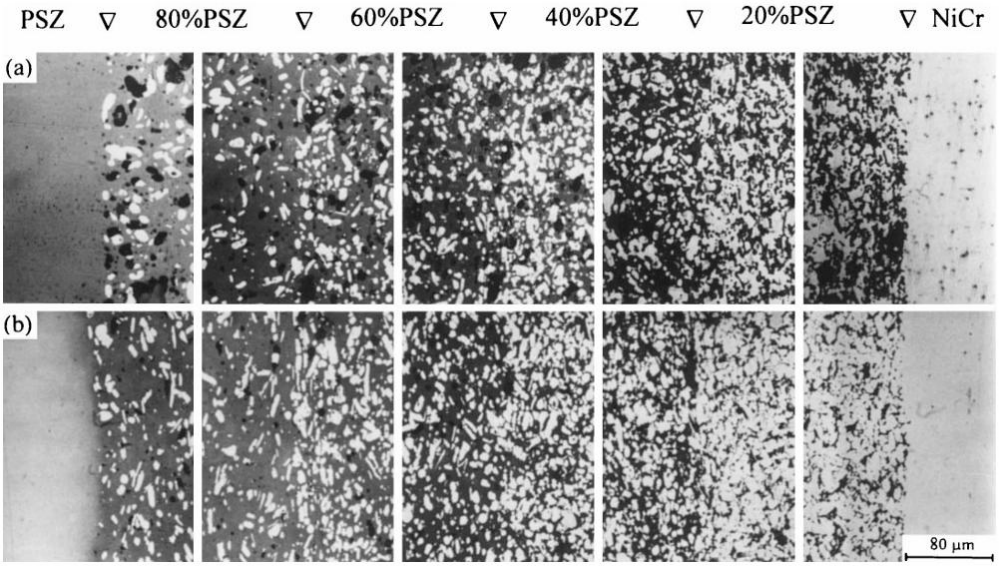

Figure II-7 Cross-sectional microstructure of ZrO2–NiCr FGM fabricated by (a) pressureless sintering at 1400C; (b) hot pressing at 1250C, 5MPa [43]

II.7.1.3. Nickel-Alumina ($Ni-Al_2O_3$) FGMs

These FGMs combine the hardness, corrosion resistance, and thermal stability of Al_2O_3 with the ductility and toughness of nickel, which further enhance their performance under conditions of combined thermal and mechanical stresses.

a. Manufacturing Methods:

Electrophoretic Deposition (EPD): Fine gradient control obtainable through using NiO and Al_2O_3 suspensions [46]

Powder Metallurgy: Good for obtaining fine grain sizes and eliminating segregation of the reinforcing phase.

b. Applications:

- Aerospace: Heat-resistant parts and shields
- Energy: Pipes for toxic fluid transport run, catalytic surfaces [47]
- Chemical processing: Corrosion-resistant liners [48]

c. Justification:

$Ni-Al_2O_3$ FGMs have high bonding strength, outstanding thermal shock resistance, and a low amount of residual stress—all of which are critical for aerospace and power generation systems [48].

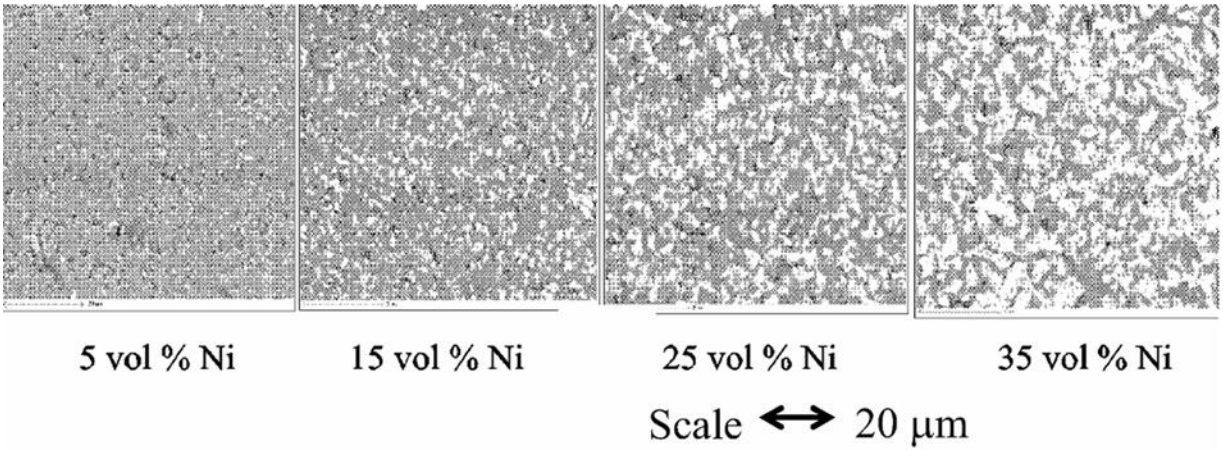

Figure II-8 Micrograph of a representative Ni-Al2O3 FGM showing made by Electrophoretic Deposition

II.7.2. Functionally Graded Porous (FGP) Structures (Foams)

FGPMs constitute engineered porosity in FGMs to allow for combined properties of lightweight structure, energy absorption, and thermal management. This section summarizes FGP structures based on primary materials: Stainless Steel, Zirconia, and Alumina.

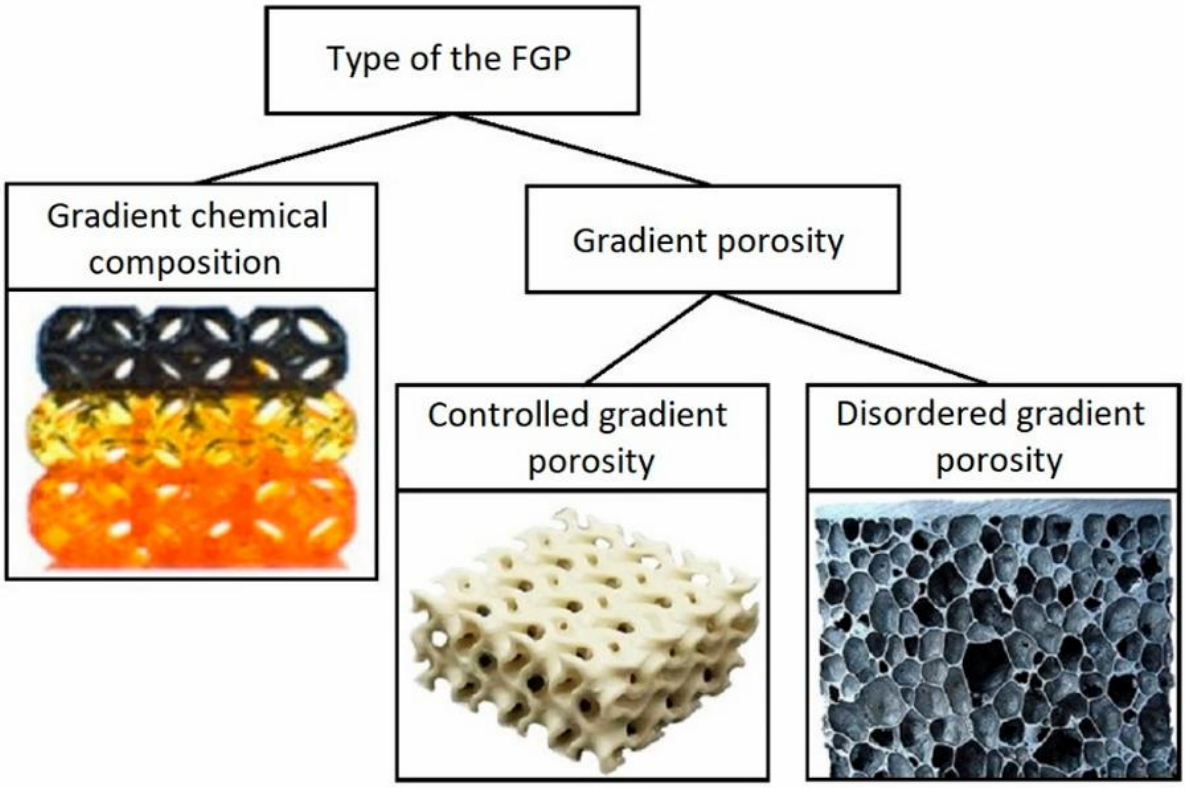

Figure II-9 FGP classification by gradient type [49]

II.7.2.1. Stainless Steel (SS) FGP Foams

SS FGP foams combine corrosion resistance, mechanical strength of stainless steel, enhanced porosity for energy absorption, and permeability for fluid transport.

a. Fabrication Methods:

- Space Holders-Powder Metallurgy: This method provides precise control of pore formation through the use of removable agents NaCl or K_2CO_3 [50].
- Liquid Metallurgy: For closed-cell foams, injecting gas into a molten metal.
- Additive Manufacturing: For example, Powder Bed Fusion to create tailored porous implants [51].

b. Applications:

- Automotive: Crash absorbers, vibration damping
- Heat Exchangers: Systems with high surface area for cooling
- Biomedical: Implants (porous 316L SS), bone scaffold
- Filtration: Fluid and gas filters
- Construction and Fuel Cells: Sound dampers, foam-core panels [50], [52]

c. Justification:

SS foams make excellent choices for structural and medical applications because of their high energy absorption, corrosion resistance, biocompatibility, and customizable pore geometry [52], [53].

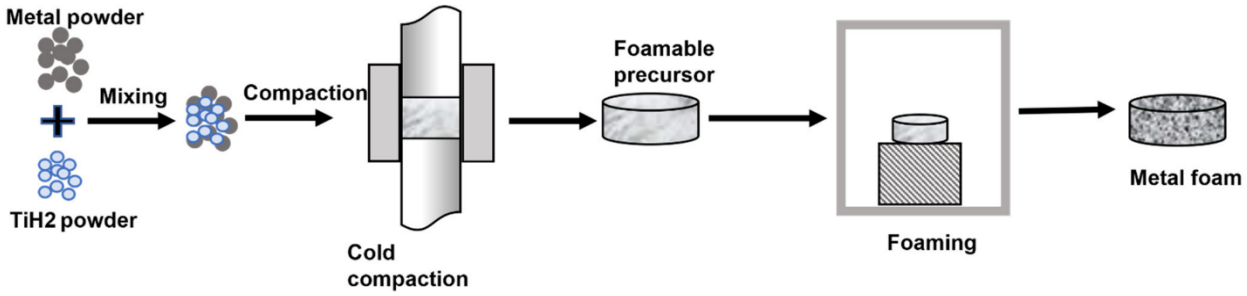

Figure II-10 Schematic diagram of powder metallurgy technique for metallic foams [49]

II.7.2.2. Zirconia (ZrO_2) FGP Foam

ZrO_2 foams have high thermal and chemical stability, mechanical strength, and are well-suited for high-temperature and biomedical applications

a. Production Techniques:

- Direct Foaming: Produces strong, machinable green bodies [54].
- Additive Manufacturing: FDM, DLP, SLA, Binder Jetting for precision control [49].
- Sintering: Sintering temperatures from 900°C to 1600°C apply, chiefly for Y-TZP [54].

b. Applications:

- Molten Metal Filtration: For steels and superalloy [55]
- Thermal Insulation: Kilns, barrier coatings
- Catalyst Supports: Large surface area for gas-phase reactions
- Biomedical: Load-bearing implants, dental applications [54], [56]

c. Justification: Withstand temperature up to 1700°C, resistant to oxidation and most acids, and allow for controlled pore design optimizing strength and functionality [57], [58].

Figure II-11 Zirconia Ceramic Foam Filters [55]

II.7.2.3. Aluminia (Al_2O_3) FGP Foams

Alumina foams combine strength and chemical stability of Al_2O_3 with a porous structure for thermal insulation, filtration, and catalytic applications.

a. Manufacturing Methods:

- Polymeric Sponge Method: Produces open-cell foam with very high permeability [59].
- Direct Foaming: Produces strong and less easily shaped structures.
- Others: Includes Bayer process, sintering, sol-gel, hydrothermal synthesis [60].

b. Applications

- Thermal Protection: Furnaces, solar thermal systems [61], [62]
- Filtration: Molten metals, hot gases
- Catalysis: Toxic gas treatment, auto-emission control
- Structural: Lightweight aerospace components, energy absorbers [56], [63]

c. Justification:

They maintain high mechanical integrity at temperatures up to 1700°C and exhibit excellent chemical resistance, high surface area, and low thermal conductivity, ensuring energy efficiency and structural performance [64].

Figure II-12 Alumina Ceramic Foam Filters [57]

III. Modelization of porous rotors structure

III.1. Beam theories in rotor vibration analysis:

In the modeling and analysis of rotor dynamics, beam theories provide a foundational framework for describing the mechanical behavior of rotating shafts. These theories are indispensable for predicting natural frequencies, critical speeds, mode shapes, and dynamic responses under various operating conditions. The selection of a suitable beam theory directly influences the accuracy of vibration analysis, especially when accounting for shear deformation, rotary inertia, and material heterogeneity such as porosity.

III.2. General assumptions of beam theories

Before presenting individual theories, it is important to state the general assumptions shared across classical beam theories:

- The beam is initially straight and prismatic (constant cross-section).
- Material follows linear elastic behavior.
- Plane sections remain plane after deformation.
- Small deformations are assumed.
- Transverse displacements dominate (bending is the primary deformation mode).

III.3. Euler–Bernoulli beam theory

The Euler–Bernoulli beam theory (EBBT) is effective for modeling long and slender rotors where shear deformation and rotary inertia are negligible. However, it becomes inaccurate when applied to thick beams or high-speed rotating systems, as it fails to account for the shear and inertial effects that significantly influence the dynamic behavior in such cases.

III.3.1. Assumptions of EBBT

- Plane sections remain plane and perpendicular to the neutral axis (no shear deformation).
- Neglects rotary inertia.

- Suitable for slender beams and low-frequency applications.

III.3.2. Displacement field of EBBT

$$\vec{U}_{EBT}(x,y,z,t) = \begin{bmatrix} u_0(x,t) + z\frac{\partial w_0(x,t)}{\partial x} - y\frac{\partial v_0(x,t)}{\partial x} \\ v_0(x,t) + \phi(x,t)z \\ w_0(x,t) + \phi(x,t)y \end{bmatrix} \quad \text{III-1}$$

III.4. Timoshenko beam theory

The Timoshenko beam theory (TBT), first proposed by Stephen P. Timoshenko in the 1920s, represents a comprehensive model that significantly improves upon classical theories. It accounts for:

- Shear deformation, which is important in thick beams and composite/porous structures.
- Rotary inertia, which becomes increasingly relevant in high-speed rotating shafts.
- Flexural and transverse displacements, allowing for coupled bending and shear effects.

These features make the Timoshenko theory particularly relevant for analyzing porous rotor systems, where the presence of voids alters stiffness and mass distributions, leading to non-classical dynamic behaviors.

III.4.1. Assumptions of TBT

- Plane sections remain plane but not necessarily perpendicular to the neutral axis (shear deformation is allowed).
- Includes rotary inertia.
- Applicable to thick beams and materials with nonuniform properties (e.g., porous or FGMs).

III.4.2. Comparison of Beam Theories

Euler–Bernoulli Beam Theory (EBT) and Timoshenko Beam Theory (TBT), represent progressively refined models for analyzing the mechanical behavior of beams. EBT assumes that plane cross-sections remain perpendicular to the neutral axis, neglecting shear deformation, which limits its accuracy in thick or short beams. TBT introduces independent rotations to account for

shear deformation and rotary inertia, making it more suitable for moderately thick beams. The Table IV-1 represent a summarize differences between the EBT and TBT. Physically, this progression reflects an increasing ability to capture the true deformation characteristics of real beam structures, especially in complex applications like porous and functionally graded rotors.

Table III-1 Comparison of Beam Theories

Feature	EBT	TBT
Shear deformation	Neglected	Included (constant through thickness)
Rotary inertia	Neglected	Included
Cross-section behavior	Remains plane and perpendicular to neutral axis	Remains plane but not necessarily perpendicular
Accuracy	Suitable for slender beams	Suitable for moderately thick beams
Shear correction factor	Not required	Required
Physical realism	Limited (bending only)	Moderate (bending + shear)

III.4.3. Justification for using TBT in this study

In this thesis, the Timoshenko beam model is employed to investigate the dynamic behavior of porous rotors. This choice is justified based on the following:

1. Porosity-induced shear effects: The presence of pores reduces the effective shear modulus, amplifying shear deformation—a phenomenon accurately captured by Timoshenko theory.
2. Gyroscopic and rotary inertia effects: At higher rotational speeds, ignoring rotary inertia leads to errors in critical speed and stability predictions.
3. Material grading and heterogeneity: Timoshenko theory's flexibility allows incorporation of spatially varying material properties, crucial for modeling FG porous structures.

The model is further enhanced by integrating material property gradation and porosity functions derived from micromechanical formulations.

III.5. Application of TBT in rotor vibration analysis

The Timoshenko beam model is employed to analyze the shaft and validate the kinematic hypotheses at any point on the shaft along its length as presented in Figure IV-1. The Timoshenko Beam Theory (TBT) is used, assuming moderate thickness and accounting for shear deformation

and rotary inertia also linear elastic behavior of the material is assumed, without considering plastic deformation or damage mechanics. This model incorporates accounts for both shear deformation and rotary inertia, making it particularly suitable for the analysis of rotating shafts. Compared to simpler beam theories such as Euler-Bernoulli beam theory, TBT offers more accurate results when dealing with thick and flexible rotating shafts, high-speed rotations, and complex vibration modes, where shell theory may be less effective in capturing localized bending and gyroscopic effects. This theoretical framework is crucial for capturing the gyroscopic effects and the rotary inertia that significantly influence the dynamic behavior of rotating PFGM shafts. We believe this theory provides the necessary accuracy for our specific application and offers a more comprehensive model for studying these systems.

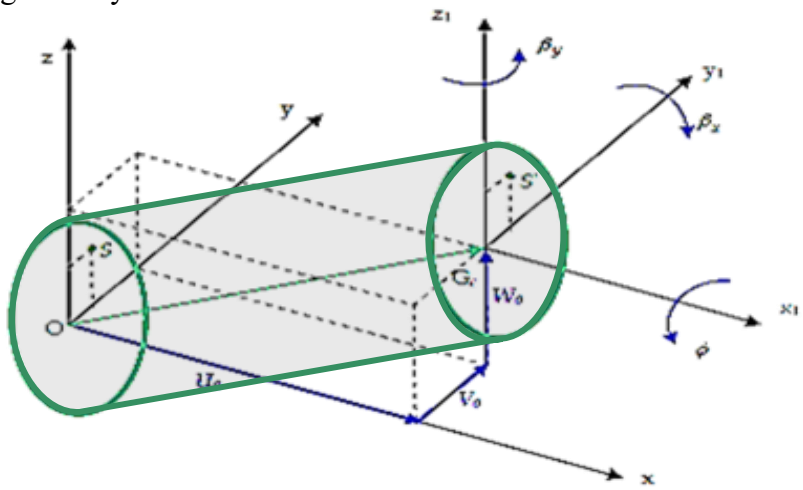

Figure III-1 Displacements of a cross-section of the shaft

III.5.1. Displacement field of TBT

Given these assumptions, the displacement field (U, V, W) can be expressed as follows:

$$\vec{U}_{TBT}(x,y,z,t) = \begin{bmatrix} u_0(x,t) + z\beta_x(x,t) - y\beta_y(x,t) \\ v_0(x,t) + \phi(x,t)z \\ w_0(x,t) + \phi(x,t)y \end{bmatrix} \quad \text{III-2}$$

$U_0(x,t)$: Longitudinal displacement.

$V_0(x,t)$: Transversal horizontal displacement.

$W_0(x,t)$: Transversal vertical displacement.

ϕ : Angular displacement.

β_x : Rotation angles about y.

β_y : Rotation angles about z.

t : Time.

III.5.2. Stress tensor

The stress (σ, τ) -strain (ε, γ) relations are as follows:

$$\begin{cases} \sigma_{xx} = Q_{11}\varepsilon_{xx} \\ \tau_{x\theta} = \tau_{\theta x} = k_s Q_{66}\gamma_{x\theta} \\ \tau_{xr} = \tau_{rx} = k_s Q_{55}\gamma_{xr} \end{cases} \quad \text{III-3}$$

Where: $Q_{11} = \frac{E}{1-\upsilon^2}$; $Q_{55} = Q_{66} = \frac{E}{2(1+\nu)}$

Here, k_s, E and ν; represent the shear correction factor, Young's modular and Poisson's ratio, respectively. And Q_{ii} the elasticity constant.

The cylindrical coordinate system (x, r, θ) is utilized to describe the strain components (see Figure V-3) expressed as follows:

$$\begin{cases} \varepsilon_{xx} = \frac{\partial U_0}{\partial x} + r\sin\theta\,\frac{\partial \beta_x}{\partial x} - r\cos\theta\,\frac{\partial \beta_y}{\partial x} \\ \varepsilon_{rr} = \varepsilon_{\theta\theta} = \varepsilon_{r\theta} = 0 \\ \varepsilon_{x\theta} = \varepsilon_{\theta x} = \frac{1}{2}\left(\beta_y \sin\theta + \beta_x \cos\theta - \sin\theta\,\frac{\partial V_0}{\partial x} + \cos\theta\,\frac{\partial W_0}{\partial x} + r\frac{\partial \phi}{\partial x}\right) \\ \varepsilon_{xr} = \varepsilon_{rx} = \frac{1}{2}\left(\beta_x \sin\theta - \beta_y \cos\theta - \sin\theta\,\frac{\partial W_0}{\partial x} + \cos\theta\,\frac{V_0}{\partial x}\right) \end{cases} \quad \text{III-4}$$

k_s : Shear correction factor.

E : Young modular.

ν : Poisson's ratio.

Q_{ii} : Elasticity constant.

x : Longitudinal axe.

r : Radius coordinate.

θ : Angle coordinate.

Various definitions of shear correction factors can be found in the literature. In this study, the formulation proposed by Cowper [65] is adopted, where k_s is the shear constant which we insert as a correction factor to account for the fact that τ_{xz} is not (in reality) uniform over the height of the section [66]. Mentioned also by Rajiv Tiwari [67], and Hutchinson [68].

$$k_s = \frac{6(1+\nu)(1+\bar{r})^2}{(7+6\nu)(1+\bar{r})^2+(20+12\nu)\bar{r}^2} \quad \text{III-5}$$

With: $\bar{r} = R_i/R_o$

III.6. Hierarchical beam element formulation

The using of hierarchical p-element technique (p-FEM) instead of an analytical solution to provides higher accuracy and better convergence for complex geometries and boundary conditions, where analytical solutions become intractable. The hierarchical p-element method also allows for efficient computational modeling of high-order dynamic effects.

The spinning flexible shaft is discretized using a p-FEM with two nodes 1 and 2 as shown in Figure IV-2. The nodal degrees of freedom for each node include $U_0, V_0, W_0, \beta_x, \beta_y,$ and ϕ .

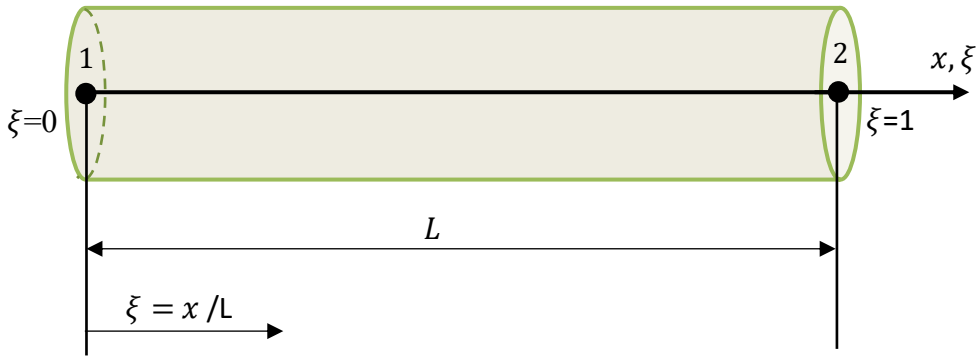

Figure III-2 Beam element with two nodes

The local and non-dimensional coordinates are related by:

$$\xi = x / L \quad (0 \le \xi \le 1) \tag{III-6}$$

$U_0, V_0, W_0, \beta_x, \beta_y,$ and ϕ can be rewritten as follows:

$$\begin{cases} U_0 = [N_U]\{q_U\} = \sum_{m=1}^{p_U} x_m(t).f_m(\xi) \\ V_0 = [N_V]\{q_V\} = \sum_{m=1}^{p_V} y_m(t).f_m(\xi) \\ W_0 = [N_W]\{q_W\} = \sum_{m=1}^{p_W} z_m(t).f_m(\xi) \\ \beta_x = [N_{\beta_x}]\{q_{\beta_x}\} = \sum_{m=1}^{p_{\beta_x}} \beta_{x_m}(t).f_m(\xi) \\ \beta_y = [N_{\beta_y}]\{q_{\beta_y}\} = \sum_{m=1}^{p_{\beta_y}} \beta_{y_m}(t).f_m(\xi) \\ \phi = [N_\phi]\{q_\phi\} = \sum_{m=1}^{p_\phi} \phi_m(t).f_m(\xi) \end{cases} \tag{III-7}$$

With $[N]$ representing the shape function matrix, it can be defined as follows:

$$\left[N_{U,V,W,\beta_x,\beta_y,\phi}\right] = \left[f_1 f_2 \dots \dots f_{p_U,p_V,p_W,p_{\beta_x},p_{\beta_y},p_\phi}\right] \quad \text{III-8}$$

In this work $q_U = q_V = q_W = q_{\beta_x} = q_{\beta_y} = q_\phi = p$ represents the number of shape functions for displacements. The set of shape f_i functions employed in this study is provided in reference [69] as follows:

$$\begin{cases} f_1 = 1 - \xi \\ f_2 = \xi \\ f_{r+2} = \sin(\delta_r\, \xi), \quad \delta_r = r\pi \ ; \ r = 1\,,2\,,3\,, \dots \end{cases} \quad \text{III-9}$$

III.7. Modelization of shaft

III.7.1. Strain energy

The formulation of strain energy (E_{Ss}) of the shaft are as follows:

$$E_{sS} = \frac{1}{2}\int_V (\sigma_{xx}\varepsilon_{xx} + 2\tau_{x\theta}\gamma_{x\theta} + 2\tau_{xr}\gamma_{xr})\, dV \quad \text{III-10}$$

After developing equations (IV-3) and (IV-4), the final forms of the strain energy:

$$E_{sS} = \frac{1}{2}A_{11}\int_0^L \left(\frac{\partial U_0}{\partial x}\right)^2 dx + \frac{1}{2}B_{11}\begin{bmatrix}\int_0^L \left(\frac{\partial \beta_x}{\partial x}\right)^2 dx + \\ \int_0^L \left(\frac{\partial \beta_x}{\partial x}\right)^2 dx\end{bmatrix} + \frac{1}{2}B_{66}\int_0^L \left(\frac{\partial \phi}{\partial x}\right)^2 dx + \frac{1}{2}(A_{55} + A_{66})\begin{bmatrix}\int_0^L \left(\frac{\partial V_0}{\partial x}\right)^2 dx + \int_0^L \left(\frac{\partial W_0}{\partial x}\right)^2 dx + \\ \int_0^L \beta_x^2\, dx + \int_0^L \beta_y^2\, dx + \\ 2\int_0^L \beta_x \frac{\partial W_0}{\partial x} dx - \int_0^L \beta_y \frac{\partial V_0}{\partial x} dx\end{bmatrix} \quad \text{III-11}$$

Where:

$$\begin{cases} A_{11} = 2\pi \int_{R_i}^{R_o} Q_{11}(r)\, r\, dr \\ A_{55} = A_{66} = \pi \int_{R_i}^{R_o} \mathrm{k_s} Q_{55}(r)\, r\, dr \\ B_{66} = 2\pi \int_{R_i}^{R_o} \mathrm{k_s} Q_{66}(r)\, r^3\, dr \\ B_{11} = \pi \int_{R_i}^{R_o} Q_{11}(r)\, r^3\, dr \end{cases} \quad \text{III-12}$$

III.7.2. Kinetic energy

The formulation of kinetic energy (E_{kS}) of the shaft are as follows:

$$E_{kS} = \frac{1}{2}\int_V \rho \left(\vec{\dot{R}}_{P/O}.\vec{\dot{R}}_{P/O}\right) dV \quad \text{III-13}$$

$\vec{R}_{P/O}$, ρ are the displacement vector and the density, respectively.

The final kinetic energy of a shaft is obtained as follows:

$$E_{kS} = \frac{1}{2}\int_0^L \left[I_m^s\left(\dot{U}_0^2 + \dot{V}_0^2 + \dot{W}_0^2\right) + I_d^s\left(\dot{\beta}_x^2 + \dot{\beta}_y^2\right) - 2\Omega I_p^s \beta_x \dot{\beta}_y + 2\Omega I_p^s \dot{\phi} + I_p^s \dot{\phi}^2 + \Omega^2 I_p^s + \Omega^2 I_d^s\left(\beta_x^2 + \beta_y^2\right)\right] dx \quad \text{III-14}$$

The moments of inertia of the shaft are:

$$\begin{cases} I_m^s = 2\pi \int_{R_i}^{R_o} \rho(r)\, r\, dr \\ I_d^s = \pi \int_{R_i}^{R_o} \rho(r)\, r^3\, dr \\ I_p^s = 2\pi \int_{R_i}^{R_o} \rho(r)\, r^3\, dr \end{cases} \quad \text{III-15}$$

L, R_o, R_i represent length, outer radius and inner radius of the shaft respectively.

III.7.3. Matrices of shaft

After applying the Euler-Lagrange derivation, we obtained the following matrices for the free vibration of the rotational shaft:

$$[M^S] = \begin{bmatrix} [M_U] & 0 & 0 & 0 & 0 & 0 \\ 0 & [M_V] & 0 & 0 & 0 & 0 \\ 0 & 0 & [M_W] & 0 & 0 & 0 \\ 0 & 0 & 0 & [M_{\beta_x}] & 0 & 0 \\ 0 & 0 & 0 & 0 & [M_{\beta_y}] & 0 \\ 0 & 0 & 0 & 0 & 0 & [M_\phi] \end{bmatrix} \quad \text{III-16}$$

$$[K^S] = \begin{bmatrix} [K_U] & 0 & 0 & 0 & 0 & 0 \\ 0 & [K_V] & 0 & 0 & [K_1] & 0 \\ 0 & 0 & [K_W] & [K_2] & 0 & 0 \\ 0 & 0 & [K_2]^T & [K_{\beta_x}] & 0 & 0 \\ 0 & [K_1]^T & 0 & 0 & [K_{\beta_y}] & 0 \\ 0 & 0 & 0 & 0 & 0 & [K_\phi] \end{bmatrix} \quad \text{III-17}$$

$$[G^S] = \begin{bmatrix} 0 & 0 & 0 & 0 & 0 & 0 \\ 0 & 0 & 0 & 0 & 0 & 0 \\ 0 & 0 & 0 & 0 & 0 & 0 \\ 0 & 0 & 0 & 0 & [G_1] & 0 \\ 0 & 0 & 0 & -[G_1]^T & 0 & 0 \\ 0 & 0 & 0 & 0 & 0 & 0 \end{bmatrix} \quad \text{III-18}$$

III.8. Modelization of disc

III.8.1. Kinetic energy

The disk attached to the shaft (Figure IV-3) is assumed to be rigid and made of isotropic materials. According to equation (IV-13) and in a similar way, the kinetic energy of the disk is written as follows:

$$E_{kD} = \frac{1}{2}\int_0^L \left[I_m^D\left(\dot{U}_0^2 + \dot{V}_0^2 + \dot{W}_0^2\right) + I_d^D\left(\dot{\beta}_x^2 + \dot{\beta}_y^2\right) - 2\Omega I_p^D \beta_x \dot{\beta}_y + 2\Omega I_p^D \dot{\phi} + I_p^D \dot{\phi}^2 + \Omega^2 I_p^D + \Omega^2 I_d^D\left(\beta_x^2 + \beta_y^2\right)\right] dx \quad \text{III-19}$$

$$\begin{cases} I_m^D = \mathrm{M}^D = \pi\left({R_d}^2 - {R_o}^2\right) e_d \rho_d \\ I_d^D = \frac{\mathrm{M}^D}{12}\left(3{R_d}^2 + {R_o}^2 + {e_d}^2\right) \\ I_p^D = \frac{\mathrm{M}^D}{12}\left({R_d}^2 + {R_o}^2\right) \end{cases} \quad \text{III-20}$$

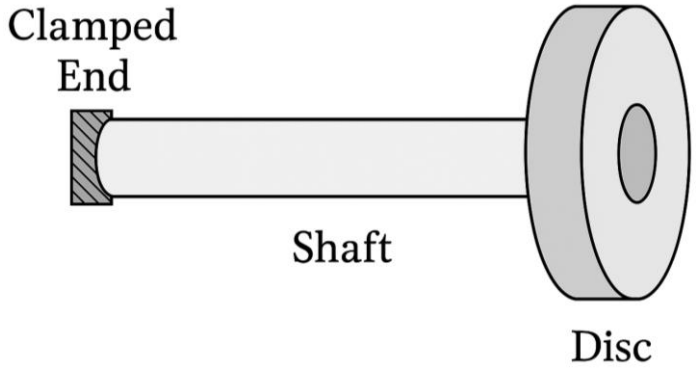

Figure III-3 Shaft with disc structure under clamped end

III.8.2. Matrices of disc

A same work in the shaft it's making with the disc:

$$[M^D] = \begin{bmatrix} [I_m^D] & 0 & 0 & 0 & 0 & 0 \\ 0 & [I_m^D] & 0 & 0 & 0 & 0 \\ 0 & 0 & [I_m^D] & 0 & 0 & 0 \\ 0 & 0 & 0 & [I_d^D] & 0 & 0 \\ 0 & 0 & 0 & 0 & [I_d^D] & 0 \\ 0 & 0 & 0 & 0 & 0 & [I_p^D] \end{bmatrix} \quad \text{III-21}$$

$$[G^D] = \begin{bmatrix} 0 & 0 & 0 & 0 & 0 & 0 \\ 0 & 0 & 0 & 0 & 0 & 0 \\ 0 & 0 & 0 & 0 & 0 & 0 \\ 0 & 0 & 0 & 0 & \Omega[I_p^D] & 0 \\ 0 & 0 & 0 & -\Omega[I_p^D]^T & 0 & 0 \\ 0 & 0 & 0 & 0 & 0 & 0 \end{bmatrix} \quad \text{III-22}$$

III.9. Modelization of bearing and damping

Bearings and damping elements are key components in rotor dynamics (figure IV-4) as they strongly influence stability, vibration amplitudes, and critical speeds. Bearings provide stiffness and constrain rotor motion, while damping mechanisms dissipate vibrational energy and help control resonance. In Porous shafts, accurate modeling of these effects is essential because the interaction between material gradation, porosity, and support conditions leads to complex dynamic behavior. Therefore, bearing stiffness and damping are introduced into the mathematical model to represent realistic boundary conditions, improve prediction of critical speeds, and ensure reliable analysis of rotor system performance.

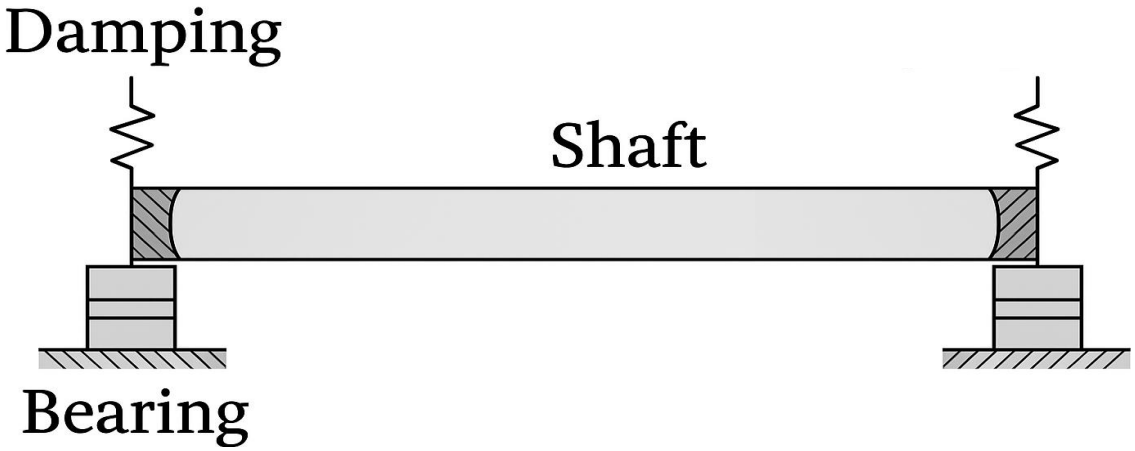

Figure III-4 Shaft under bearing and damping condition

The virtual work δA of the forces acting on the element beam is:

$$\delta A = F_{V_0}\delta_{V_0} + F_{W_0}\delta_{W_0} \qquad \text{III-23}$$

Where F_{V_0} and F_{W_0} are the generalized forces expressed by:

$$\begin{Bmatrix} F_{V_0} \\ F_{W_0} \end{Bmatrix} = -\begin{bmatrix} C_{yy} & C_{yz} \\ C_{zy} & C_{zz} \end{bmatrix}\begin{Bmatrix} \dot{V}_0 \\ \dot{W}_0 \end{Bmatrix} - \begin{bmatrix} K_{yy} & K_{yz} \\ K_{zy} & K_{zz} \end{bmatrix}\begin{Bmatrix} V_0 \\ W_0 \end{Bmatrix} \qquad \text{III-24}$$

We introduce the shape functions $[N]$ and the generalized coordinates $\{q_U\}$, so we obtained:

$$[K^B] = \begin{bmatrix} 0 & 0 & 0 & 0 & 0 & 0 \\ 0 & [K_{yy}] & [K_{yz}] & 0 & 0 & 0 \\ 0 & [K_{zy}] & [K_{zz}] & 0 & 0 & 0 \\ 0 & 0 & 0 & 0 & 0 & 0 \\ 0 & 0 & 0 & 0 & 0 & 0 \\ 0 & 0 & 0 & 0 & 0 & 0 \end{bmatrix} \quad \text{III-25}$$

$$[C^D] = \begin{bmatrix} 0 & 0 & 0 & 0 & 0 & 0 \\ 0 & [C_{yy}] & [C_{yz}] & 0 & 0 & 0 \\ 0 & [C_{zy}] & [C_{zz}] & 0 & 0 & 0 \\ 0 & 0 & 0 & 0 & 0 & 0 \\ 0 & 0 & 0 & 0 & 0 & 0 \\ 0 & 0 & 0 & 0 & 0 & 0 \end{bmatrix} \quad \text{III-26}$$

III.10. Global matrices of the rotors system

Finelly the general equation of motion and the global matrices are attaining:

$$[M]\{\ddot{q}\} + [G]\{\dot{q}\} + [K]\{q\} = \{0\} \quad \text{III-27}$$

III.10.1. Global mass matrix

$$[M] = [M^S] + [M^D] \quad \text{III-28}$$

$$[M] = \begin{bmatrix} [M_U] + [I_m^D] & 0 & 0 & 0 & 0 & 0 \\ 0 & [M_V] + [I_m^D] & 0 & 0 & 0 & 0 \\ 0 & 0 & [M_W] + [I_m^D] & 0 & 0 & 0 \\ 0 & 0 & 0 & [M_{\beta_x}] + [I_d^D] & 0 & 0 \\ 0 & 0 & 0 & 0 & [M_{\beta_y}] + [I_d^D] & 0 \\ 0 & 0 & 0 & 0 & 0 & [M_\phi] + [I_p^D] \end{bmatrix} \quad \text{III-29}$$

III.10.2. Global gyroscopic matrix

$$[G] = [G^S] + [G^D] + [C^D] \quad \text{III-30}$$

$$[G] = \begin{bmatrix} 0 & 0 & 0 & 0 & 0 & 0 \\ 0 & [C_{yy}] & [C_{yz}] & 0 & 0 & 0 \\ 0 & [C_{zy}] & [C_{zz}] & 0 & 0 & 0 \\ 0 & 0 & 0 & 0 & [G_1] + \Omega[I_p^D] & 0 \\ 0 & 0 & 0 & -[G_1]^T - \Omega[I_p^D]^T & 0 & 0 \\ 0 & 0 & 0 & 0 & 0 & 0 \end{bmatrix} \quad \text{III-31}$$

III.10.3. Global stiffness matrix

$$[K] = [K^S] + [K^B] \quad \text{III-32}$$

$$[K] = \begin{bmatrix} [K_U] & 0 & 0 & 0 & 0 & 0 \\ 0 & [K_V] + [K_{yy}] & [K_{yz}] & 0 & [K_1] & 0 \\ 0 & [K_{zy}] & [K_W] + [K_{zz}] & [K_2] & 0 & 0 \\ 0 & 0 & [K_2]^T & [K_{\beta_x}] & 0 & 0 \\ 0 & [K_1]^T & 0 & 0 & [K_{\beta_y}] & 0 \\ 0 & 0 & 0 & 0 & 0 & [K_\phi] \end{bmatrix} \quad \text{III-33}$$

III.10.4. Solving the equation of motion system

To resolve the previous system (IV-27), it's should be transmitting form the second order differential equations to a first order differential equations; for this objective, is necessary to formulate the system as follow:

$$\begin{cases} [M]\{\ddot{q}\} + [G]\{\dot{q}\} + [K]\{q\} = \{0\} \\ -[I]\{\dot{q}\} + [I]\{\dot{q}\} = \{0\} \end{cases} \quad \text{III-34}$$

After that we can obtain the following simplify first order differential equation:

$$[A]\{\dot{Q}\} + [B]\{Q\} = \{0\} \quad \text{III-35}$$

With:

$$\begin{cases} [A] = \begin{bmatrix} -[I] & [0] \\ [G] & [M] \end{bmatrix} \\ [B] = \begin{bmatrix} [0] & [I] \\ [K] & [0] \end{bmatrix} \\ \{Q\} = \begin{Bmatrix} q \\ \dot{q} \end{Bmatrix} \\ \{\dot{Q}\} = \begin{Bmatrix} \dot{q} \\ \ddot{q} \end{Bmatrix} \end{cases} \quad \text{III-36}$$

III.11. Algorithmic framework of calculation program

The proposed algorithmic framework illustrate in the Figure IV-5 has been drafted in accordance with the ISO 5807 standard for flowchart representation. By adhering to ISO 5807 conventions, the framework employs standardized symbols and hierarchical organization, facilitating effective communication of the program's logic and modular loop structure to both technical and non-technical audiences to understand calculation process.

The algorithmic framework for evaluating the dynamic behavior of porous rotors follows a hierarchical loop-based structure, tailored to incorporate a wide range of physical, material, and operational parameters. The algorithm begins with an initialization phase, where the geometric parameters of the shaft and the number of polynomials for the p-FEM are specified. Other model-specific parameters such as material types, porosity distributions, grading indices, and rotational speeds are systematically handled within their respective loops to maintain modularity and clarity in implementation.

At the Major Loop representing various materials systems for PFGM or single materials for FGP. Each material combination possesses distinct mechanical properties that significantly influence the dynamic behavior of the rotor system. Within each material system, the Outer Loop addresses the variation in porosity distribution models, which define how the pores are spatially distributed across the rotor's volume. This loop extracts and applies the appropriate mathematical model describing the porosity distribution. Following this, the Middle Loop iterates over the porosity coefficients $\alpha \; or \; e_0$, representing the intensity or magnitude of porosity. At each step, the current porosity value is applied to modify the effective material properties accordingly. The presence of porosity reduces both stiffness and mass, and this loop is crucial for capturing these effects in the eigenvalue analysis.

Nested within is the Inner Loop over the grading indices n, which control the rate of material gradation from one constituent to another (e.g., from metal-rich to ceramic-rich). For each grading index, effective FGM properties are calculated (FPG case $n = 0$), followed by symbolic integrations required for p-FEM stiffness and mass matrix formulations. Component-level matrices are then assembled and augmented with the stiffness of the bearings and supports (banding stiffness). The Innermost Loop handles the rotational speed Ω, accounting for the gyroscopic effects in the dynamic system. At each speed increment, the gyroscopic matrix is computed and the global stiffness $[K]$, mass $[M]$, and gyroscopic $[G]$ matrices are assembled. These are used to form the system matrices $[A]$ and $[B]$ for eigenvalue analysis. Boundary conditions are subsequently applied. If the system is modeled as free-free, no modification is required. Otherwise, matrices $[A]$ and $[B]$ are adjusted to reflect the specific constraints.

Finally, the eigenvalue problem is solved, and natural frequencies are extracted and filtered. The loop structure is systematically closed, starting from the innermost level (rotational speed) up to the major material loop, ensuring that all combinations of materials, porosity models, grading indices, and operational speeds are evaluated.

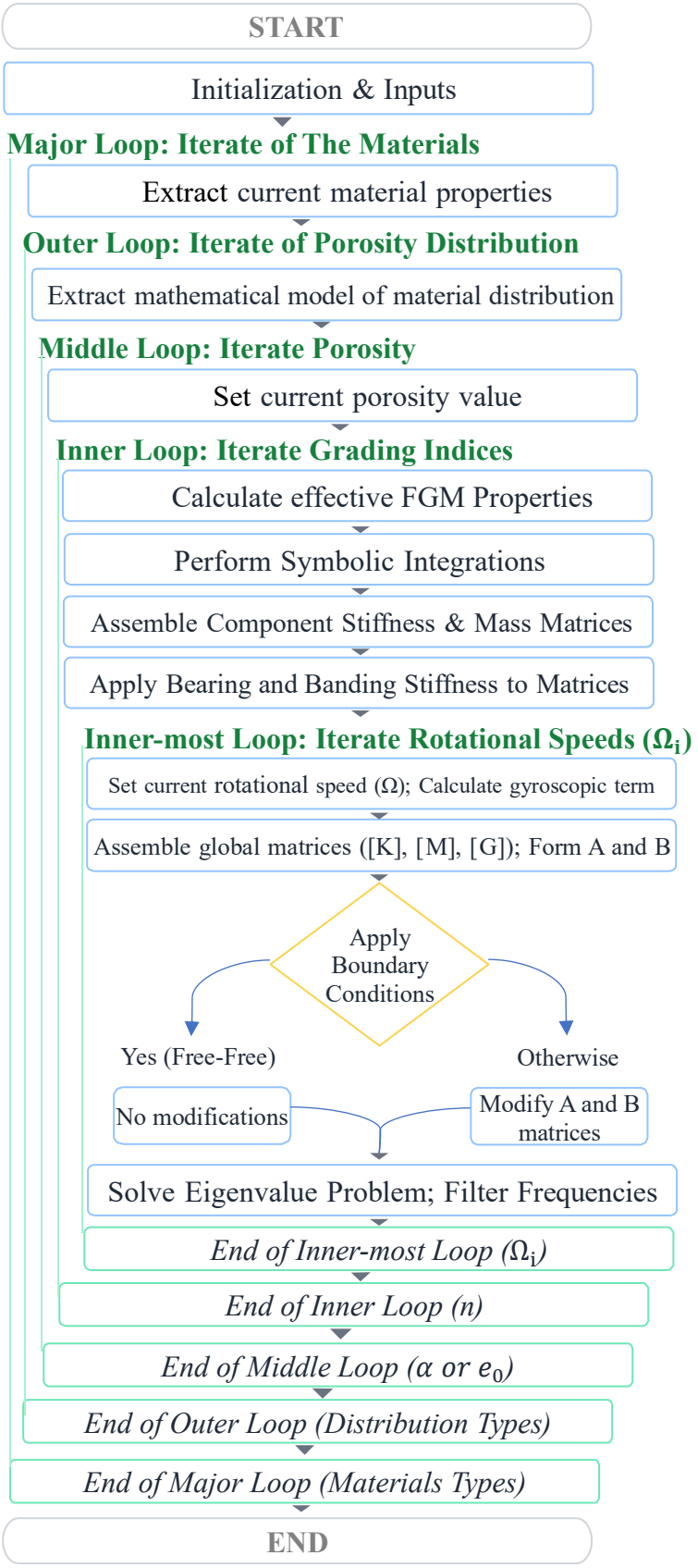

Figure III-5 flowchart represent the calculation program algorithm.

III.12. Mechanical properties of PFGM

The characterization of the PFGM in the cylindrical form is illustrated in figure IV-6, employing even porosity, uneven porosity types of porosity distribution illustrate in figure IV-7 modeling by Vijaykumar Vaka et al. [22]. The shaft material is homogeneous at the microscopic level, with a gradual material as defined by the PFGM model. These models are defined by the mathematical formulations in the equations IV-39 for even porosity and the equations IV-40 for uneven porosity.

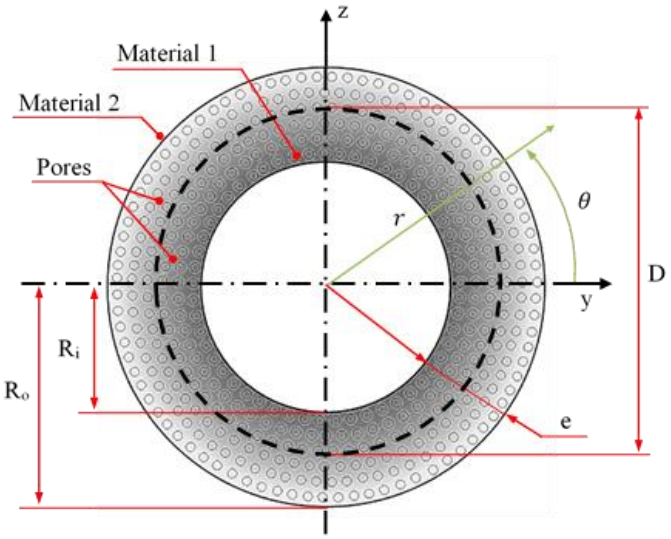

Figure III-6 Structure characterization, inner and outer radius of Even Porous FGM shaft.

$P(r)$ present the expression of material properties of PFGM by power low gradation with even porosity model. Including the outer (P_o) and the inner (P_i) material properties.

$$P(r) = (P_o - P_i)\left(\frac{r-R_i}{e}\right)^n + P_i - (P_o + P_i)\left(\frac{\alpha}{2}\right) \quad \text{III-37}$$

$$P(r) = (P_o - P_i)\left(\frac{r-R_i}{e}\right)^n + P_i - (P_o + P_i)\left(\frac{\alpha}{2}\right)\left(1 - \frac{2|R_o|}{r}\right) \quad \text{III-38}$$

Where the thickness is $e = R_o - R_i$, n the power low index, and α the coefficient of porosity.

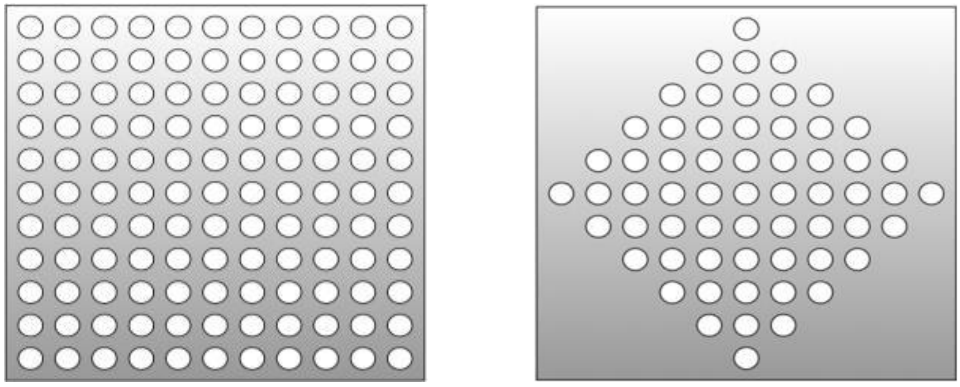

A: even porosity B: uneven porosity

Figure III-7 Different porosity distribution for an PFGM structure [22]

The function $P(r)$ in terms of the radius r represent Young's modulus $E(r)$, density $\rho(r)$, or Poisson's ratio $\upsilon(r)$. These relationships are expressed as follows:

Even porosity:
$$\begin{cases} E(r) = (E_o - E_i)\left(\frac{r-E_i}{e}\right)^n + E_i - (E_o + E_i)\left(\frac{\alpha}{2}\right) \\ \rho(r) = (\rho_o - \rho_i)\left(\frac{r-\rho_i}{e}\right)^n + \rho_i - (\rho_o + \rho_i)\left(\frac{\alpha}{2}\right) \\ \upsilon(r) = (\upsilon_o - \upsilon_i)\left(\frac{r-\upsilon_i}{e}\right)^n + \upsilon_i - (\upsilon_o + \upsilon_i)\left(\frac{\alpha}{2}\right) \end{cases} \quad \text{III-39}$$

Uneven porosity:
$$\begin{cases} E(r) = (E_o - E_i)\left(\frac{r-E_i}{e}\right)^n + E_i - (E_o + E_i)\left(\frac{\alpha}{2}\right)\left(\frac{2|R_o|}{r}\right) \\ \rho(r) = (\rho_o - \rho_i)\left(\frac{r-\rho_i}{e}\right)^n + \rho_i - (\rho_o + \rho_i)\left(\frac{\alpha}{2}\right)\left(\frac{2|R_o|}{r}\right) \\ \upsilon(r) = (\upsilon_o - \upsilon_i)\left(\frac{r-\upsilon_i}{e}\right)^n + \upsilon_i - (\upsilon_o + \upsilon_i)\left(\frac{\alpha}{2}\right)\left(\frac{2|R_o|}{r}\right) \end{cases} \quad \text{III-40}$$

$$R_o \le r \le R_i \quad 0 \le n \le \infty \quad \alpha \ll 1$$

III.13. Mechanical properties of FGP

Two types of FGP distributions, namely Type 1 (symmetric porosity distribution), Type 2 (non-symmetric porosity distribution) are considered in cylindrical shaft, as shown in Figure IV-8. The elastic modulus and mass density of porous materials vary through the thickness direction based on the assumption of a typical mechanical feature of the open-cell metal foam. The variation of Young's modulus $E(r)$, shear modulus $G(r)$ and density $\rho(r)$ through the thickness direction of the cylindrical shaft is described by Equations IV-41 and IV-42.

Symmetric distribution :
$$\begin{cases} E(r) = E_1\left[1 - e_0 cos\left(\frac{\pi r}{e}\right)\right] \\ G(r) = G_1\left[1 - e_0 cos\left(\frac{\pi r}{e}\right)\right] \\ \rho(r) = \rho_1\left[1 - e_m cos\left(\frac{\pi r}{e}\right)\right] \end{cases} \quad \text{III-41}$$

Non-symmetric distribution :
$$\begin{cases} E(r) = E_1\left[1 - e_0 sin\left(\frac{\pi r}{2e} + \frac{\pi}{4}\right)\right] \\ G(r) = G_1\left[1 - e_0 sin\left(\frac{\pi r}{2e} + \frac{\pi}{4}\right)\right] \\ \rho(r) = \rho_1\left[1 - e_m sin\left(\frac{\pi r}{2e} + \frac{\pi}{4}\right)\right] \end{cases} \quad \text{III-42}$$

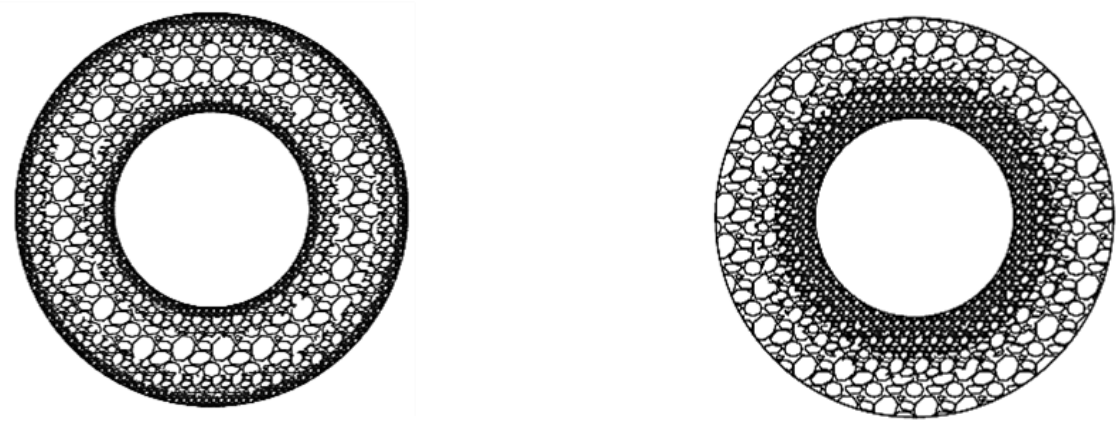

(a) Symmetric distribution (b) Non-symmetric distribution

Figure III-8 Cross-section for an FGP cylindrical shaft with different porosity distribution [70]

The porosity coefficient e_0 is defined as follows:

$$e_0 = 1 - \frac{E_0}{E_1} = 1 - \frac{G_0}{G_1} \quad (0 < e_0 < 1) \quad \text{III-43}$$

where E_0 and E_1 denote the minimum and maximum values of elasticity modulus in radial direction. The relationship of elasticity modulus and shear modulus is defined as follow:

$$G_i = \frac{E_i}{2(1+\nu)} \quad (i = 0,1) \quad \text{III-44}$$

The porosity coefficient for mass density is defined as

$$e_m = 1 - \frac{\rho_0}{\rho_1} \ (0 < e_m < 1) \quad \text{III-45}$$

In which ρ_0 and ρ_1 denote the minimum and maximum values respectively. For parameters e_0 and e_m, the relationship of which are defined as:

$$e_m = 1 - \sqrt{(1 - e_0)} \quad \text{III-46}$$

IV. Results and discussions

IV.1. Convergence and comparison studies

The graph presented in Figure V-1 illustrates the variation of the first three modes of natural frequencies ($\omega\ [Hz]$) as a function of the number of shape functions (or polynomial order p) for different boundary conditions: Simply supported (S-BC), Clamped– Clamped (C-BC), and simply supported– Clamped (CS-BC). The materials used in this study are stainless are stainless steel for the inner material and nickel for the outer material, with parameters $n = 0.5$, $\alpha = 0.2$. The geometric parameters are defined as: $e/D = 0.05$, $L/D = 20$. D: medium diameter of shaft.

It can be observed that rapid convergence occurs as the polynomial order p increases. The graphs begin to stabilize after reaching the seventh order. Additionally, it is noteworthy that the simply supported cases exhibit better stability compared to the other boundary conditions. For the subsequent studies, $p = 10$ has been chosen.

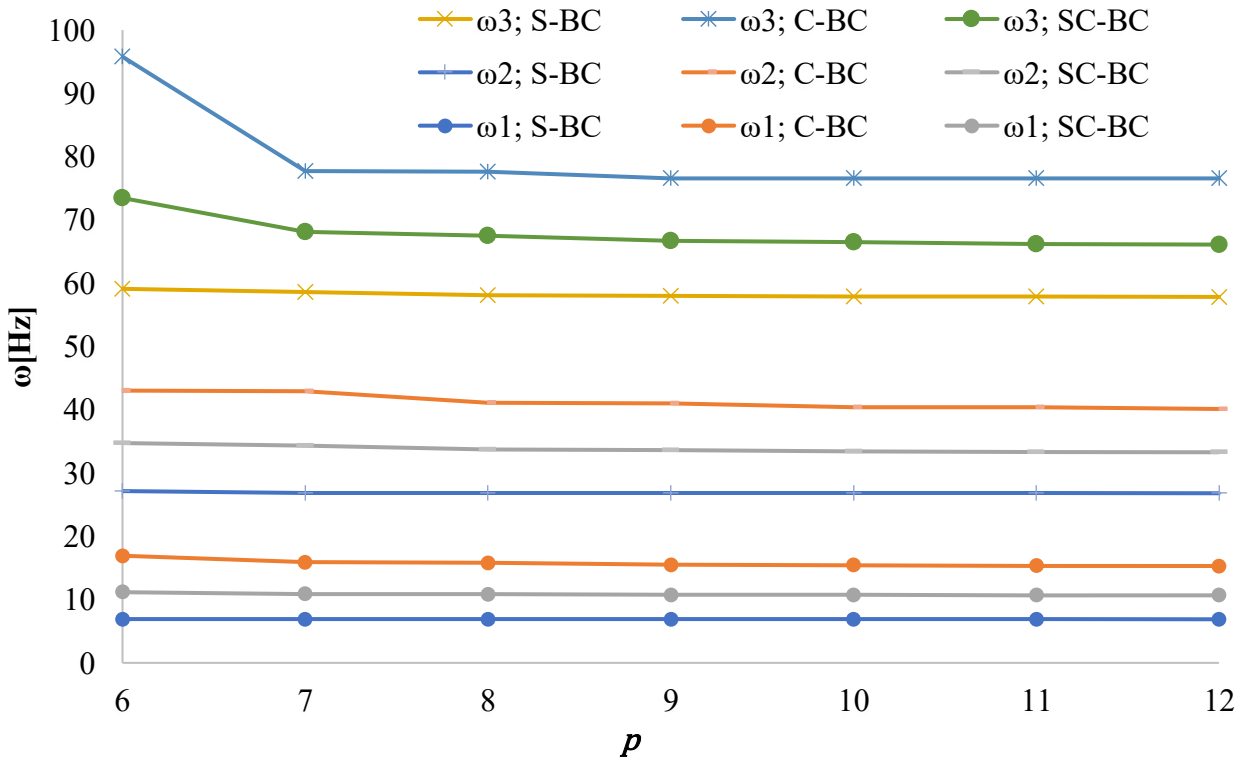

Figure IV-1 Convergence study for three first modes of natural frequencies in function in the number of shape functions with different boundary conditions.

Table V-1 presents the calculated first four normal modes of homogenous beam using the p-beam element. The obtained frequencies are compared with exact solutions provided by Szeidl and Kiss [3]. The frequency parameter used is as follow: (A: Aire of cross-section)

$$\lambda = \sqrt{\omega . \sqrt{\frac{\rho . A . L^4}{E . I}}} \qquad \text{IV-1}$$

Table IV-1 FEM-p values and exact values of the four first modes of the homogenous beam.

BC	**S -BC**		**SC -BC**		**C -BC**	
$\boldsymbol{\lambda}$	Present	Exact [3]	Present	Exact [3]	Present	Exact [3]
1	03.2101	03.1416	04.0137	03.9270	04.9031	04.7300
2	06.3821	06.2832	07.1678	07.0686	08.0466	07.8532
3	09.4832	09.4248	10.2327	10.2102	11.1582	10.2102
4	12.4872	12.5664	13.1966	13.3518	14.0758	10.9956

Table V-2 shows a comparison of the three first steady-state natural frequencies of cylindrical shaft with the result provided by Elhannani et al. [71]. The FGM mixture Stainless Steel–Nickel, is considered for this comparison, with the following geometric parameters: e = 0.002m, D/e = 500, L/D = 20.

Table IV-2 Three first modes for FGM (SS-Ni) beam

Material	**Ni**		**FGM (SS-Ni)**		**SS**	
Source	Present	[71]	Present	[71]	Present	[71]
ω1	06.9264	06.9257	07.1059	07.0985	07.2972	07.2965
ω2	26.9253	26.9240	27.6197	27.5960	28.3591	28.3580
ω3	52.4292	52.4370	53.6398	53.7470	54.9302	54.9380

Table V-3 presents a comparison with the results from Loy et al. [5], examining the variations in natural frequencies (Hz) for different power law indices n and the effect of the thickness ratio (e/R), where R represents the radius of the shell. Table V-4 compares the first natural frequencies of cylindrical shell, with results obtained by Assem et al. [26], showing the influence of graded index. The geometric parameters used for this comparison used are: $R = 1m$, $e/R = 0.002$, $L/R = 20$.

Table IV-3 Geometric parameter e/R influence in natural frequency for FGM beam

e/R	n	0(SS)	0(Ni)	0.5	0.7	1	2	5	15	30
0.002	Present	7.2229	6.8577	7.0962	7.0671	7.0348	6.9746	6.9156	6.8793	6.8688
	[5]	7.2250	6.8577	7.0972	7.0691	7.0384	6.9820	6.9251	6.8856	6.8726
0.05	Present	174.06	165.21	171.07	170.38	169.60	168.15	166.69	165.77	165.50
	[5]	174.83	168.99	178.06	174.13	173.36	171.98	170.60	169.66	169.35

Table IV-4 Graded index influence in first natural frequency for FGM cylindrical shaft.

n	Present	[26]
0	13.4754	13.2537
0.5	13.7048	13.4667
0.7	13.7601	13.5181
1	13.8230	13.5766
2	13.9437	13.6889
5	14.0670	13.8036
15	14.1454	13.8766
30	14.1683	13.8980

These comparisons demonstrate that the results obtained from our model and simulations closely align with those reported in existing literature, thereby validating the accuracy and effectiveness of our modelling, analysis, and simulation methods.

Table V-5 presents a comparison of dimensionless natural frequencies for a simply supported even PFGM cylindrical beam, with the results from Ebrahimi et al. [7] and Sathujoda et al. [19]. The frequency parameter used in these results is the same λ illustrated in equation VI-1, considering the inner material properties. In [7], the study focused on a rectangular beam, while Sathujoda et al. [19] examined a cylindrical beam, considering the effect of a disk when investigating rotational speed.

Table IV-5 Dimensionless natural frequencies of Porous FGM cylindrical shaft

n	0,5			1			2			5		
α	Present	[19]	[7]	Present	[19]	[7]	Present	[19]	[7]	Present	[19]	[7]
0	4.4209	4.5283	4.5158	4.1684	3.9695	3.9582	3.9046	3.5659	3.5552	3.6061	3.2436	3.2332
0.1	4.4905	4.5947	4.5821	4.1967	3.9621	3.9509	3.8995	3.5188	3.5082	3.5701	3.1736	3.1633
0.2	4.5896	4.6806	4.6678	4.2385	3.9516	3.9405	3.8983	3.4599	3.4494	3.5312	3.0888	3.0786

Table V-6 compares the dimensionless natural frequencies of a functionally graded porous (FGP) cylindrical shaft for both symmetric and non-symmetric porosity distributions at various porosity levels, with results from the present study validated against reference [70] that studying the vibration behavior of FGP cylindrical shells. The frequencies decrease as the porosity coefficient e_0 increases, reflecting the expected reduction in structural stiffness. The present results show good agreement with the reference, particularly at low porosity, while slightly higher values at larger e_0 suggest improved sensitivity in the current model. Differences between symmetric and non-symmetric cases become more noticeable at higher porosity, demonstrating the model's capability to accurately capture the influence of porosity distribution.

Table IV-6 Dimensionless natural frequencies of FGP cylindrical shaft

e_0	Symmetric distribution		Non-symmetric distribution	
	Present	[70]	Present	[70]
0	1.2803	1.2429	1.2803	1.2429
0.2	1.2384	1.2155	1.2384	1.2037
0.4	1.1943	1.1893	1.1945	1.1598
0.6	1.1510	1.1677	1.1502	1.1093
0.8	1.1141	1.1633	1.1145	1.0507

Comparisons across all the tables confirm the accuracy and robustness of the p-FEM based on the TBT in analyzing the dynamic vibration behavior of steady-state cylindrical PFGM and FGP shafts. The p-FEM hierarchical beam model demonstrated in this paper can be used for more complex rotor designs, including those with variable cross-sections and hybrid materials. The close agreement with values reported in the literature for various boundary conditions, materials, geometric parameters, and porosity levels further validates the reliability of the results presented in this study.

IV.2. Parametric study of PFGM shaft

In this section, the influence of various physical and geometrical parameters on free vibration behavior of cylindrical PFGM shafts is investigated under both steady-state and rotational conditions. These parameters include material gradation, porosity distribution, geometric ratios, and boundary conditions, which all play a crucial role in the dynamic behavior of the shafts. The FGM used in this study is a mixture of two materials: Steel SUS304, Zirconia and Alumina for the inner layer and Nickel for the outer layer. Their material properties at the temperature $T = 300\ °K$ (The effect of temperature variations is not considered in this study) are presented in Table V-7 from Loy et al. [5].

Table IV-7 Materials properties at $T = 300\ °K$ [5]

Materials	**SUS304 (SS)**	**Nickel (Ni)**	**Zirconia (ZrO_2)**	**Alumina (Al_2O_3)**
$\boldsymbol{E\ [N/m^2] \times 10^{11}}$	2.0104	2.05098	1.68	3.8
$\boldsymbol{\rho\ [kg/m^3]}$	8166	8900	5700	3800
$\boldsymbol{\upsilon}$	0.3262	0.31	0.24	0.23

IV.2.1. Effect of n, α, boundary conditions, and modes

The tables bellow Table V-8 and Table V-9 presents the effect of boundary conditions (BCs), porosity α and the graded index n on the three first modes of steady-state natural frequencies for even and uneven porosity respectively; The geometric parameters used for this analysis are as follows: $D = 1m$; $e/D = 0.002$; $L/D = 20$. The first natural frequencies with various volume fraction of even porosity $\alpha = [0;\ 0.1;\ 0.2;\ 0.3;\ 0.4;\ 0.5]$ and graded index $n = [0.5;\ 1;\ 2;\ 5]$ under different BCs (S-BC, SC-BC, and C-BC).

Table IV-8 First three modes natural frequencies of various Even PFGM with different BC

α	Mode	n											
		0.5	1	2	5	0.5	1	2	5	0.5	1	2	5
		S-BC				C-BC				SC-BC			
		ω [Hz]											
0	1	07.0268	07.0717	07.1176	07.1647	15.7089	15.8063	15.9059	16.0079	10.9131	10.9819	11.0523	11.1243
	2	27.3074	27.4793	27.6552	27.8353	40.9244	41.1717	41.4248	41.6839	33.9441	34.1536	34.3680	34.5875
	3	58.7786	59.1405	59.5109	59.8901	76.0228	76.4682	76.9242	77.3910	67.2735	67.6778	68.0916	68.5152
0.1	1	06.9521	07.0000	07.0491	07.0995	15.5761	15.6805	15.7876	15.8976	10.8083	10.8818	10.9572	11.0346
	2	27.0465	27.2303	27.4189	27.6124	40.6495	40.9162	41.1898	41.4706	33.6665	33.8914	34.1222	34.3591
	3	58.3067	58.6956	59.0946	59.5041	75.6683	76.1517	76.6478	77.1571	66.8458	67.2823	67.7302	68.1900
0.2	1	06.8859	06.9378	06.9912	07.0462	15.4595	15.5733	15.6905	15.8112	10.7158	10.7957	10.8779	10.9625
	2	26.8155	27.0153	27.2210	27.4328	40.4109	40.7030	41.0038	41.3135	33.4224	33.6678	33.9205	34.1807
	3	57.8911	58.3157	58.7527	59.2029	76.5569	76.9964	77.4506	77.9201	66.4746	66.9534	67.4463	67.9541
0.3	1	06.8271	06.8845	06.9437	07.0050	15.3571	15.4836	15.6144	15.7497	10.6340	10.7225	10.8140	10.9086
	2	26.6107	26.8322	27.0612	27.2980	40.2041	40.5303	40.8676	41.2164	33.2077	33.4808	33.7630	34.0550
	3	57.5247	57.9973	58.4858	58.9911	77.4739	77.9914	78.5282	79.0856	66.1528	66.6881	67.2414	67.8139
0.4	1	06.7745	06.8394	06.9069	06.9772	15.2664	15.4105	15.5602	15.7161	10.5611	10.6616	10.7661	10.8747
	2	26.4276	26.6792	26.9407	27.2127	40.0234	40.3964	40.7842	41.1877	33.0172	33.3284	33.6518	33.9883
	3	57.1988	57.7375	58.2975	58.8802	78.4038	79.0258	79.6746	80.3522	65.8714	66.4840	67.1209	67.7837
0.5	1	06.7262	06.8022	06.8817	06.9651	15.1839	15.3532	15.5305	15.7164	10.4945	10.6123	10.7357	10.8650
	2	26.2600	26.5548	26.8636	27.1874	39.8601	40.3000	40.7609	41.2444	32.8436	33.2093	33.5924	33.9943
	3	56.9008	57.5342	58.1977	58.8937	79.3335	80.1024	80.9108	81.7618	65.6164	66.3394	67.0970	67.8918

Table IV-9 First three modes natural frequencies of various Uneven PFGM with different BC

α	Mode	n											
		0.5	1	2	5	0.5	1	2	5	0.5	1	2	5
		S-BC				C-BC				SC-BC			
		ω [Hz]											
0	1	07.0052	07.0501	07.0961	07.1431	15.7815	15.8795	15.9797	16.0823	10.9557	11.0247	11.0953	11.1676
	2	27.4093	27.5819	27.7586	27.9394	41.2236	41.4734	41.7290	41.9907	34.0885	34.2995	34.5154	34.7364
	3	58.9745	59.3392	59.7123	60.0943	76.8427	77.2949	77.7577	78.2316	67.7864	68.1953	68.6138	69.0422
0.1	1	07.0910	07.1337	07.1774	07.2220	15.9354	16.0281	16.1227	16.2194	11.0751	11.1407	11.2076	11.2759
	2	27.7075	27.8714	28.0387	28.2095	41.5510	41.7860	42.0261	42.2712	34.4131	34.6124	34.8160	35.0240
	3	59.5311	59.8755	60.2272	60.5864	77.2880	77.7105	78.1421	78.5830	68.3012	68.6853	69.0776	69.4784
0.2	1	07.1875	07.2288	07.2709	07.3138	16.1100	16.1988	16.2894	16.3817	11.2103	11.2733	11.3376	11.4031
	2	28.0440	28.2015	28.3621	28.5258	41.9246	42.1485	42.3767	42.6094	34.7804	34.9712	35.1658	35.3641
	3	60.1593	60.4887	60.8244	61.1667	77.8031	78.2027	78.6101	79.0255	68.8876	69.2530	69.6254	70.0052
0.3	1	07.2962	07.3366	07.3777	07.4195	16.3076	16.3937	16.4814	16.5707	11.3630	11.4243	11.4868	11.5504
	2	28.4232	28.5765	28.7325	28.8913	42.3488	42.5645	42.7841	43.0076	35.1951	35.3799	35.5681	35.7596
	3	60.8665	61.1852	61.5095	61.8397	78.3942	78.7762	79.1650	79.5607	69.5526	69.9040	70.2616	70.6257
0.4	1	07.4186	07.4585	07.4991	07.5404	16.5308	16.6153	16.7013	16.7886	11.5353	11.5958	11.6573	11.7198
	2	28.8502	29.0010	29.1543	29.3102	42.8288	43.0388	43.2524	43.4694	35.6624	35.8434	36.0274	36.2144
	3	61.6613	61.9729	62.2897	62.6116	79.0678	79.4365	79.8113	80.1923	70.3037	70.6452	70.9922	71.3450
0.5	1	07.5565	07.5964	07.6370	07.6782	16.7829	16.8667	16.9518	17.0382	11.7299	11.7901	11.8513	11.9134
	2	29.3309	29.4809	29.6333	29.7880	43.3705	43.5771	43.7868	43.9997	36.1886	36.3676	36.5494	36.7340
	3	62.5536	62.8614	63.1739	63.4912	79.8314	80.1905	80.5552	80.9255	71.1498	71.4847	71.8248	72.1700

IV.2.2. Effect of n, α, boundary conditions, and situation motion

IV.2.2.1. Even PFGM

In figure V-2 for the case of steady-state of even PFGM, and in figures V-3 for the case of rotational state Forward mode at a speed of $500\,rad/s$. The geometric parameters used in the model are $e/D = 0.02;\ L/D = 10$.

The influence of porosity and the graded index is evident across all plots. As porosity increases, the natural frequency decreases, while an increase in the FGM index results in a corresponding increase in natural frequency. For both the steady-state and rotational-state cases, the maximum natural frequencies are $56.2104\,Hz$ and $55.56\,Hz$, respectively, observed with C boundary conditions at $\alpha = 0$ and $n = 5$ (without porosity). Conversely, the minimum natural frequencies are $54.2\,Hz$ and $53.4748\,Hz$, respectively, found with CC boundary conditions at $\alpha = 0.5$ and $n = 0.5$.

The increase in natural frequency is attributed to the higher rigidity of the material, as the shaft resists deformation more effectively. This increased stiffness requires more energy (or a higher frequency) to achieve the same amplitude of vibration. After performing these calculations, it was concluded that the same pattern is observed in both cases the steady-state (figures V-2-a (S-BC), figures V-2-b (C-BC), and figures V-2-c (SC-BC)) and rotational-state (figures V-3-a (S-BC), figures V-3-b (C-BC), and figures V-3-c (SC-BC)).

Similarly, boundary conditions have a significant effect on the natural frequency of the PFGM cylindrical shaft. The natural frequency of the shaft under S-BC is smaller compared to SC-BC, and both are smaller than the natural frequencies observed with C-BC. This is due to more constrained at the nodes under clamped conditions, which results in increased stiffness and consequently higher natural frequencies.

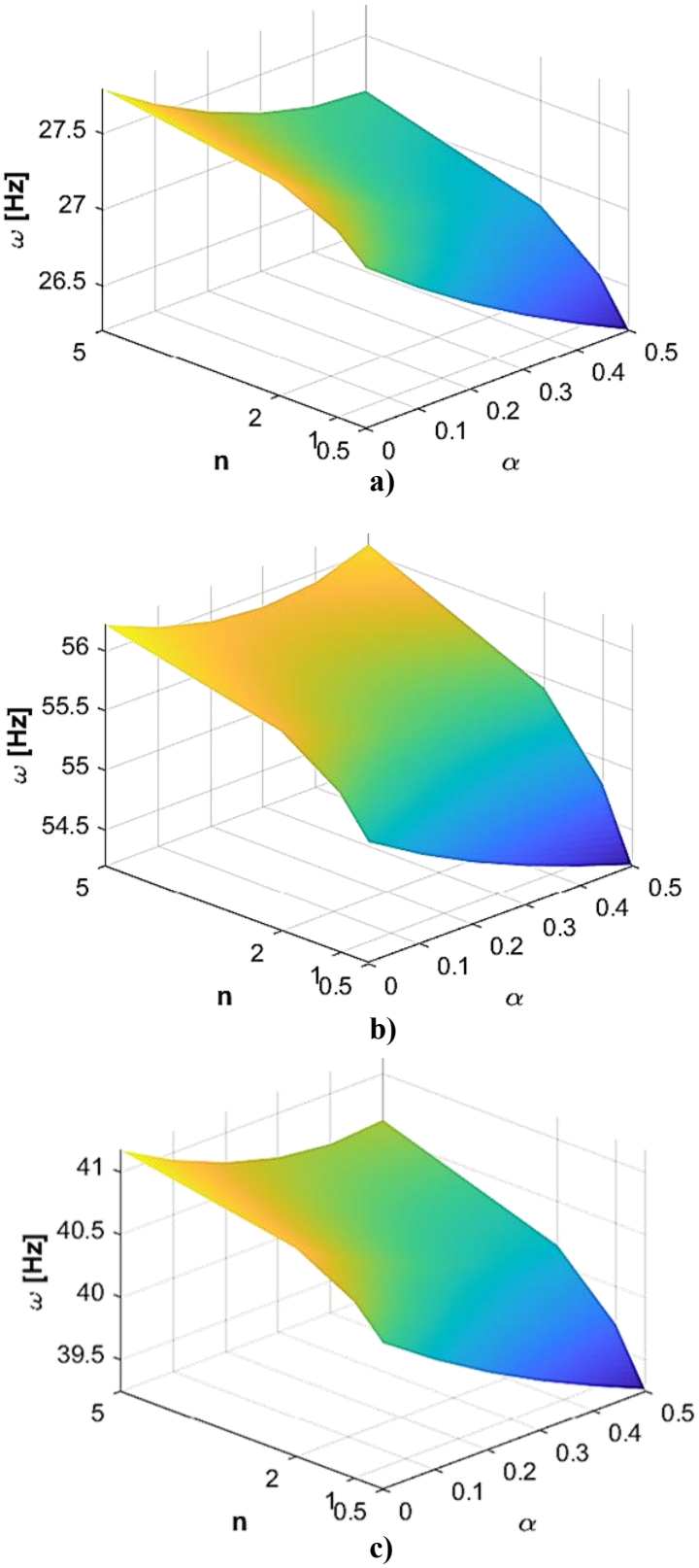

Figure IV-2 first steady-state natural frequencies of Even PFGM for different BC. a) S-BC; b) C-BC; c) SC-BC.

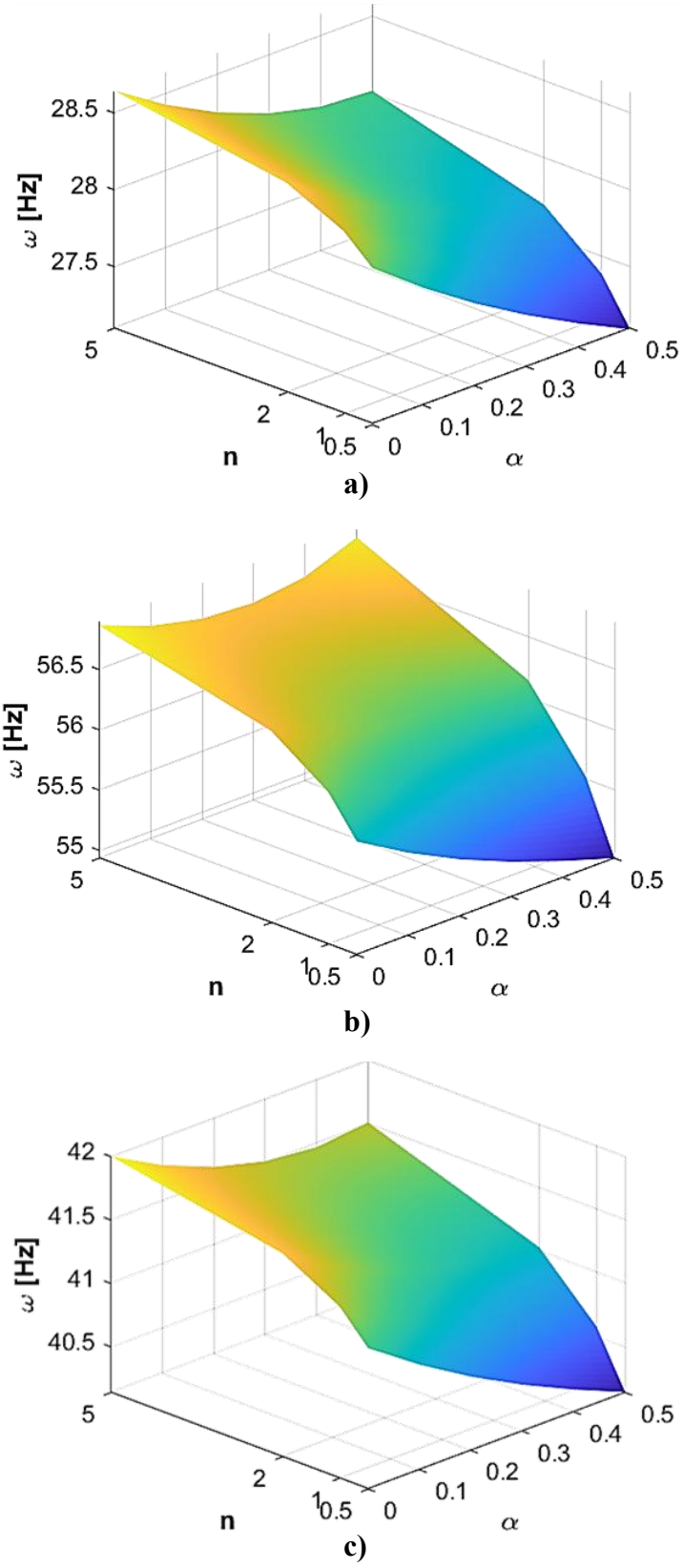

Figure IV-3 first rotational natural frequencies of Even PFGM for different BC. a) S-BC; b) C-BC; c) SC-BC.

IV.2.2.2. Uneven PFGM

In both the steady-state (Figure V-4) and rotational-state at 500 rad/s (Figure V-5) cases, the boundary conditions have the most significant effect on the natural frequency. As seen in the graphs, the C-BC consistently yields the highest natural frequencies, as clamping restricts both translational and rotational movement, making the shaft much stiffer. In contrast, the S-BC results in the lowest natural frequencies because it only restricts translation, providing less resistance to deformation. The SC-BC provides an intermediate level of stiffness, with its natural frequencies falling between those of the S-BC and C-BC conditions. This hierarchy of stiffness— C-BC > SC-BC > S-BC — is clearly demonstrated by the frequency values in all plots.

First, as the porosity distribution parameter (α) increases, the natural frequency decreases. A higher α value means there are more voids in the material. These voids reduce the overall stiffness of the shaft, which in turn lowers its natural frequency. Second, as the non-uniformity FGM index (n) increases, the natural frequency also decreases. The non-uniformity index defines the material gradient along the length of the shaft. For this specific type of uneven PFGM, an increase in n likely means a larger portion of the lighter, less stiff material (e.g., the ceramic component) is concentrated at critical locations, which reduces the shaft's overall rigidity and, consequently, its natural frequency.

A final key observation is the increase in natural frequency due to rotation. Comparing the first set of figures (steady-state) with the second set (rotational-state at 500 rad/s), it is clear that the natural frequencies are significantly higher in the rotating case. This is a direct consequence of the centrifugal stiffening effect. When the shaft rotates, the centrifugal forces generate a tensile stress along its length, which acts to increase the overall stiffness. This stiffening raises the natural frequency, a critical factor in the design and analysis of high-speed rotating components like turbine shafts and helicopter blades. This effect is independent of the boundary conditions, and is observed across all three cases.

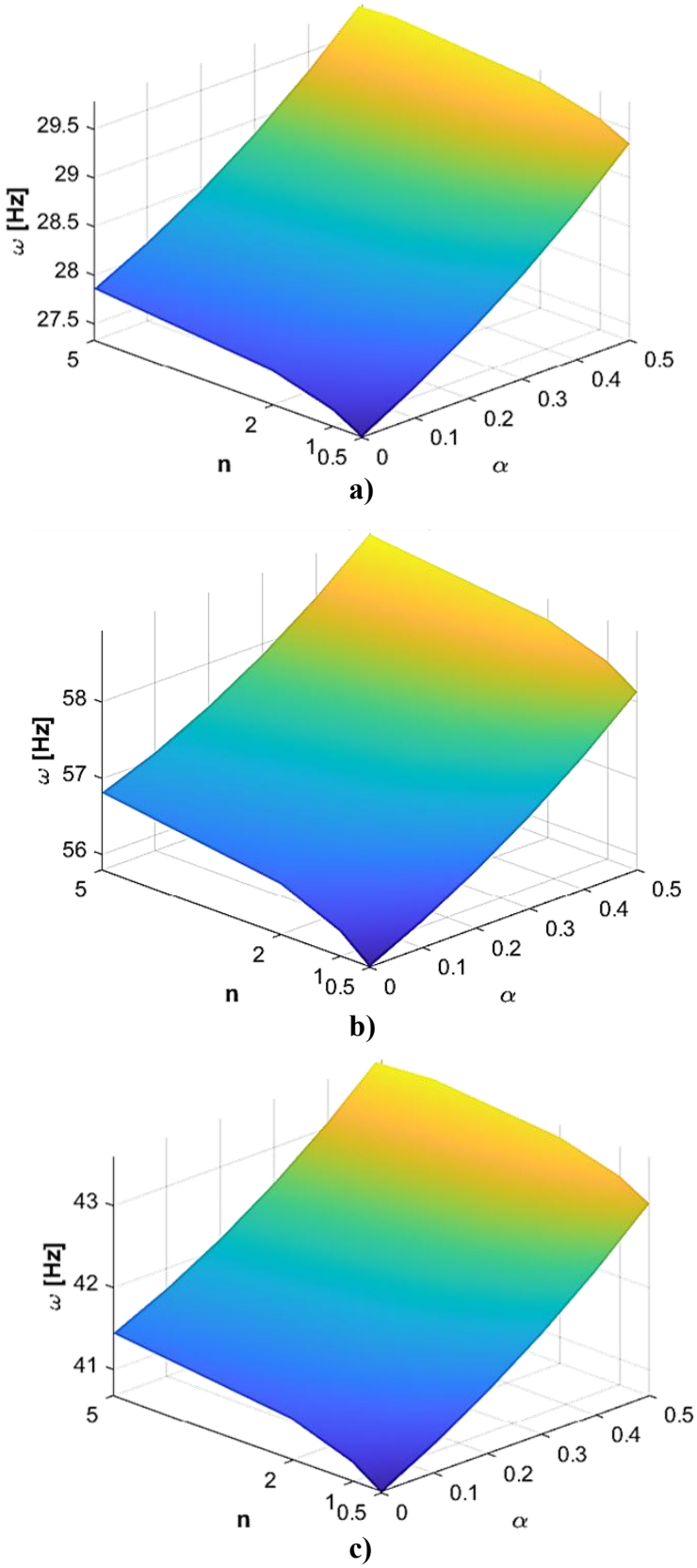

Figure IV-4 first steady-state natural frequencies of Uneven PFGM for different BC. a) S-BC; b) C-BC; c) SC-BC.

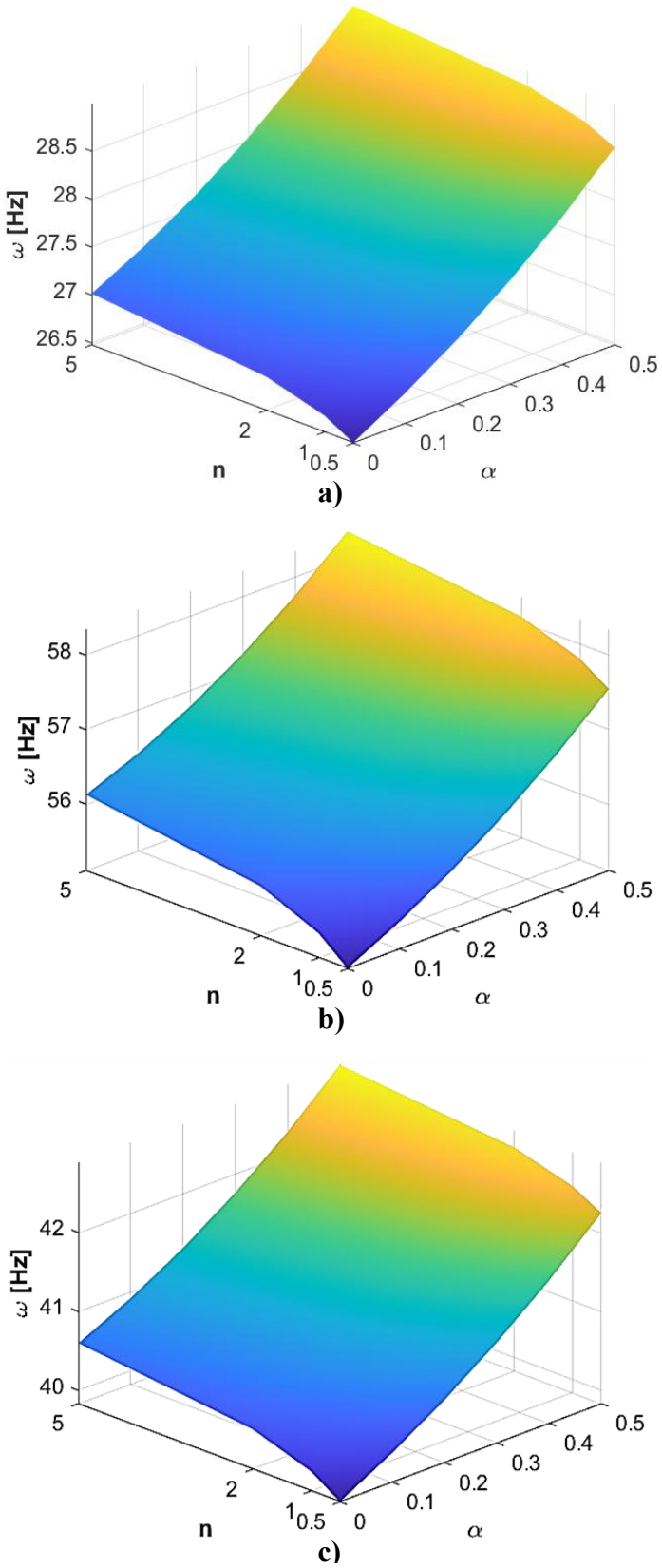

Figure IV-5 first rotational natural frequencies of Uneven PFGM for different BC. a) S-BC; b) C-BC; c) SC-BC.

IV.2.1. Effect of α, boundary conditions, and modes:

Figure V-6 illustrates the first three vibration modes for various coefficients of even porosity α under S-BC, C-BC and SC-BC, with the graded index fixed at $n = 0.5$. It can be seen that the waves in the third mode are higher than those in both the second and first modes. This indicates that BCs have a significant impact, as they are closely related to the structural rigidity and inflexibility of the system.

It is concluded that BC have a greater influence on the vibrational behavior of both steady-state and rotational-state of FGM shaft compared to the porosity fraction. This is due to minor alteration in the structure, specifically related to their low mass fraction. The results highlight the importance of boundary conditions, which can be tuned to enhance the stability and performance of rotating structures.

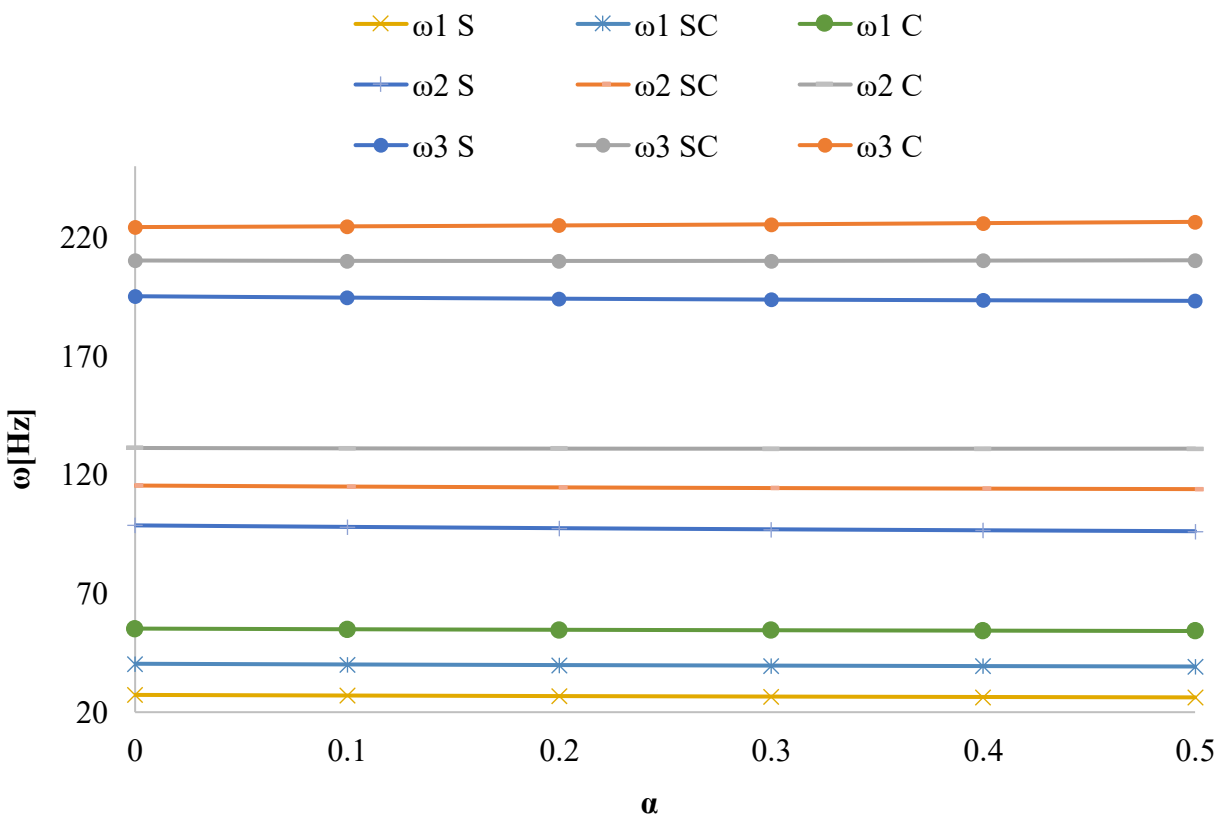

Figure IV-6 Three first modes of steady natural frequencies for various porosity with S-BC, C-BC, and SC-BC.

IV.2.2. Geometric effect in Campbell's diagram

The following studies examine the gyroscopic effect on the first natural rotational frequencies $\omega[Hz]$ as a function of the rotational speed Ω $[RPM]$ (Campbell's diagram) for even and uneven different porosity volume fraction, with the graded index $n = 0.5$ under simply supported boundary condition. The influence of the thickness ratio (e/D) on the shaft dynamics is illustrated in Figures V-7 and V-8 for even and uneven PFGM configurations, respectively, with a constant slenderness ratio of $L/D = 10$. Furthermore, the effect of the slenderness ratio (L/D) is demonstrated in Figures V-9 and V-10 for both even and uneven PFGM shafts, respectively, considering a fixed thickness ratio of $e/D = 0.02$.

The geometric configuration of a rotating shaft significantly affects the natural frequencies and thus the Campbell diagram. When an external torque is applied, it induces precession, which describes a cone in space, causing the axis of rotation to move perpendicular to the applied torque. This results in two distinct types of processional motion: Forward (FW) precession, which occurs at a higher frequency, and Backward (BW) precession, which occurs at a lower frequency.

For different porosity fractions, an increase in porosity leads to a reduction in rigidity, resulting in a decrease in the natural rotational frequencies. From Figure V-7-a ($\alpha = 0$), V-7-b ($\alpha = 0.2$), and V-7-c ($\alpha = 0.5$), so from Figure V-8-a ($\alpha = 0$), V-8-b ($\alpha = 0.2$), and V-8-c ($\alpha = 0.5$), it can be observed that a higher thickness ratio ($e/D = 0.05$) results in higher rotational frequencies for both FW and BW modes at a given shaft rotational speed compared to a lower thickness ratio ($e/D = 0.002$). Although, a small difference in e/D may not significantly impact the rotational frequency due to the negligible deformation caused by the inclination of the rotating shaft arc, it remains an important parameter to consider. In Figure V-9-a ($\alpha = 0$), V-9-b ($\alpha = 0.2$), and V-9-c ($\alpha = 0.5$), so in Figure V-10-a ($\alpha = 0$), V-10-b ($\alpha = 0.2$), and V-10-c ($\alpha = 0.5$),the slenderness ratio L/D has a significant influence on natural vibrations, exhibiting an opposite relationship with natural rotational frequency. The curves for $L/D = 5$ are higher than those for $L/D = 10$ and $L/D = 20$ across different even porosity levels. This is attributed to the direct relationship between the length of the shaft and its transverse deformations, with shaft stiffness decreasing as the L/D ratio increases.

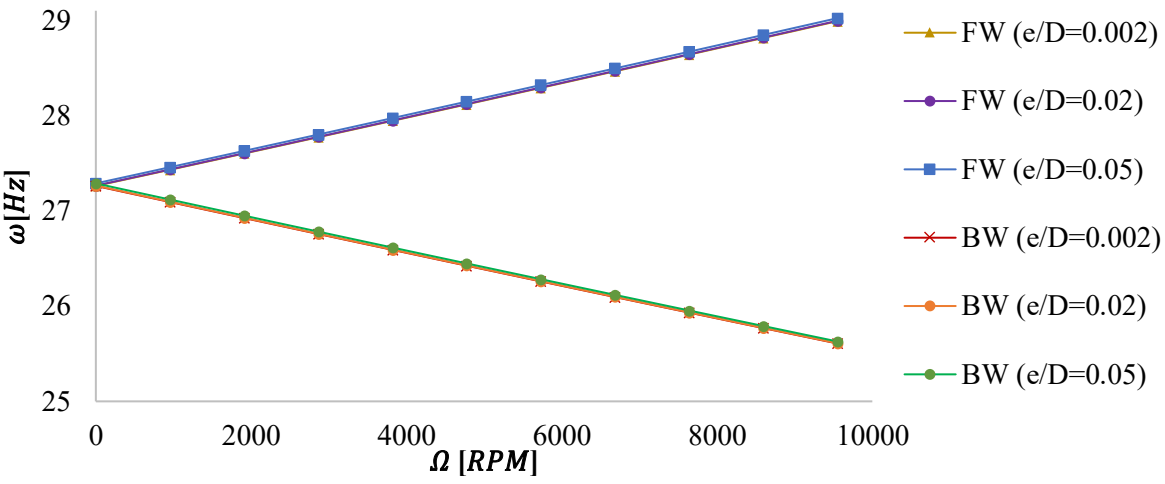

a)

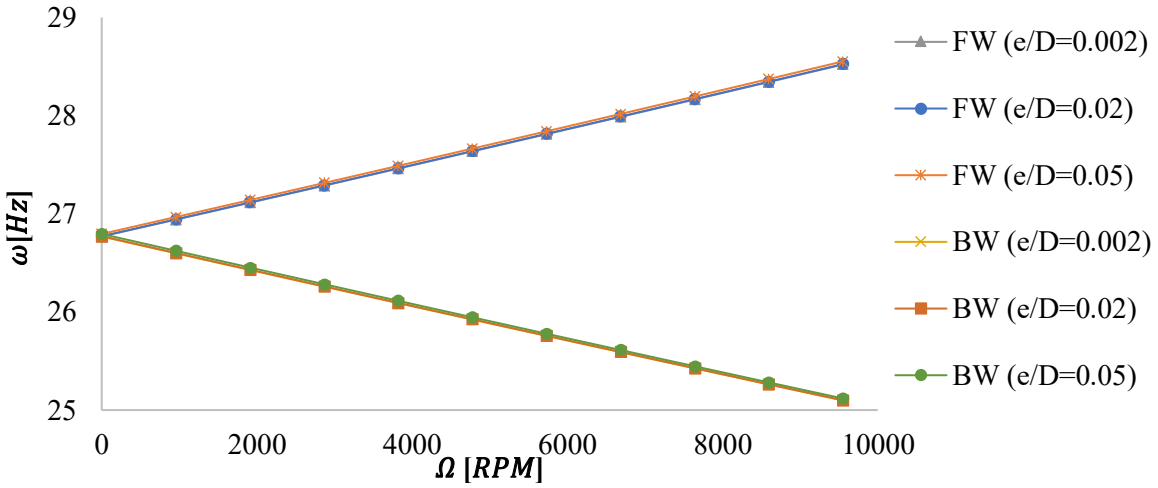

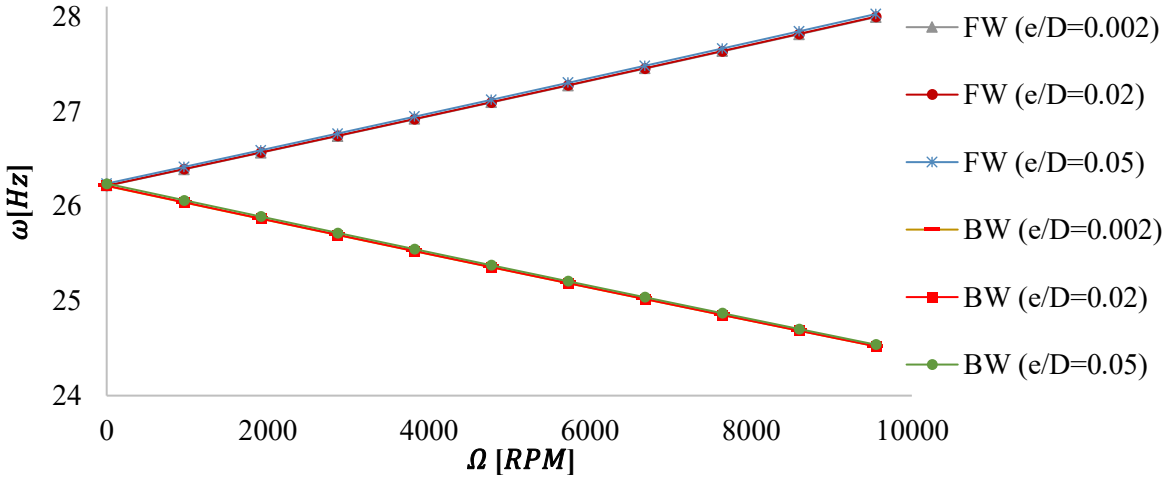

Figure IV-7 Campbell's diagrams for different thickness ratios of even PFGM.
a) $\alpha = 0$; b) $\alpha = 0.2$; c) $\alpha = 0.5$

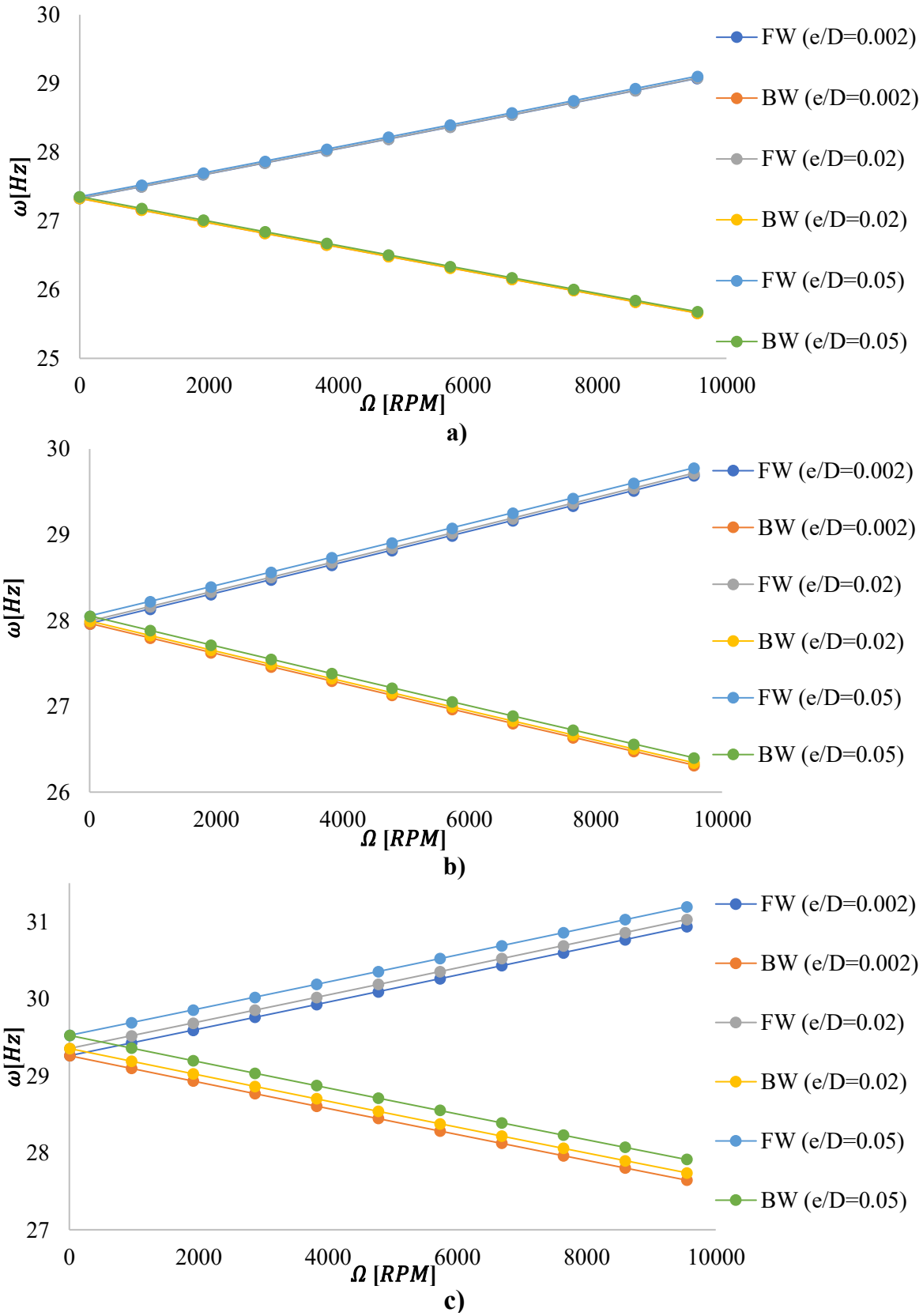

Figure IV-8 Campbell's diagrams for different thickness ratios of uneven PFGM.
a) $\alpha = 0$; b) $\alpha = 0.2$; c) $\alpha = 0.5$

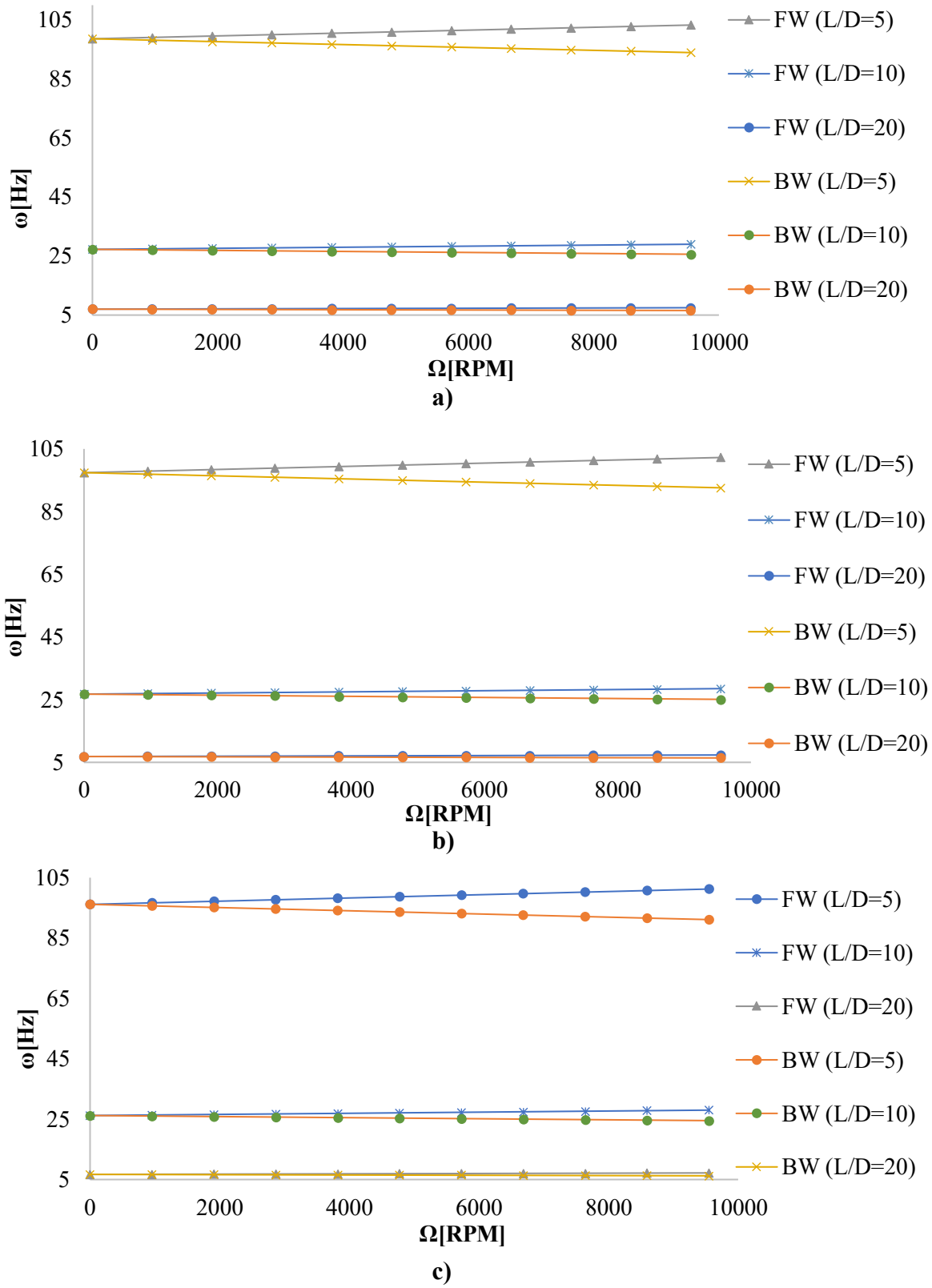

Figure IV-9 Campbell's diagrams for different slenderness ratios of even PFGM.
a) $\alpha = 0$; b) $\alpha = 0.2$; c) $\alpha = 0.5$.

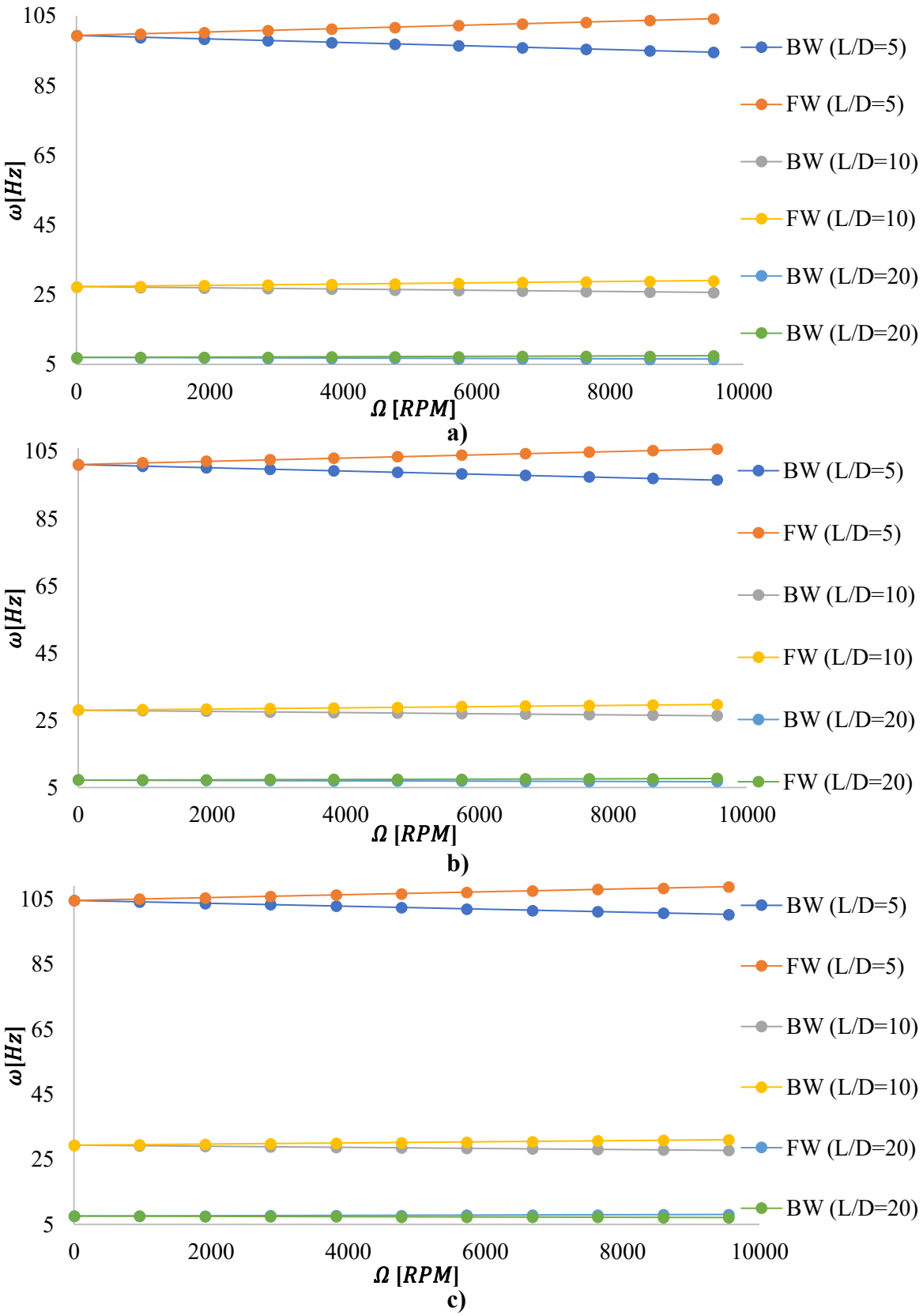

Figure IV-10 Campbell's diagrams for different slenderness ratios of uneven PFGM. a) $\alpha = 0$; b) $\alpha = 0.2$; c) $\alpha = 0.5$.

IV.3. Critical Speed of PFGM shaft

IV.3.1. Effect of geometric parameters and boundary conditions

The graphs in Figure V-11 illustrate the first critical speed (Ω in RPM) of an even PFGM rotating shaft as a function of the porosity volume fraction α for different boundary conditions. Additionally, the effect of varying the L/D parameter is shown in Figure V-11-a ($L/D = 5$), V-11-b ($L/D = 10$), and V-11-c ($L/D = 20$) with $e/D = 0.02. n = 0.5$.

It can be observed that the critical speed decreases slightly as α increases under S boundary conditions, while it remains relatively constant with slight fluctuations as α increases under the SC boundary conditions. At $L/D = 5$, the critical speed increases slightly with increasing α under clamped boundary conditions, and for the other slenderness ratios, the critical speed is the highest among the three boundary conditions.

Under SC-BC and C-BC, the critical speeds are less sensitive to changes in porosity compared to S-BC. Under S-BC, an increase in porosity results in a reduction in critical speed, indicating a decrease in overall stiffness. The critical speed decreases as the length L increases or the diameter D decreases, leading to a higher L/D ratio. Porosity influences both the stiffness and mass distribution of the structure, thereby affecting the critical speeds.

Understanding the effect of porosity on critical speeds is crucial for designing rotors made from functionally graded materials or porous materials. Ensuring that the operating speeds are well below the critical speeds for all expected porosity levels to guarantee the safe operation of the rotor system. Additionally, monitoring changes in porosity during operation due to factors such as wear and corrosion can facilitate the predictive maintenance and avoiding unexpected resonance.

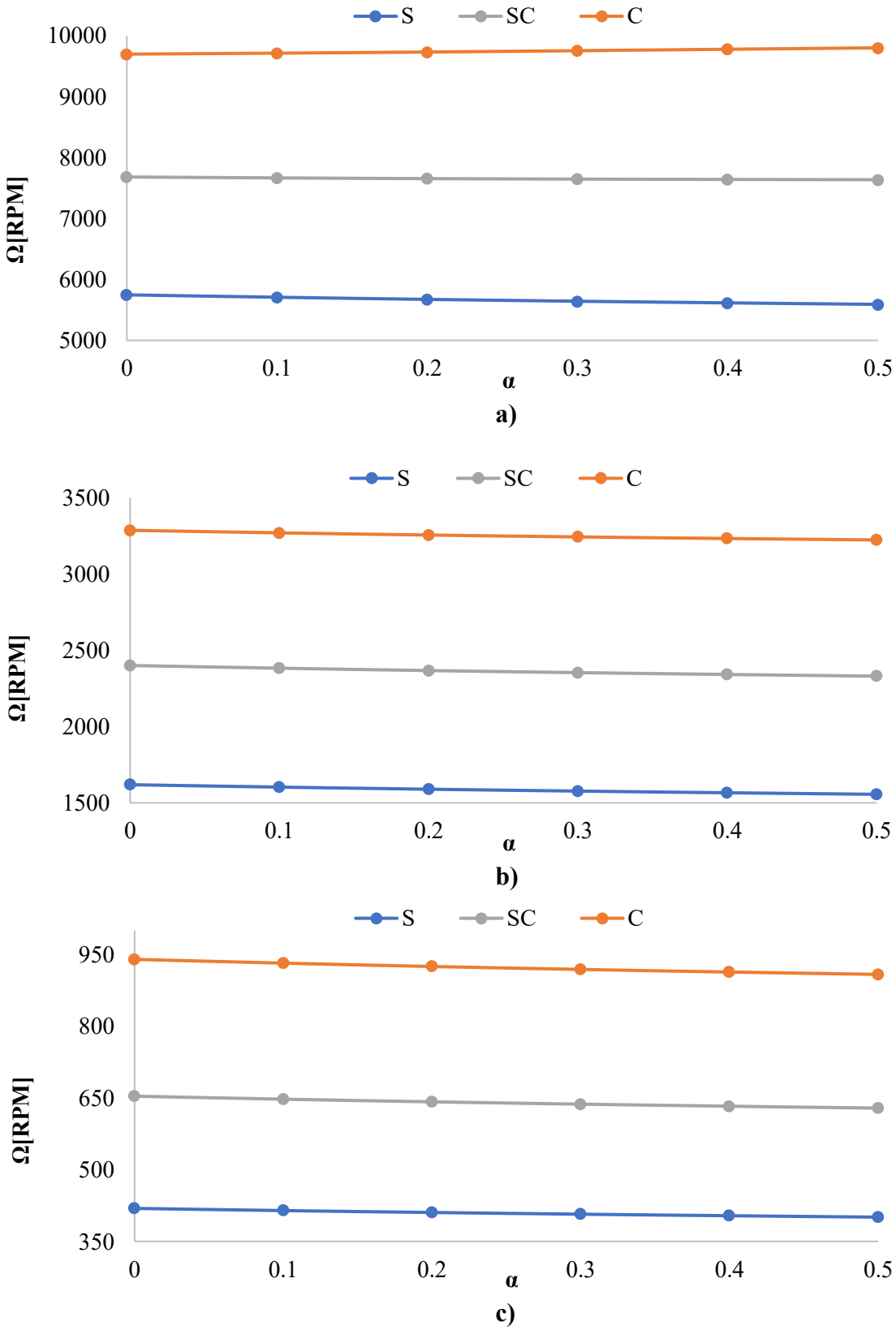

Figure IV-11 First critical speeds in function in porosity α of Even PFGM under various boundary conditions (S-BC, C-BC, and SC-BC). a) $L/D = 5$; b) $L/D = 10$; c) $L/D = 20$.

IV.3.2. The influence of the FGM types in critical speed of PFGM shaft

The two figures (V-12 and V-13) illustrate the relationship between the first critical speed, porosity coefficient α, and the type of FGMs (SS-Ni, Ni-ZrO_2, Ni-Al_2O_3) for both even and uneven porosity distributions respectively, under simply supported boundary condition, $L/D = 10, e/D = 0.02, and\ n = 0.5$.

First, the even porous FGMs, the critical speed decreases as the porosity coefficient α increases for all three materials. This is the expected behavior, as increasing porosity reduces the material's stiffness more significantly than its mass, thereby lowering the critical speed. In contrast, for the uneven porous FGMs, the critical speed increases with increasing α for all three materials. This is a unique and significant finding. The increase suggests that for this specific uneven porosity distribution, the reduction in mass is more dominant than the reduction in stiffness, leading to a net increase in the critical speed. This indicates that the geometric arrangement of the pores, not just their volume fraction, is a critical factor in determining the dynamic behavior of the shaft.

Next, in both the even and uneven porosity cases, the Ni-Al_2O_3 FGM consistently has the highest critical speed, while the SS-Ni FGM has the lowest. This is because the critical speed is directly related to the material's stiffness-to-mass ratio. Since aluminum oxide (Al_2O_3) is a very stiff and relatively light ceramic, the Ni-Al_2O_3 composite provides the best dynamic performance. Zirconia (ZrO_2) is also a strong ceramic, placing the Ni-ZrO_2 composite in the middle, and the all-metallic SS-Ni shaft has the lowest critical speed due to its lower stiffness-to-mass ratio.

In conclusion, these figures highlight that both the material composition and the porosity distribution pattern are critical in controlling the critical speed of porous FGM shafts. While a higher porosity generally lowers the critical speed in even distributions, a specific uneven distribution can have the opposite effect, offering a potential design advantage for achieving higher operational speeds by carefully tailoring the porosity.

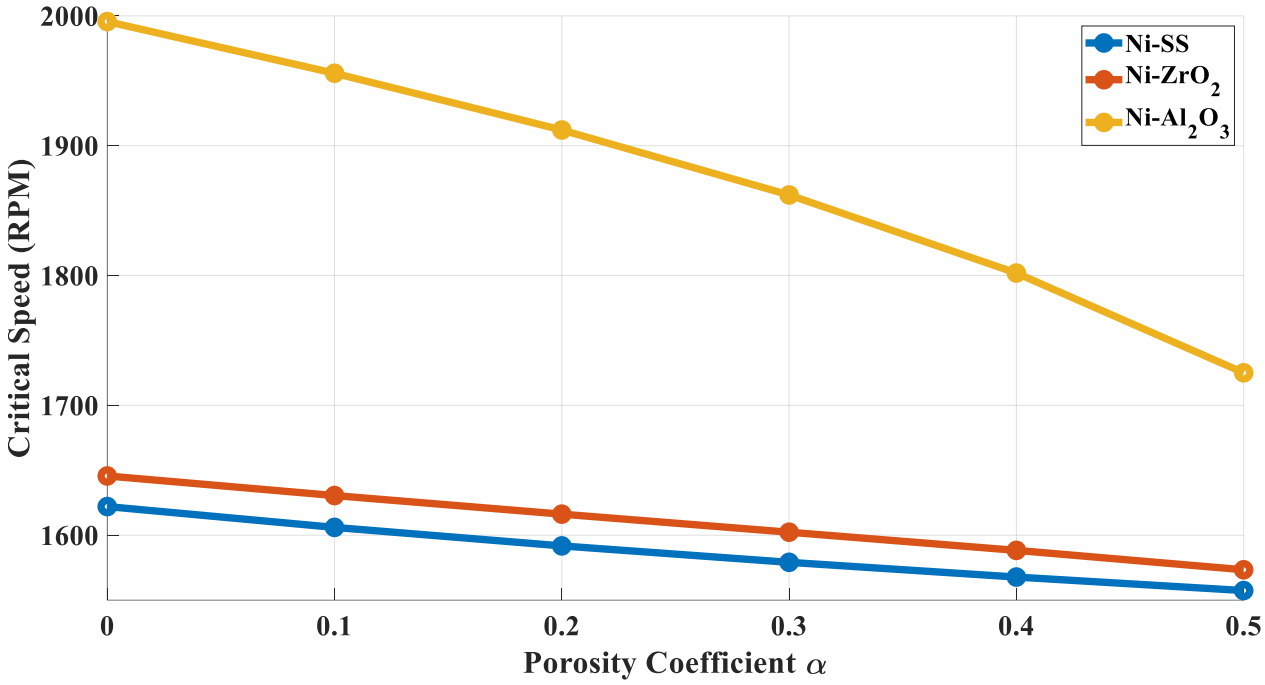

Figure IV-13 First critical speeds in function in porosity for deferent even Porous FGMs types (SS-Ni, Ni-ZrO2, and Ni-Al2O3) in function in porosity α.

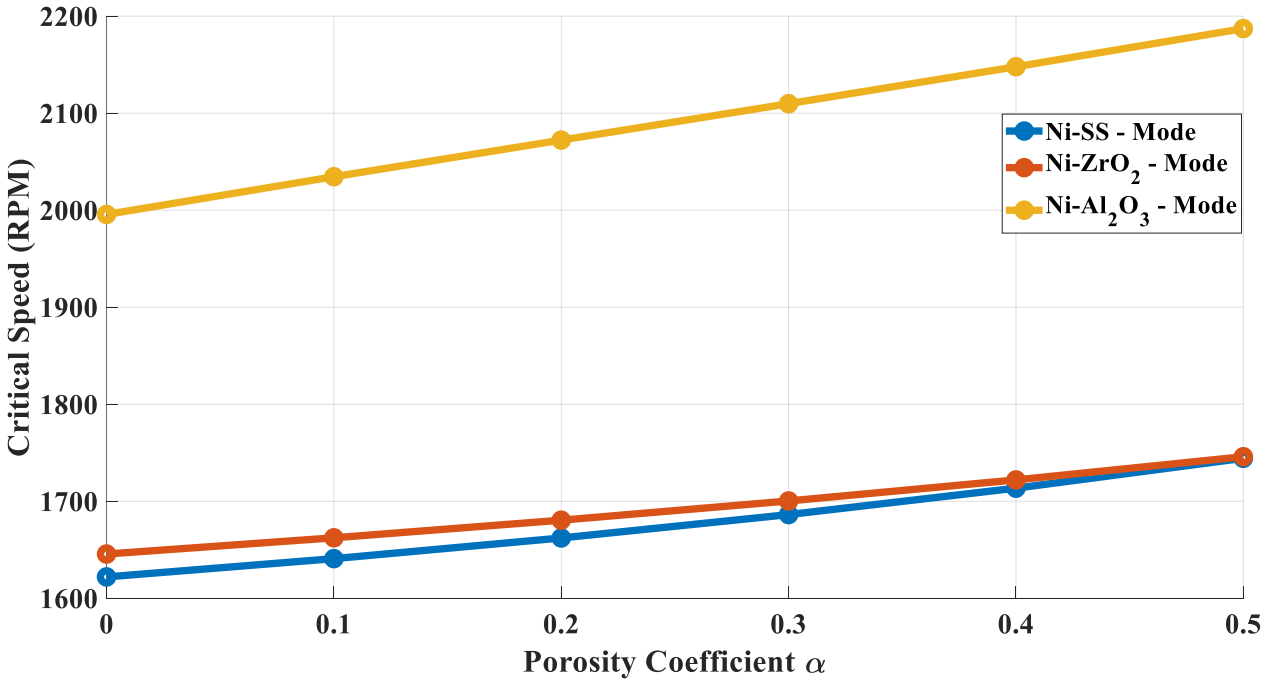

Figure IV-12 First critical speeds in function in porosity for deferent uneven Porous FGMs types (SS-Ni, Ni-ZrO2, and Ni-Al2O3) in function in porosity α.

IV.3.3. The influence of the bearing in critical speed of PFGM shaft

The influence of bearing stiffness on the critical speed of PFGM shafts with symmetric supports is illustrated in Figures IV-14 and IV-15 for two porosity distributions even and uneven respectively. For the case of even porosity distribution, the results show a clear monotonic decrease in the first critical speed with increasing porosity coefficient α. This trend is physically consistent, since a higher porosity fraction reduces the overall stiffness of the shaft while simultaneously lowering its effective density, with the stiffness reduction being dominant. The role of the bearings is observed as a vertical shift: higher bearing stiffness values ($K_{yy} = K_{zz} = 1.74\ e8$) elevate the critical speed across all porosity levels compared to lower bearing stiffness ($K_{yy} = K_{zz} = 1.74\ e6$), while the slope of the decline with porosity remains nearly identical. This indicates that, in the even porosity case, the shaft material properties govern the trend, whereas the bearing stiffness primarily adjusts the baseline of dynamic performance.

In contrast, the case of uneven porosity distribution demonstrates a more complex and non-monotonic behavior. For porosity values up to approximately $\alpha = 0.3 - 0.4$, the critical speed decreases similarly to the even distribution, reflecting the expected softening effect. However, beyond this range a pronounced divergence occurs; the critical speed rises sharply for the systems with lower and moderate bearing stiffnesses, while it increases more gradually in the case of stiff bearings. This phenomenon can be attributed to a mode veering or modal interaction effect**,** wherein the redistribution of mass and stiffness due to uneven porosity shifts the dynamic balance between shaft bending and rotor–bearing coupled modes. Specifically, the uneven porosity concentrates less material near the neutral axis while retaining stiffness at the outer layers, thereby increasing the stiffness-to-mass ratio in higher-order forms. As a result, the rotor may undergo a modal exchange in which the tracked first critical speed corresponds to a higher branch, producing the apparent jump observed in the results.

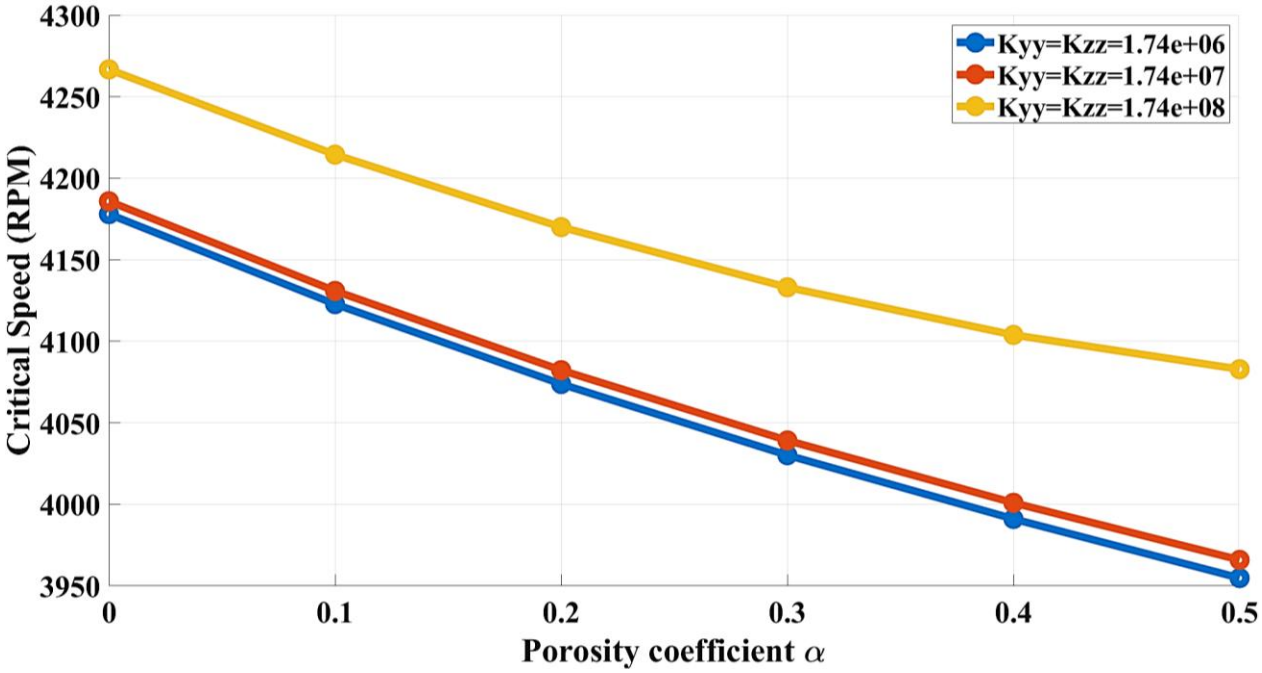

Figure IV-14 First critical speeds in function in porosity of even PFGM shaft, for deferent symmetric Bearing values

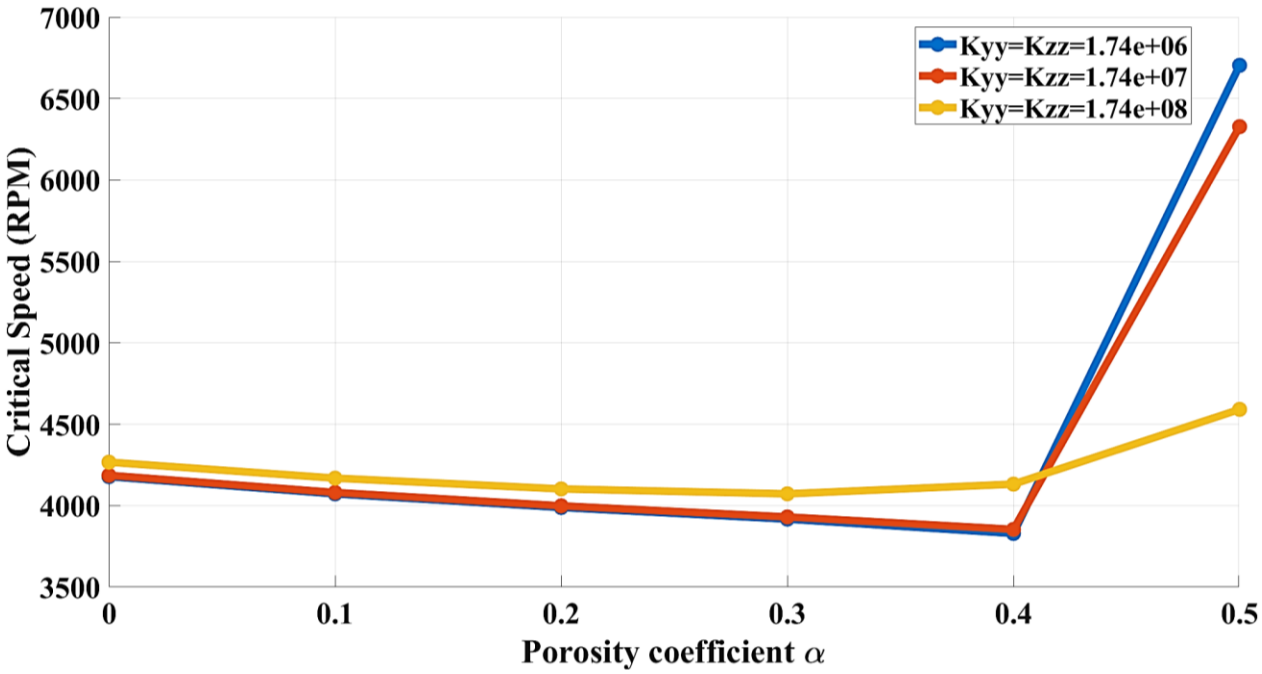

Figure IV-15 First critical speeds in function in porosity of uneven PFGM shaft, for deferent symmetric Bearing values

IV.3.4. The influence of the damping in critical speed of PFGM shaft

The two figures (IV-16 and IV-17) illustrate the variation of the first critical speed with respect to porosity for PFGM shafts under even and uneven porosity distributions respectively, while considering different symmetric damping values.

For the even porosity distribution, the critical speed decreases gradually with increasing porosity coefficient. This trend is expected since porosity weakens the shaft's stiffness due to the reduction in effective load-bearing material, thereby lowering the natural frequencies. However, the influence of damping is clearly visible in the magnitude of the critical speed. Higher damping values tend to reduce the overall level of the critical speed but also smooth out the decline with porosity, suggesting that damping acts as an energy dissipation mechanism that mitigates dynamic instabilities.

In contrast, for the uneven porosity distribution, the critical speed reduction with increasing porosity is more pronounced compared to the even case. This is attributed to the asymmetry in the material distribution, which introduces local stiffness degradation and mass imbalance effects, amplifying the sensitivity of the rotor system to porosity. Moreover, damping still moderates the behavior, but its stabilizing role is less effective in uneven porosity shafts than in even ones. This indicates that asymmetric porosity distributions magnify the detrimental effects of porosity on rotor dynamics, making the system more prone to instability.

The case of $\alpha = 0.5$ is particularly important because it represents a balanced porosity distribution. At this value, the uneven porosity profile becomes nearly symmetric, which reduces the negative influence of asymmetry on shaft stiffness. As a result, the first critical speed for $\alpha = 0.5$ is higher than for other uneven distributions and much closer to the symmetric case. This shows that $\alpha = 0.5$ acts as a special configuration where the shaft regains stability and dynamic performance despite having porosity.

Comparatively, the even distribution demonstrates higher robustness against porosity, while the uneven distribution highlights the critical importance of porosity design in rotor systems. From a design perspective, applying symmetric damping can partially alleviate the negative influence of porosity, but ensuring even porosity distributions remains the most effective strategy to maintain higher critical speeds and overall stability.

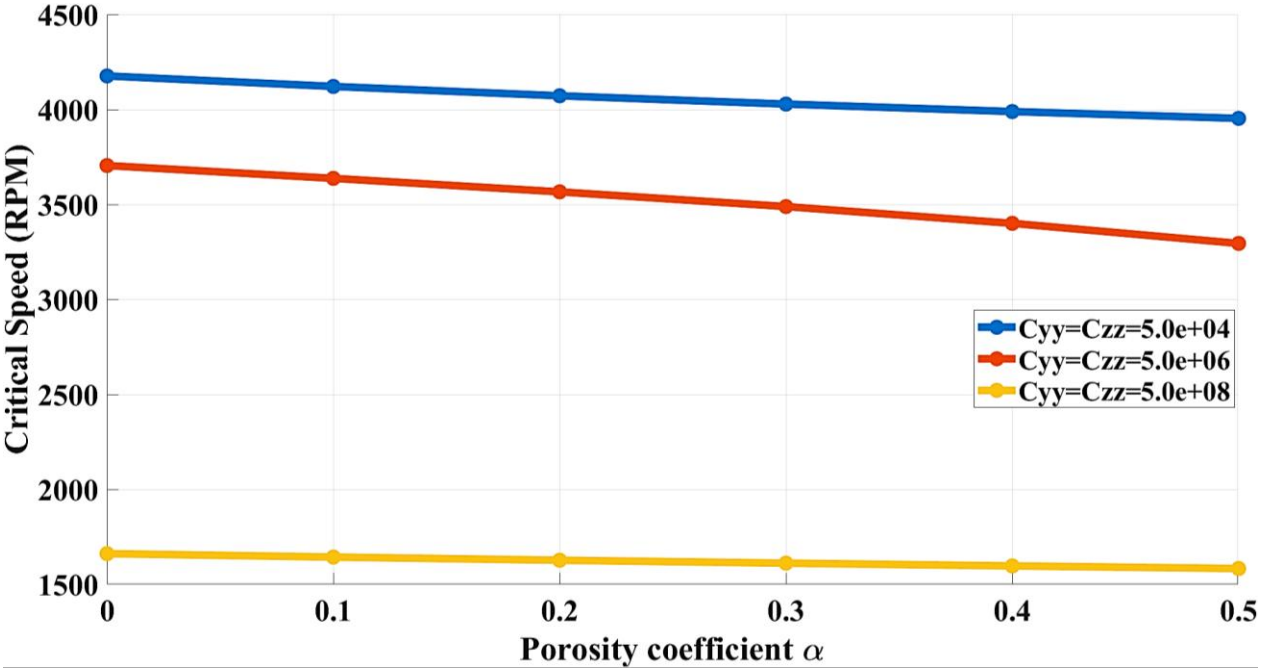

Figure IV-17 First critical speeds in function in porosity of uneven PFGM shaft, for deferent symmetric Damping values

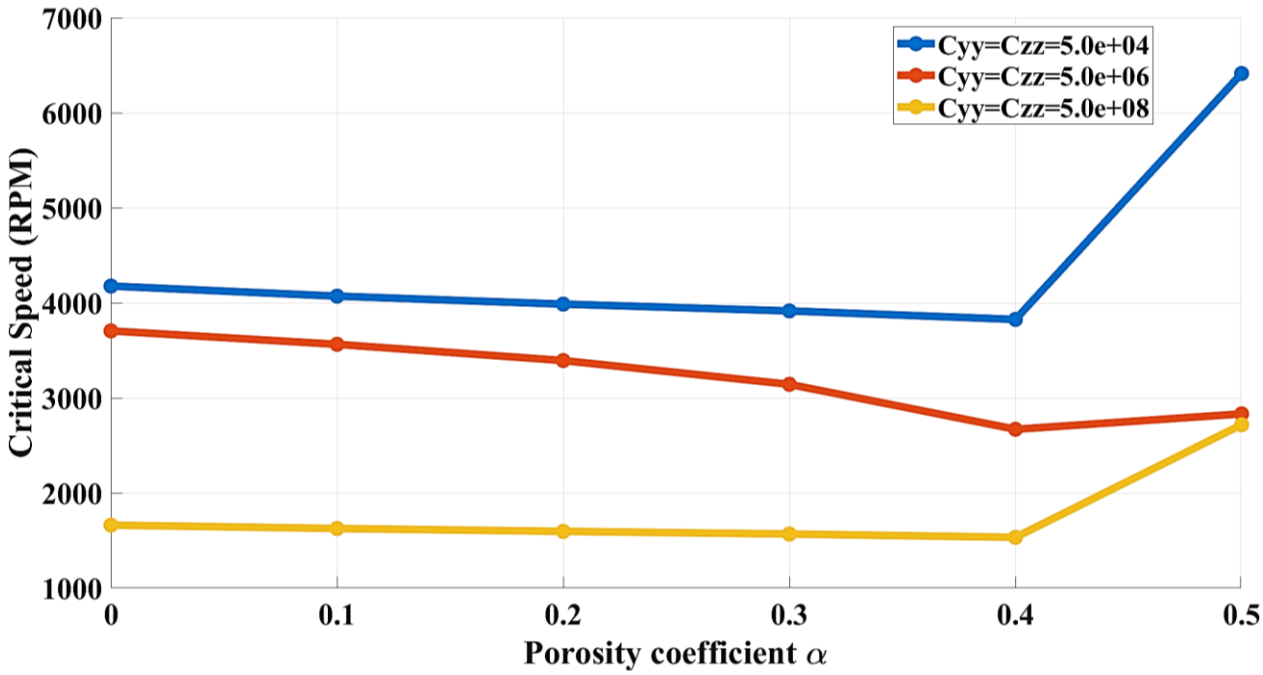

Figure IV-16 First critical speeds in function in porosity of even PFGM shaft, for deferent symmetric Damping values

IV.3.5. The influence of the disk in critical speed of PFGM shaft

This study analyzes how the first critical speeds is affected by two main factors: the mass of an attached disk and the distribution of porosity in the PFGM shaft. The most significant finding is that the disk's mass has a powerful and predictable effect on these critical speeds. Just as a heavy pendulum swing more slowly than a light one, a heavier disk consistently lowers the shaft's critical speeds. This occurs because the greater mass, or inertia, reduces the system's natural vibration frequency, making it unstable at higher speeds.

The distinction in dynamic behavior becomes evident when examining the effect of porosity in the even PFGM shaft (figure IV-18). Here, the critical speed exhibits a monotonic and predictable decrease as the porosity coefficient increases. This linear degradation aligns perfectly with conventional mechanical theory, where a uniform introduction of porosity systematically weakens the shaft's flexural rigidity. This behavior represents a straightforward and reliable engineering trade-off, where the benefit of mass reduction comes at the direct and quantifiable cost of the shaft's dynamic performance, making it a safe choice for design.

In stark contrast, the uneven PFGM shaft (figure IV-19) displays a highly complex and non-monotonic response. Its critical speed initially decreases with porosity but then experiences a sharp dip at a coefficient of $\alpha = 0.4$, followed by a counter-intuitive and significant rise. This phenomenon points to a sophisticated interaction between the shaft's asymmetric stiffness and its vibration mode shape. The trough suggests the creation of a new point of instability, caused by the specific pattern of material removal, which poses a significant operational risk. The subsequent recovery, however, reveals that the relationship between the material's architecture and its stability is far from linear and can yield unexpected performance enhancements at higher porosity levels.

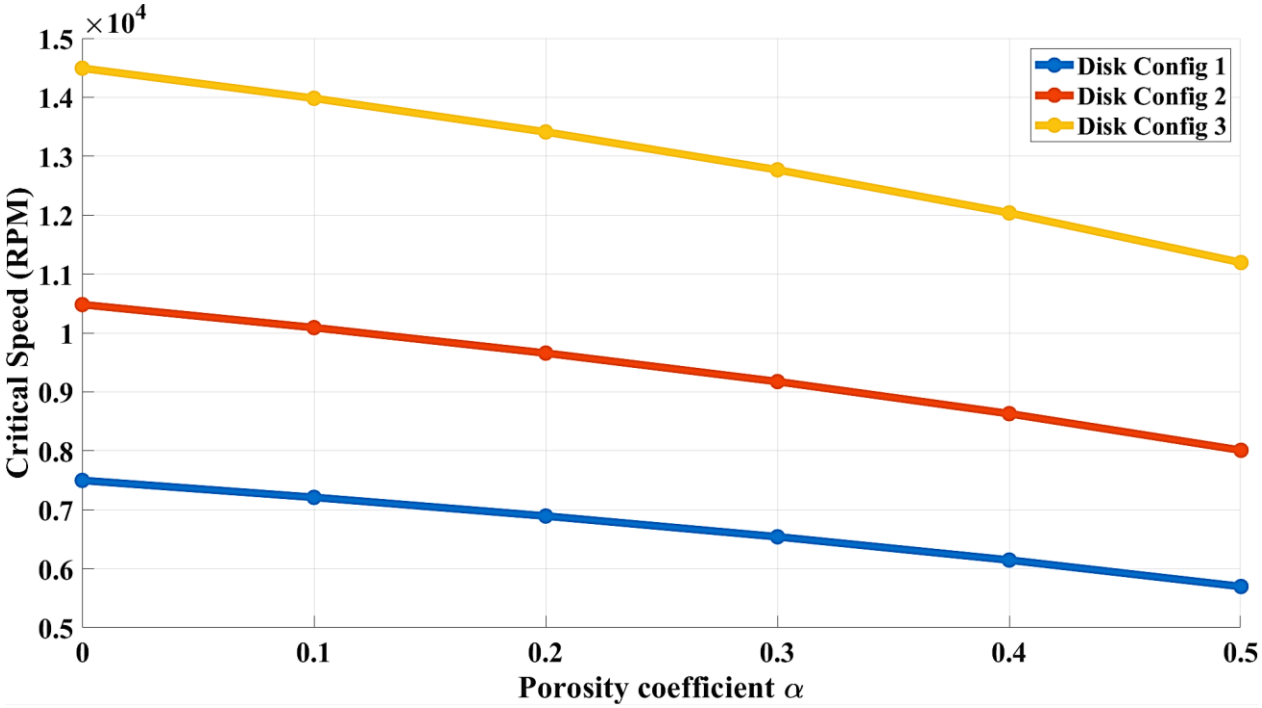

Figure IV-18 First critical speeds in function in porosity of even PFGM shaft, for deferent configurations of the disk

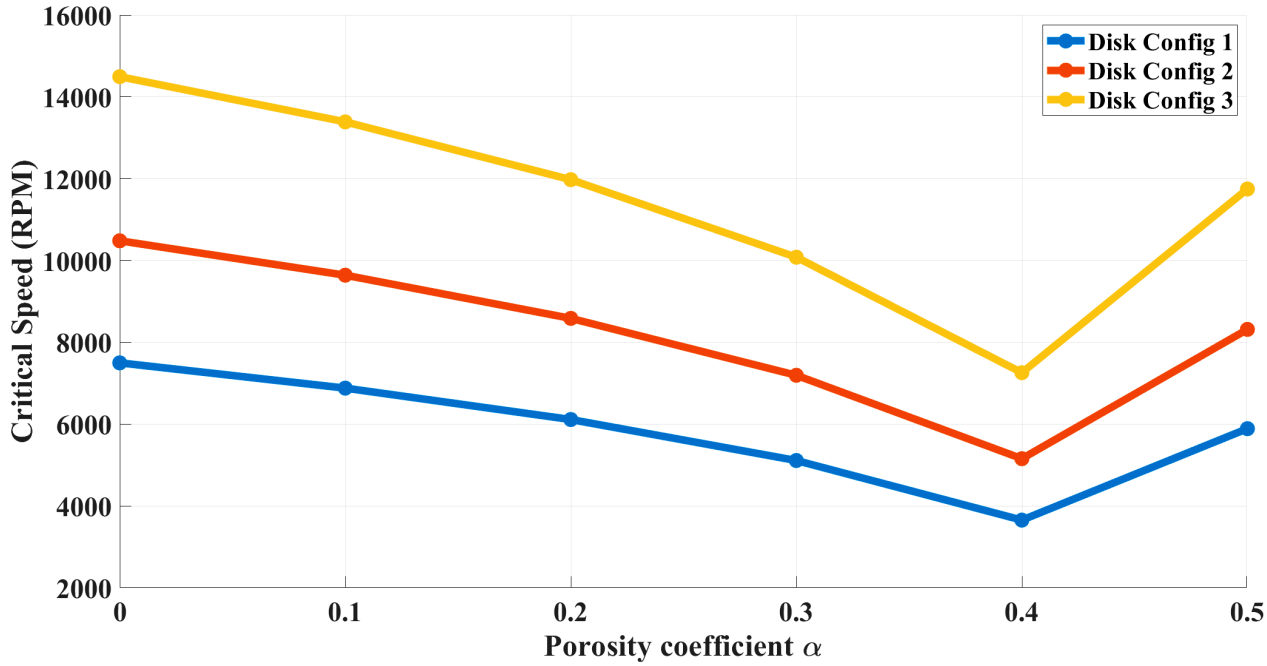

Figure IV-19 First critical speeds in function in porosity of uneven PFGM shaft, for deferent configurations of the disk

IV.4. Parametric study of FGP shaft

This parametric study aims to explore the effects of different porosity distributions on the dynamic behavior of FGP shafts. By systematically analyzing both symmetric and non-symmetric configurations, we seek to uncover insights that can inform the design of more efficient, high-performance shafts. Understanding the implications of these distributions will contribute significantly to the ongoing development of FGP materials, enhancing functionality across various engineering applications. Through this research, we aspire to unlock the full potential of FGP materials in modern engineering solutions, paving the way for innovative advancements in performance and reliability.

IV.4.1. Porosity Influence of FGP shaft under varying boundary conditions

The following graphs Figure IV-20 and IV-21 illustrate the natural frequencies of the first three vibrational modes for both symmetric and non-symmetric porosity distributions receptively for FGP shafts, analyzing the effects of the porosity coefficient e_0 under different boundary conditions: Simply Supported (S-BC), Clamped-Supported (SC-BC), and Clamped (C-BC).

The dynamic behavior of FGP shafts is influenced by the porosity coefficient e_0, the distribution of the material gradient (symmetric or non-symmetric), and the type of boundary conditions applied. As the porosity coefficient increases, a consistent decline in natural frequencies is observed across all modes. This trend is primarily attributed to the reduction in material stiffness and the corresponding increase in structural flexibility. The fundamental (first) mode is especially sensitive to this change, showing the most significant frequency reduction.

Boundary conditions play a crucial role in determining the shaft's dynamic characteristics. Clamped boundary conditions provide greater restraint and structural rigidity, resulting in higher natural frequencies and reduced sensitivity to porosity variations. In contrast, simply supported conditions allow for more flexibility, making the system more susceptible to reductions in stiffness caused by increased porosity. This sensitivity is particularly prominent in configurations with non-symmetric material distributions, where stiffness and mass are not uniformly distributed.

Comparing symmetric and non-symmetric FGP distributions reveals distinct differences in vibrational behavior. Symmetric distributions tend to produce more gradual and stable changes in

natural frequencies as porosity increases. On the other hand, non-symmetric distributions cause more pronounced and irregular variations, due to the uneven allocation of material properties, which disturbs the dynamic balance of the system. These differences underscore the importance of considering not only the amount of porosity but also how it is spatially distributed within the shaft.

In conclusion, the porosity coefficient, distribution type, and boundary condition collectively shape the dynamic performance of FGP shafts. For optimal vibration control and structural integrity, designers must carefully balance these parameters. Particularly in rotor applications, where precise dynamic behavior is critical, an informed selection of porosity profiles and boundary conditions can significantly enhance performance and reliability.

This analysis underscores the importance of understanding the interplay between porosity, boundary conditions, and dynamic behavior in FGP shafts. The findings provide valuable insights for engineers and designers aiming to optimize the performance and reliability of components utilizing FGP materials in various applications. Future studies could explore alternative porosity distribution strategies to enhance dynamic stability while maintaining desired material properties.

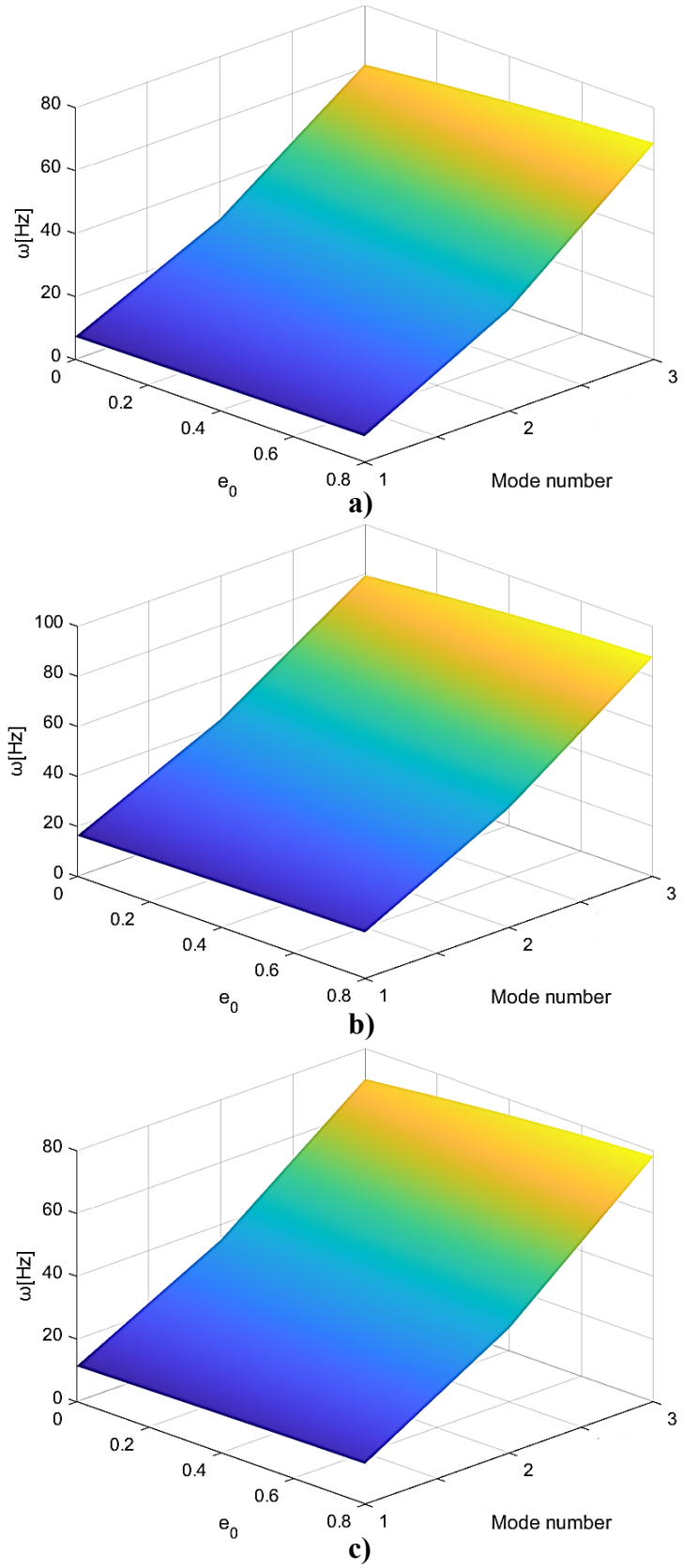

Figure IV-20 First three modes natural frequencies of various non-symmetric FGP shaft under different BCs, a) S-BC, b) C-BC, and c) SC-BC

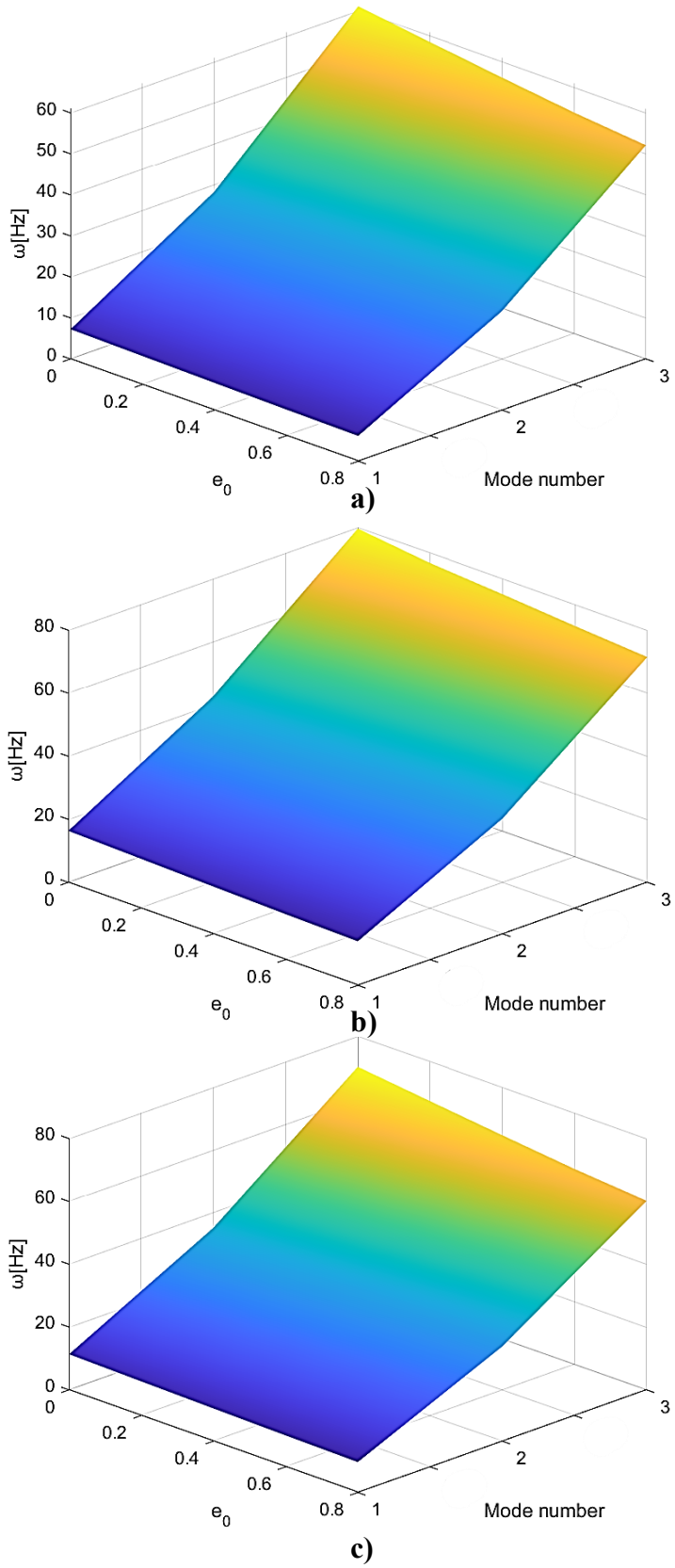

Figure IV-21 First three modes natural frequencies of symmetric FGP shaft under different BCs, a) S-BC, b) C-BC, and c) SC-BC

IV.4.2. Campbell's diagrams for FGP shafts

IV.4.2.1. Thickness ratio influence (e/D)

The Campbell's diagrams illustrate in the Figures IV-22 and IV-23 for both symmetric and non-symmetric porosity distributions respectively for FGP shafts under SC-BC conditions highlights how thickness ratio (e/D) and porosity significantly influence dynamic performance. For a solid shaft $(e_0 = 0)$, both FW and BW modes exhibit high and stable natural frequencies, reflecting excellent stiffness and minimal vibrational disturbances. This configuration demonstrates optimal behavior, with the SC-BC providing strong structural integrity.

When the symmetric porosity is introduced $(e_0 = 0.2)$, a reduction in natural frequencies becomes evident. The FW and BW modes remains relatively stable, with a small increased variability, indicating that even limited porosity can reduce stiffness and make the system more sensitive to rotational speed changes. At high porosity levels $(e_0 = 0.8)$, the reduction in stiffness is more severe. The FW and BW modes begins at a much lower frequency, suggesting greater susceptibility to dynamic behavior particularly in non-symmetric porosity distributions.

At the ratio $e/D = 0.02$ and with high porosity values $(e_0 = 0.2, 0.8)$, it is observed that the curves of FW and BW do not match the conditions $e/D = 0.002$ and $e/D = 0.05$. This behavior is explained by the increased effect of gyroscopic torque due to mass redistribution with reduced bending stiffness, resulting in a clearer separation between the FW and BW branches. In comparison, very small ratios $(e/D = 0.002)$ do not show much difference due to limited mass redistribution, while larger ratios $(e/D = 0.05)$ You regain some of the rigidity, and the curves appear more convergent. Thus, the state of $e/D = 0.02$ represents an average state sensitive to the effects of porosity and gyroscope.

Finally, the study underscores the impact of porosity distribution patterns. Symmetric distributions result in smoother and more predictable frequency behavior, while non-symmetric distributions amplify variability, especially at higher porosities. These findings emphasize the importance of optimizing porosity levels, thickness ratios, and boundary conditions together to achieve the desired balance between flexibility and stability in FGP shaft design.

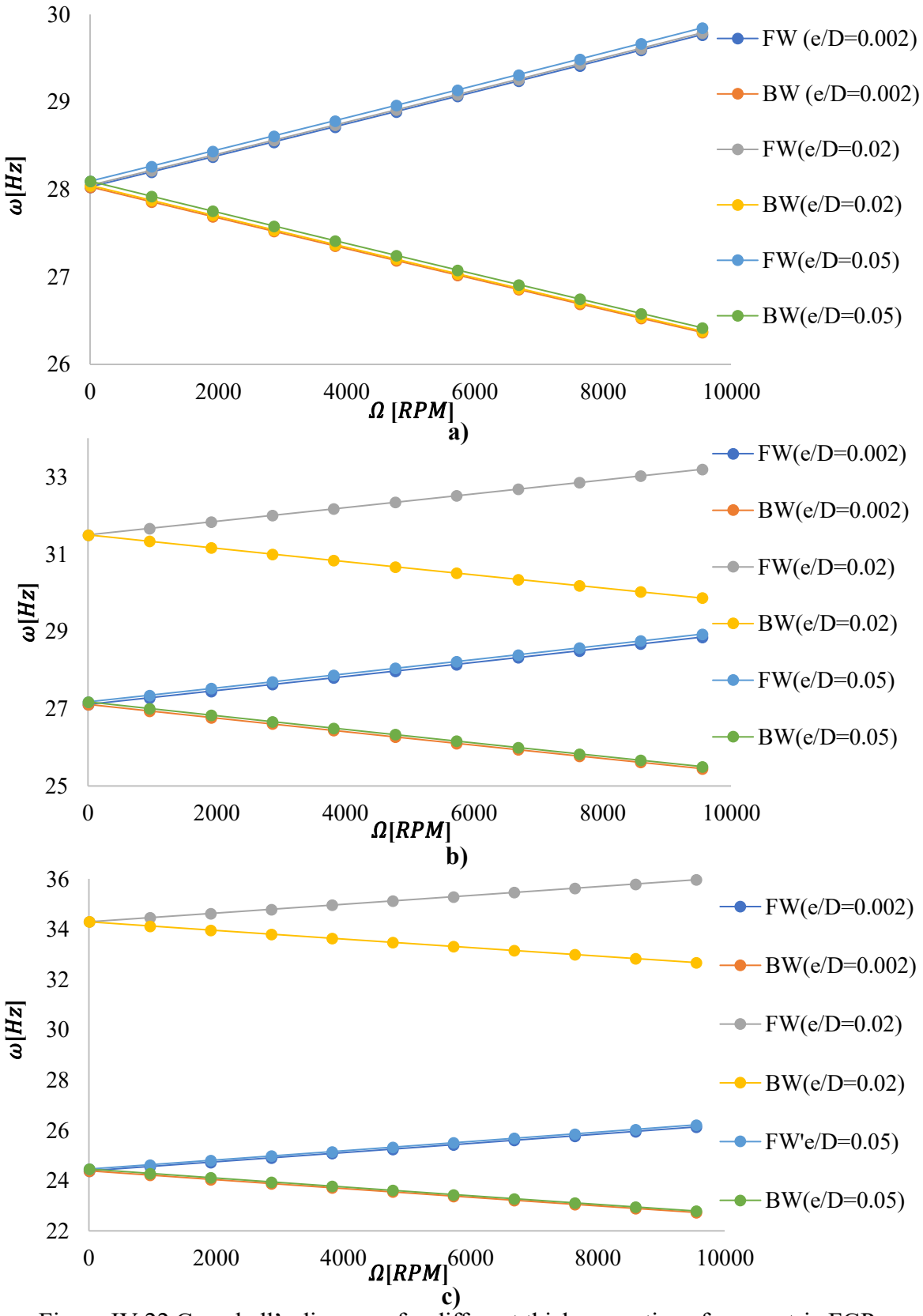

Figure IV-22 Campbell's diagrams for different thickness ratios of symmetric FGP.
a) $e_0 = 0$; b) $e_0 = 0.2$; c) $e_0 = 0.8$

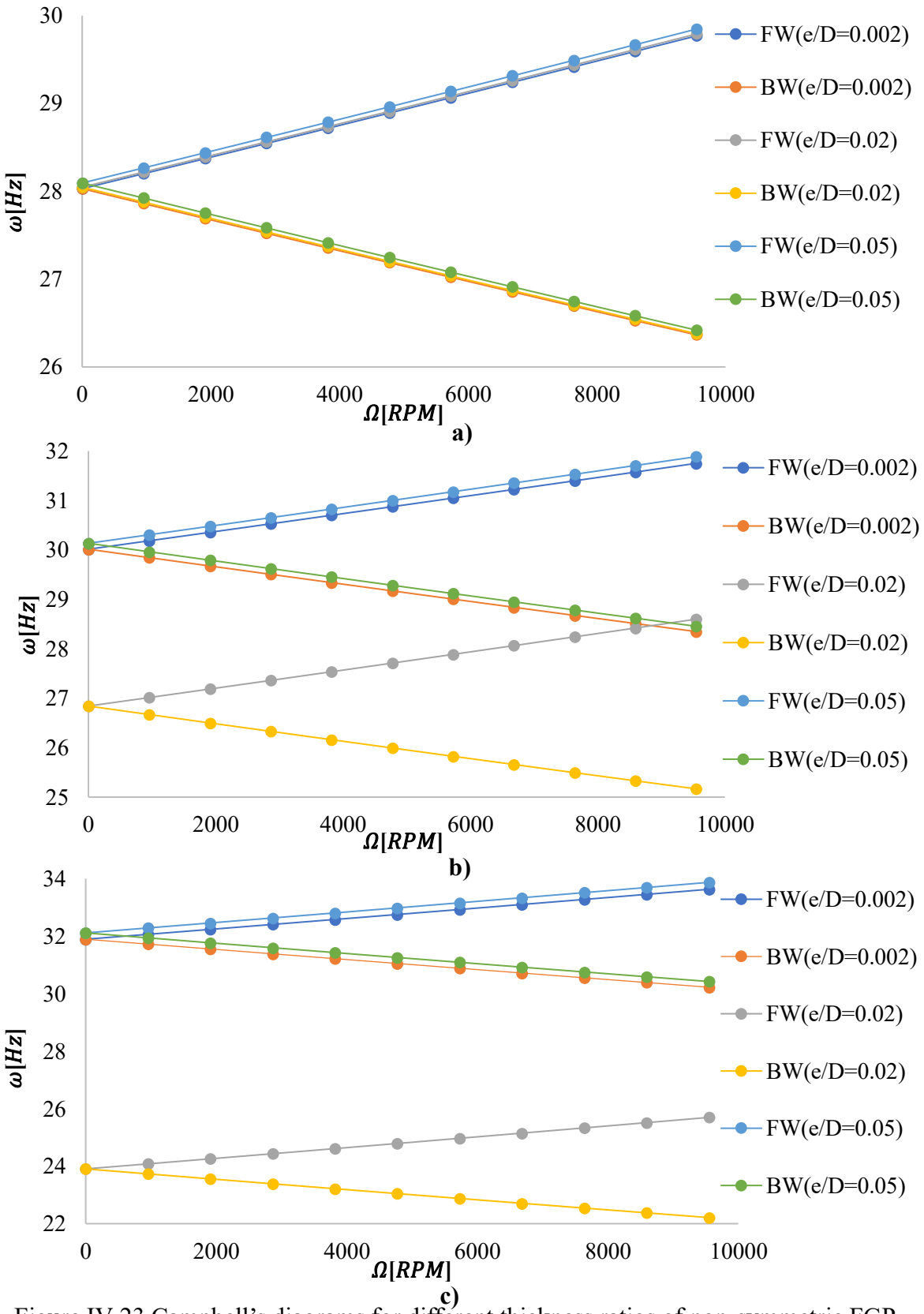

Figure IV-23 Campbell's diagrams for different thickness ratios of non-symmetric FGP.
a) $e_0 = 0$; b) $e_0 = 0.2$; c) $e_0 = 0.8$

IV.4.2.2. Slenderness ratio influence (L/D)

These Campbell's diagrams (Figure IV-24 and IV-25) illustrate the influence of slenderness ratio (L/D) and porosity coefficient (e_0) of FGP shafts under a SC–BC. A clear difference is seen between the symmetric and non-symmetric porosity distributions respectively, especially as the porosity level increases.

For the symmetric case, the results show that increasing the slenderness ratio (L/D) reduces the natural frequencies of both FW and BW modes, with the reduction being more pronounced for the higher modes. Shorter shafts ($L/D = 5$) exhibit much stiffer behavior, reflected in higher frequencies and stronger FW/BW splitting as the rotation speed increases. In contrast, slender shafts ($L/D = 20$) present significantly lower frequency bands, almost flat with respect to Ω, suggesting a reduced gyroscopic effect and higher susceptibility to flexibility. Regarding porosity, the solid shaft ($e_0 = 0$) shows the highest stiffness, while increasing porosity levels ($e_0 = 0.2, 0.8$) shift the frequency curves downward.

For the non-symmetric case, similar trends with L/D are observed, but the impact of porosity distribution is more significant. Non-symmetry introduces additional stiffness degradation in one direction, which amplifies the FW/BW separation. At higher porosity levels ($e_0 = 0.8$), the frequency reduction is more severe than in the symmetric case, especially for small shafts.

Overall, the results indicate that both slenderness ratio and porosity distribution play governing roles in the dynamic response of FGP rotors. Short and dense (solid or low-porosity) shafts are more resistant to whirl instability, while slender and highly porous shafts—particularly with non-symmetric distributions are more vulnerable to stiffness degradation and reduced frequency separation. This has important implications for the design of lightweight porous-graded rotors, where trade-offs between weight reduction, stiffness, and dynamic stability must be carefully balanced.

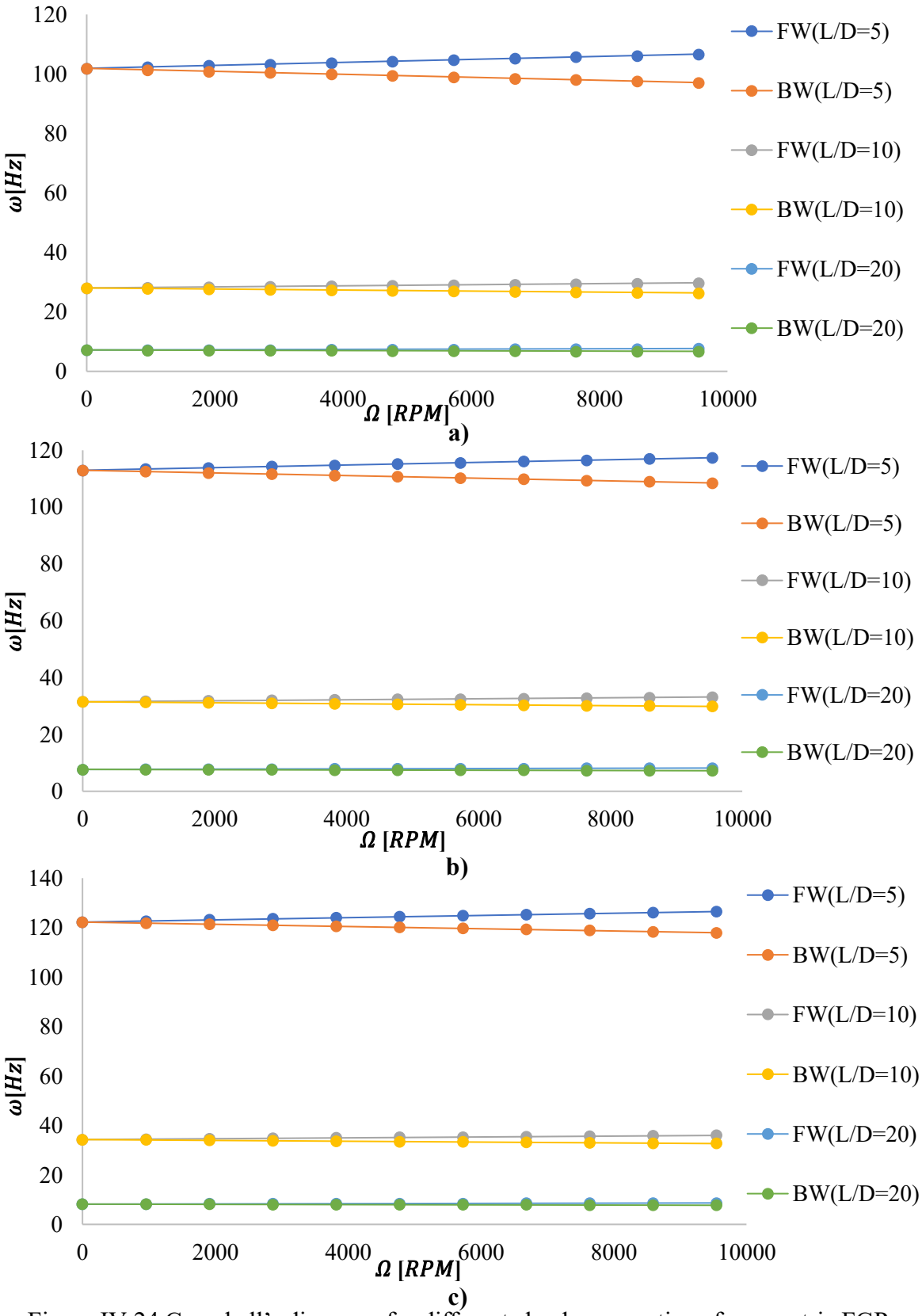

Figure IV-24 Campbell's diagrams for different slenderness ratios of symmetric FGP.
a) $e_0 = 0$; b) $e_0 = 0.2$; c) $e_0 = 0.8$

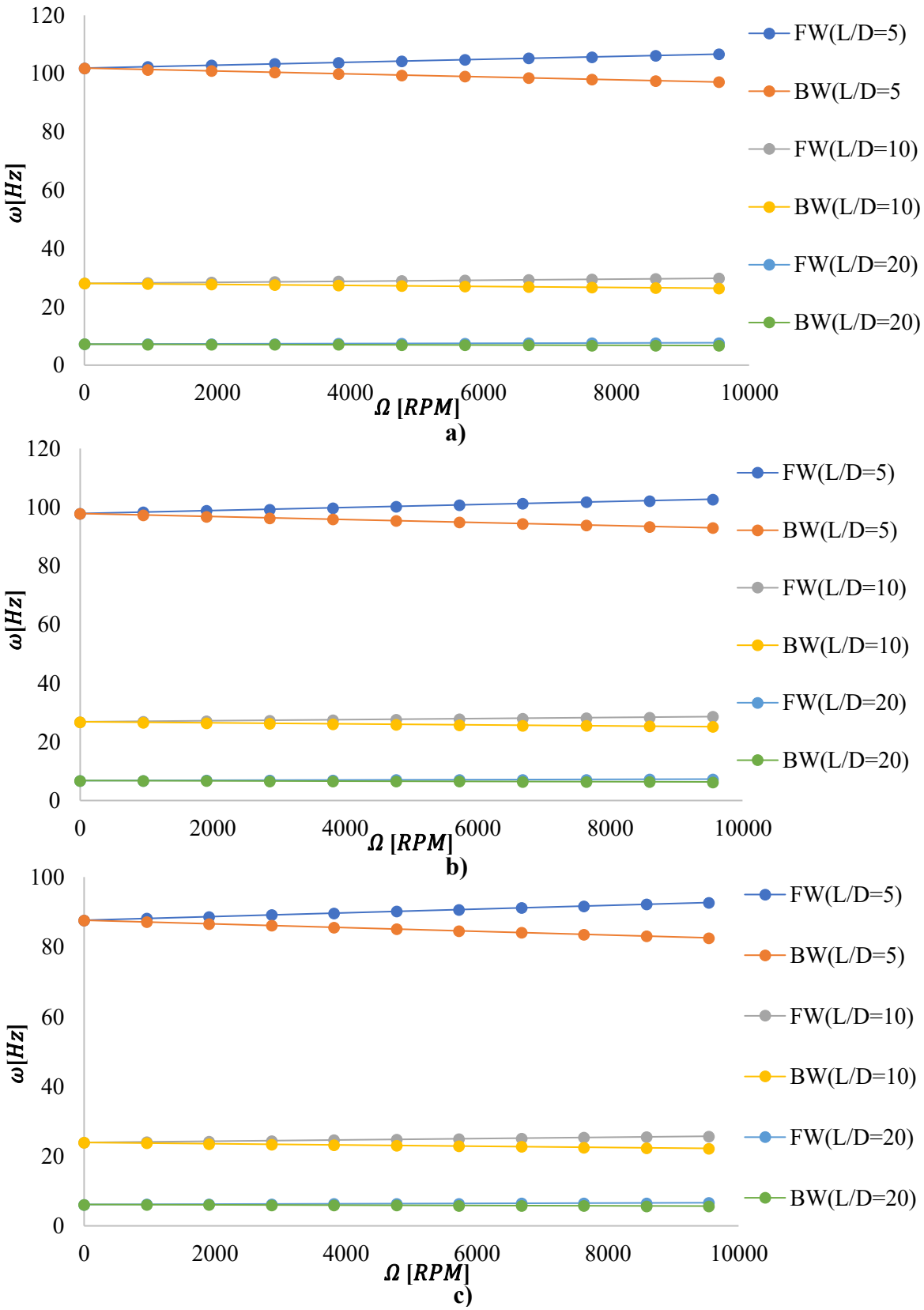

Figure IV-25 Campbell's diagrams for different slenderness ratios of non-symmetric FGP. a) $e_0 = 0$; b) $e_0 = 0.2$; c) $e_0 = 0.8$

IV.4.3. Material influence in critical speed of FGP shaft

The figures IV-26 and IV-27 highlight the effect of porosity coefficient (e_0) on the first mode critical speed of FGP shafts for different material combinations (SS, ZrO_2, and Al_2O_3), considering symmetric and non-symmetric porosity distributions respectively.

In the symmetric case, the critical speed increases with porosity up to a certain point before slightly saturating. For SS- and ZrO_2 FGP shaft, the growth is moderate: e.g., for SS, the critical speed rises from $\sim 1650\ RPM$ at $e_0 = 0$ to $\sim 1880\ RPM$ at $e_0 = 0.6 - 0.8$, a $\sim 14\%$ increase. For ZrO_2, the increase is from $\sim 1780\ RPM$ to $\sim 2030\ RPM$, about $\sim 14\%$ as well. In contrast, Al_2O_3 FGP shaft shows the most pronounced improvement, rising from $\sim 3250\ RPM$ at $e_0 = 0$ to $\sim 3730\ RPM$ at $e_0 = 0.6$ ($\approx 15\%$ increase) before slightly leveling off. This behavior is linked to the fact that symmetric porosity redistributes the stiffness uniformly across the cross-section, reducing the negative influence of porous while retaining relatively high bending rigidity. The result is that the shaft, especially with stiff ceramics like Al_2O_3, becomes dynamically more resistant and achieves higher critical speeds.

In the non-symmetric case, the effect of porosity is reversed: the critical speed decreases steadily with e_0 for all material types. For SS, the drop is from $\sim 1660\ RPM$ at $e_0 = 0$ to $\sim 1500\ RPM$ at $e_0 = 0.8$ ($\approx 10\%$ decrease). For ZrO_2, it decreases from $\sim 1780\ RPM$ to $\sim 1580\ RPM$ ($\approx 11\%$ reduction). The most significant reduction occurs for Al_2O_3, where the critical speed decreases from $\sim 3260\ RPM$ at $e_0 = 0$ to $\sim 2850\ RPM$ at $e_0 = 0.8$ ($\approx 13\%$ decrease). The deterioration is caused by the uneven stiffness distribution: when porosity is concentrated asymmetrically, bending stiffness weakens in one direction, leading to a lower dynamic stiffness and consequently lower critical speed.

Comparatively, Al_2O_3 FGP shafts always achieve the highest critical speeds due to their superior stiffness, while SS shafts give the lowest values, with ZrO_2 in between. A symmetric porosity distribution enhances critical speed by about $10 - 15\%$ as e_0 increases, offering a design advantage for lightweight, high-speed rotors. In contrast, a non-symmetric porosity distribution reduces critical speed by a similar margin, acting as a destabilizing factor. Thus, symmetric porosity is beneficial for improving dynamic stability, whereas non-symmetric porosity should be minimized in rotor design.

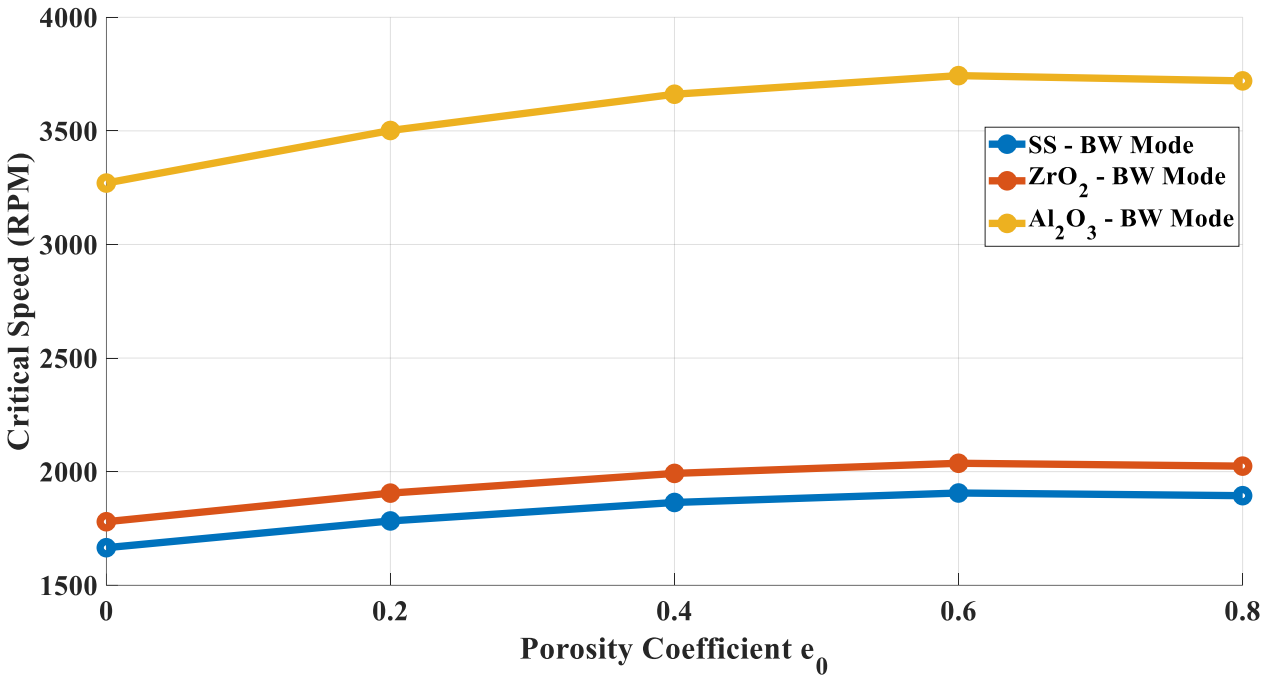

Figure IV-26 First critical speed for deferent symmetric FGP types (SS, ZrO_2, and Al_2O_3) in function in porosity e_0

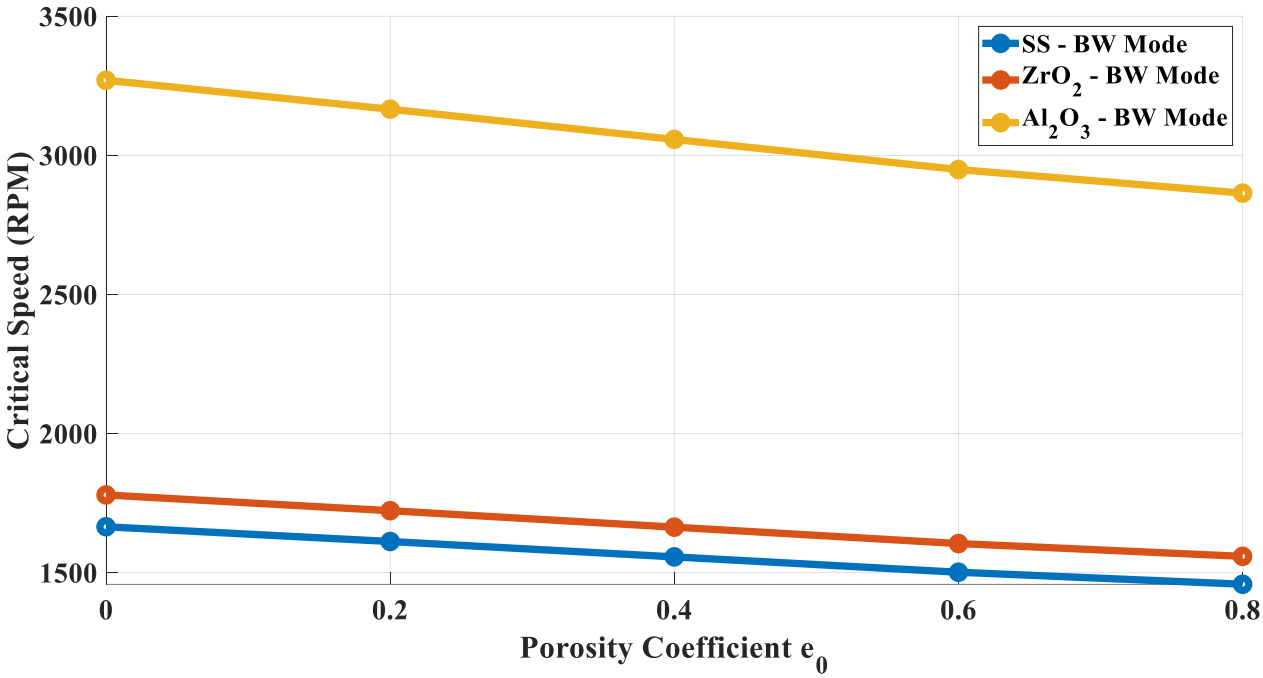

Figure IV-27 First critical speed for deferent non-symmetric FGP types (SS, ZrO_2, and Al_2O_3) in function in porosity e_0

IV.4.4. Bearing influence in critical speed of FGP shaft

This analysis provides a comparative interpretation of the first critical speeds for FGP shafts, contrasting the effects of symmetric in figure IV-28 and non-symmetric in figure IV-28 porosity distributions. A primary observation across both configurations is the direct and predictable influence of bearing stiffness on the critical speed. An increase in the stiffness coefficient consistently elevates the critical speed. This aligns with fundamental theory, as stiffer bearings increase the system's overall stiffness and, consequently, its natural frequency.

The most significant findings emerge when examining the influence of the porosity coefficient (e_0) and its spatial distribution. For the shaft with a symmetric porosity distribution, the results demonstrate a complex and non-monotonic behavior. Counter-intuitively, the critical speed initially increases with the porosity coefficient, reaching a peak value at approximately $e_0 = 0.6$ before beginning to decline. This suggests that a symmetric porosity profile can be engineered to optimize the stiffness-to-mass ratio. It is hypothesized that the porosity is introduced in areas of lower stress, such that the initial reduction in mass is more dynamically beneficial than the corresponding loss of stiffness, causing the critical speed to rise.

Conversely, the shaft featuring a non-symmetric porosity distribution exhibits a monotonic decrease in critical speed as porosity increases. This indicates that the specific type of asymmetry applied in this model results in a consistent degradation of the shaft's effective stiffness that outweighs the benefit of mass reduction across the entire range of the porosity coefficient. While asymmetry is often associated with more complex dynamics, in this instance, it leads to a predictable, linear trade-off between weight reduction and the shaft's dynamic performance.

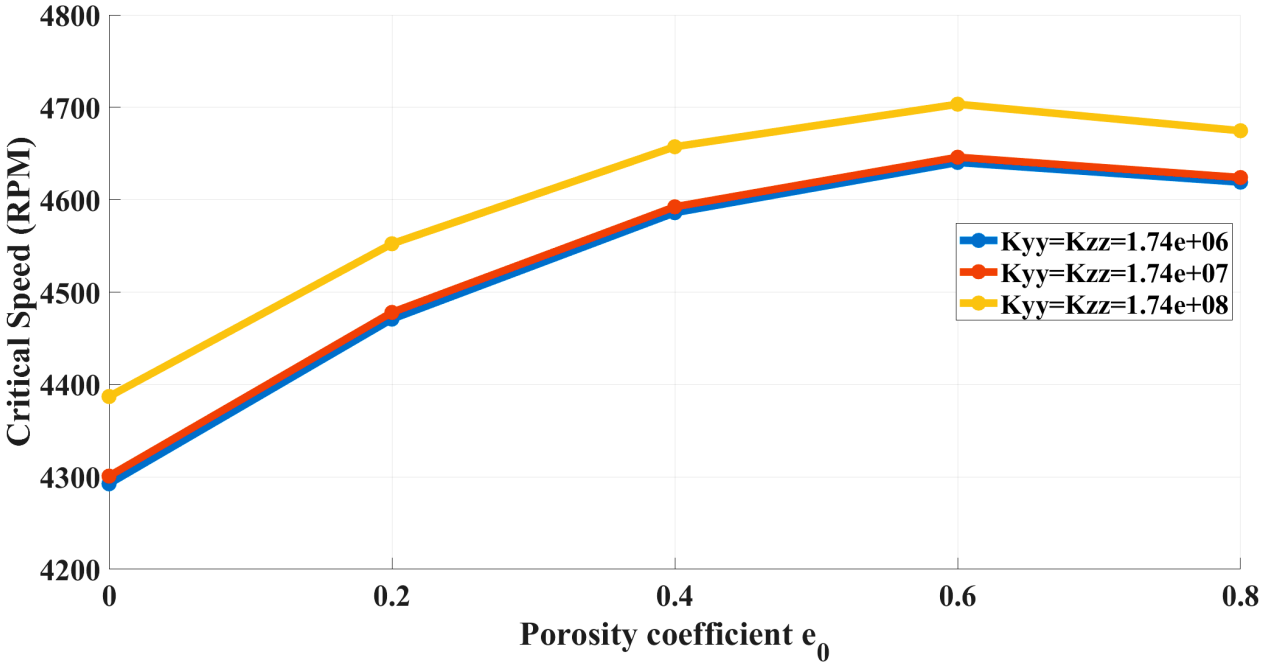

Figure IV-29 First critical speeds in function in porosity for symmetric porosity of FGP shaft, for different symmetric damping values

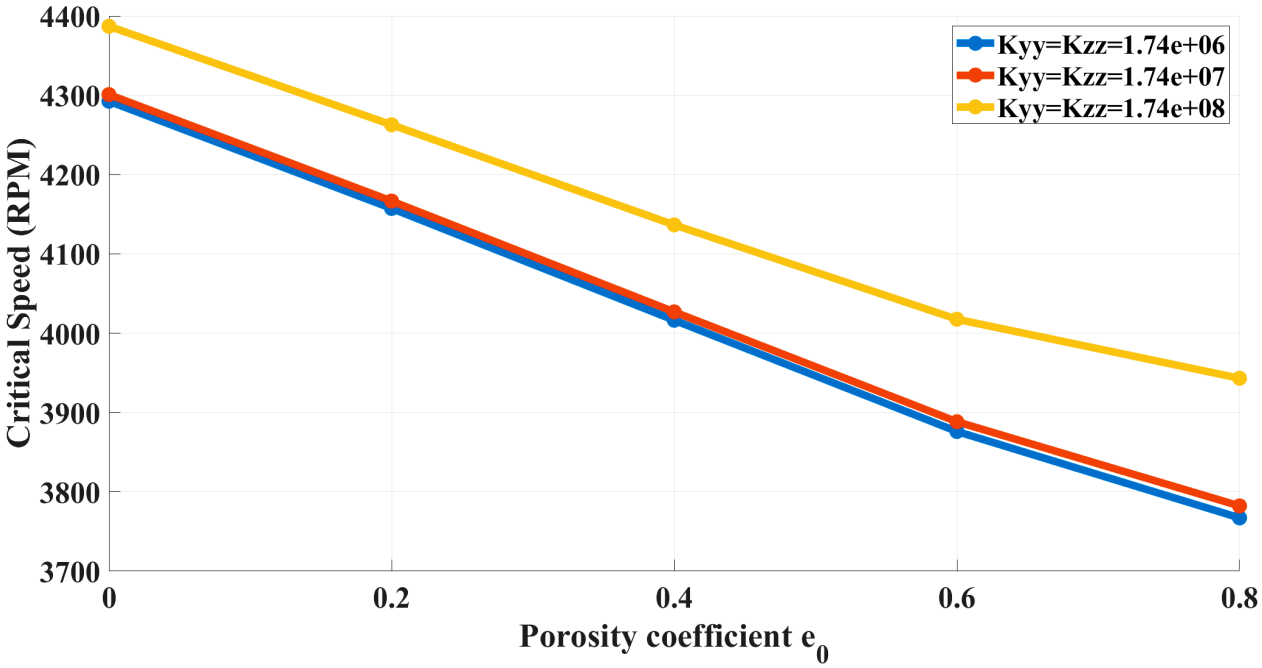

Figure IV-28 First critical speeds in function in porosity for non-symmetric porosity of FGP shaft, for different symmetric damping values

IV.4.5. Damping influence in critical speed of FGP shaft

This study investigates the first critical speeds of FGP shafts, focusing on the influence of symmetric in figure IV-30 and non-symmetric porosity distributions in figure IV-31 under various symmetric damping conditions. A primary observation across both symmetric and non-symmetric configurations is the dominant effect of the damping coefficient, $Cyy = Czz$. As the damping coefficient increases from $5.0 \times 10e4\ N \cdot s/m\ to\ 5.0 \times 10e8\ N \cdot s/m$, there is a drastic reduction in the first critical speed. This well-established phenomenon in rotordynamics is attributed to the reduction of the system's effective dynamic stiffness at high damping levels.

The influence of the porosity coefficient (e_0), however, reveals a stark contrast between the two distribution types. For the FGP shaft with a symmetric porosity distribution, the first critical speed is observed to increase as porosity increases for all damping values. This counter-intuitive result suggests that the symmetric introduction of porosity in this design optimizes the shaft's stiffness-to-mass ratio. The benefit of a significant mass reduction outweighs the corresponding loss of material stiffness.

In direct opposition to this, the shaft with a non-symmetric porosity distribution exhibits a monotonic decrease in critical speed with rising porosity. This behavior aligns with the conventional expectation that porosity degrades mechanical performance by weakening the structure. In this configuration, the stiffness reduction caused by the asymmetric removal of material is the dominant factor, overriding any benefit from mass reduction. As a result, the shaft's dynamic performance consistently declines as it is made more porous, regardless of the damping applied.

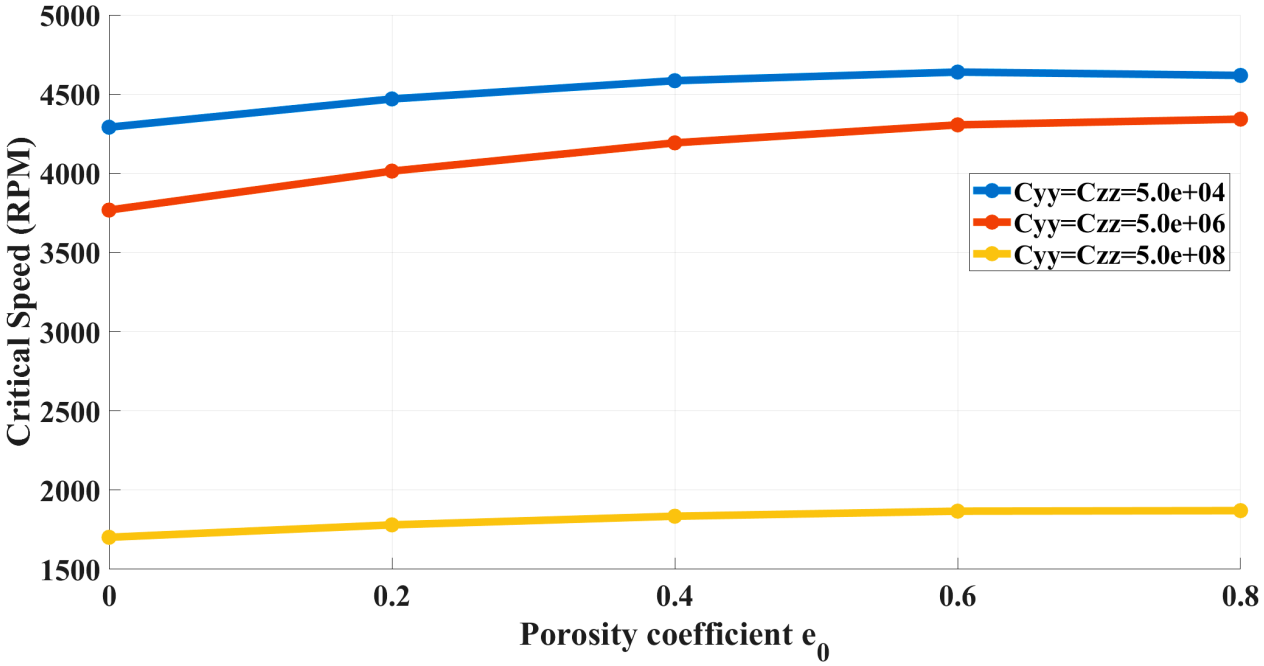

Figure IV-30 First critical speeds in function in porosity for symmetric porosity of FGP shaft, for different symmetric damping values

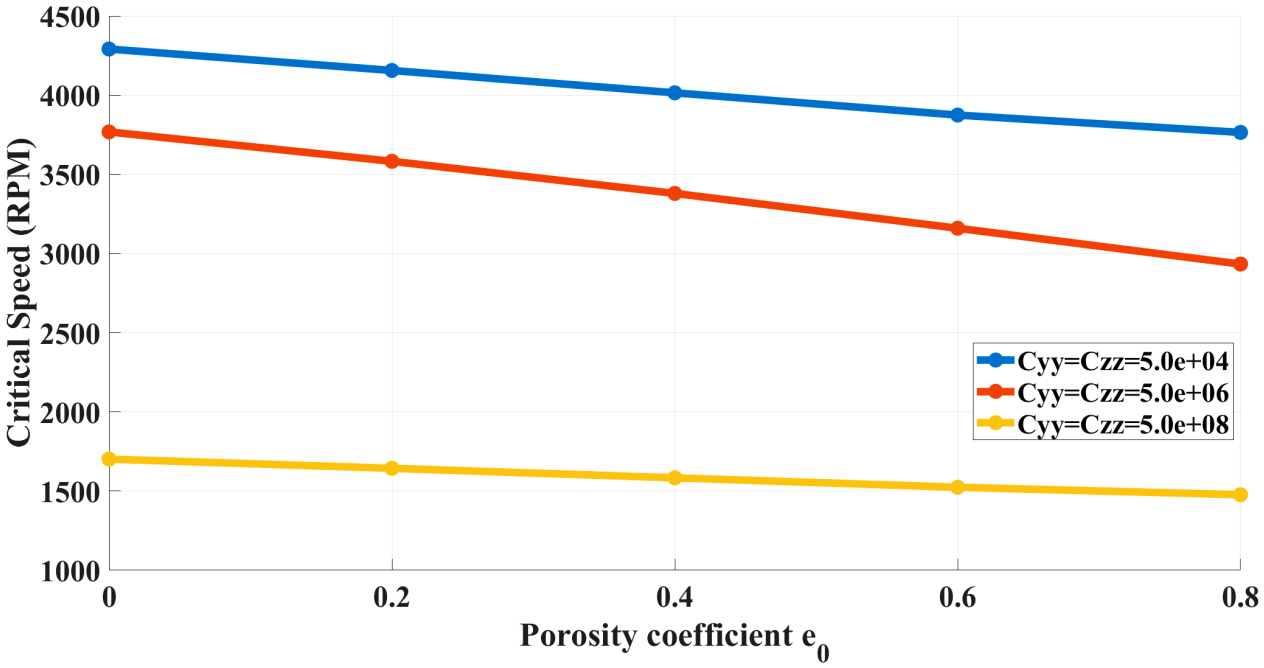

Figure IV-31 First critical speeds in function in porosity for non-symmetric porosity of FGP shaft, for different symmetric damping values

IV.4.6. Disk influence in critical speed of FGP shaft

The two figures (IV-32 and IV-33) present the variation of the first critical speed of FGP shafts with respect to the porosity coefficient e_0, considering symmetric and non-symmetric porosity distributions respectively, for three disk configurations ($m_{d1} = 14.8358\,kg$, $m_{d2} = 7.4179\,kg$, and $m_{d3} = 3.7089$). Several important points can be highlighted.

In the symmetric porosity case, the critical speed increases as porosity grows for all disk configurations. This happens because symmetric porosity reduces the shaft's mass more than it reduces its stiffness, which raises the natural frequency. The effect is stronger for lighter disks: configuration 3 (lightest disk) gives the highest critical speed, followed by configuration 2, while configuration 1 (heaviest disk) shows the lowest values. This means heavier disks reduce the dynamic stiffness of the shaft–disk system and lower the critical speed.

In the non-symmetric porosity case, the trend is similar but weaker. The critical speed still to down with porosity, but not as much as in the symmetric case. This is because non-symmetric porosity causes uneven stiffness and mass distribution, which offsets the negative effect of mass reduction. As a result, the critical speeds are always lower in the non-symmetric case than in the symmetric one, for the same disk configuration.

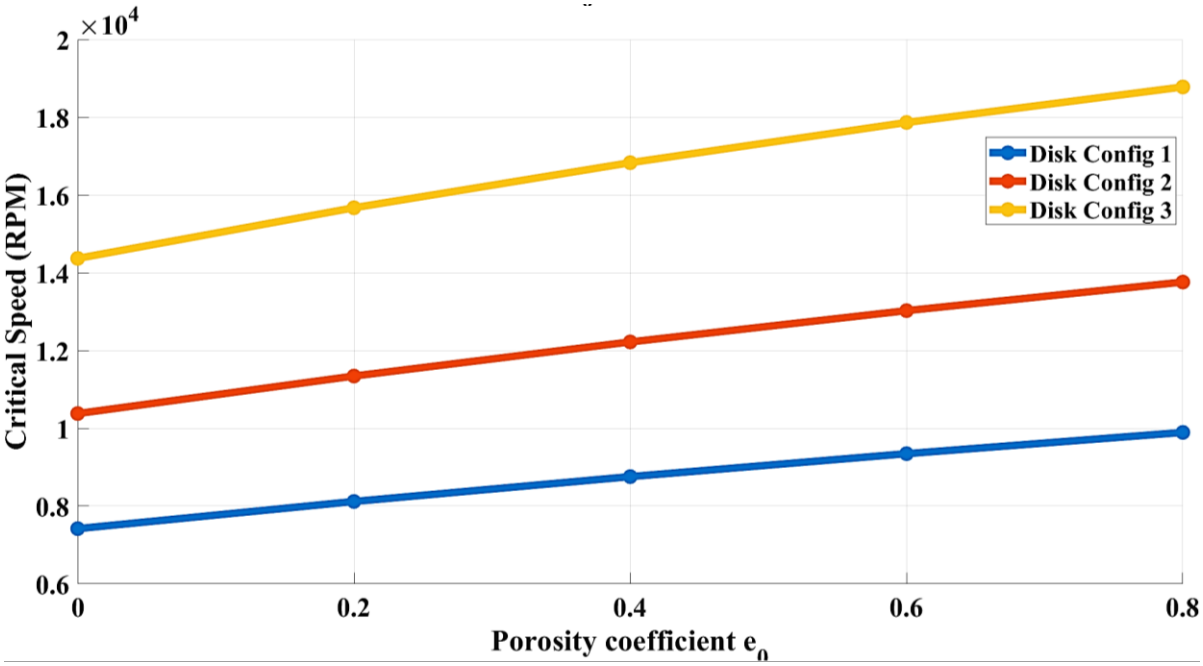

Figure IV-32 First critical speeds in function in porosity for symmetric porosity of FGP shaft, for deferent configurations of the disk

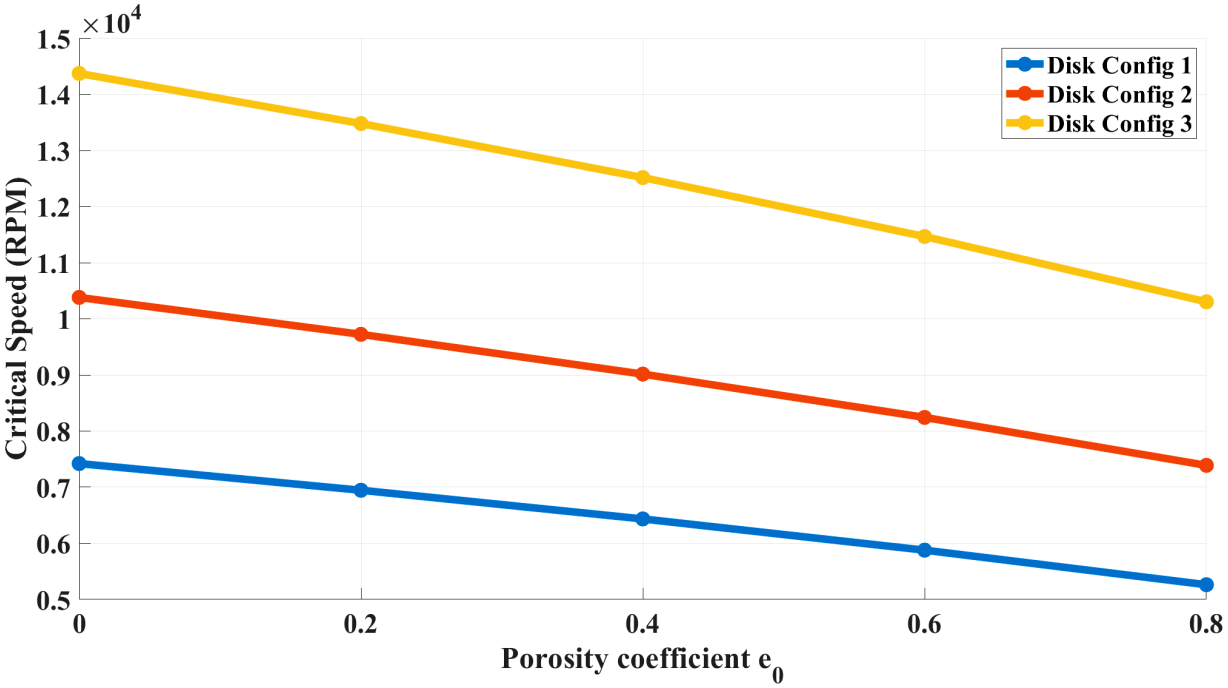

Figure IV-33 First critical speeds in function in porosity for non-symmetric porosity of FGP shaft, for deferent configurations of the disk

Conclusion

This thesis presented a comprehensive numerical investigation into the dynamic vibration behavior of rotating shafts made from Porous Functionally Graded Materials (PFGM) and Functionally Graded Porous (FGP) structures. Using a robust hierarchical p-version Finite Element Method (p-FEM) based on Timoshenko Beam Theory (TBT), the study successfully developed and validated a framework to analyze how porosity, in conjunction with material gradation, geometric parameters, and boundary conditions, influences the dynamic characteristics of rotors. The primary goal was to move beyond viewing porosity as a mere defect and instead explore its potential as a deliberate design feature for engineering lightweight, high-performance rotating machinery.

The parametric studies yielded several critical insights into the complex dynamics of porous rotors.

- A foundational finding is that the distribution of porosity is a more dominant factor than the overall porosity volume. For PFGM shafts, an even porosity distribution leads to a predictable, monotonic decrease in critical speed with increasing porosity. In stark contrast, an uneven distribution introduces complex, non-monotonic behavior, where the critical speed can drop and then rise sharply, suggesting a sophisticated interaction between the shaft's asymmetric stiffness and its vibration mode shape.

- Perhaps the most significant discovery was observed in FGP shafts. A symmetric porosity distribution was found to counter-intuitively increase the first critical speed as porosity increases. This suggests that a symmetric profile can be engineered to optimize the stiffness-to-mass ratio, where the benefit of mass reduction outweighs the corresponding loss of stiffness. Conversely, a non-symmetric distribution consistently degrades dynamic performance, causing a monotonic decrease in critical speed.

- The influence of geometric parameters and boundary conditions was reaffirmed, with stiffer conditions (Clamped-Clamped) and lower slenderness ratios (L/D) consistently yielding higher natural frequencies and critical speeds.

- External components like bearings, damping, and attached disks behaved as expected: higher bearing stiffness elevates critical speeds, higher damping tends to reduce them, and greater disk mass lowers them due to increased inertia.

The findings of this research carry significant implications for the design and application of advanced rotating machinery. This work provides quantitative evidence that engineered porosity can be a powerful tool for enhancing rotor performance, rather than simply a method for weight reduction. The discovery that symmetric porosity distributions can increase critical speed opens a new avenue for designing rotors that are both lighter and dynamically more stable, a crucial advantage in the aerospace, automotive, and energy sectors.

However, the results also serve as a critical caution: the architecture of porosity must be precisely controlled. The unpredictable and potentially destabilizing effects of uneven and non-symmetric distributions highlight the risks of improperly engineered porous structures. This thesis provides a foundational framework and valuable design insights that can help engineers harness the benefits of porous materials while mitigating the associated risks, paving the way for the next generation of efficient and reliable rotors.

While this study provides a robust numerical foundation, several avenues for future research are recommended to build upon these findings:

1. Experimental Validation: The most critical next step is the physical fabrication and experimental testing of PFGM and FGP rotors to validate the numerical predictions presented here. This would bridge the gap between theoretical analysis and real-world application.

2. Advanced Modeling: Future work should extend the models to incorporate non-linear vibration behavior, which becomes important at higher amplitudes, and thermo-mechanical coupling to account for performance in high-temperature operating environments.

3. Optimization Studies: Employing topology optimization algorithms could identify the ideal three-dimensional porosity distribution to maximize specific performance metrics, such as the critical speed-to-weight ratio.

4. Broader Material and Damage Analysis: The investigation could be expanded to include other material systems, such as hybrid composites reinforced with CNTs or graphene, and to model fatigue and damage propagation within the porous microstructure under dynamic loading.

In conclusion, this thesis successfully demonstrated that the dynamic behavior of porous rotors is intricately linked to the architecture of their internal porosity. The key takeaway is that porosity, when engineered with a symmetric and controlled distribution, can simultaneously reduce weight and enhance dynamic stability. This work shifts the perspective on porous materials from being inherently flawed to being highly tailorable, offering a new degree of freedom in the design of advanced mechanical systems. The developed p-FEM framework serves as an effective tool for predicting these complex behaviors, ultimately contributing to the creation of lighter, faster, and more reliable rotating machinery.

References

[1] H. D. Nelson and J. M. McVaugh, “The Dynamics of Rotor-Bearing Systems Using Finite Elements,” *Journal of Engineering for Industry*, vol. 98, no. 2, pp. 593–600, May 1976, doi: 10.1115/1.3438942.

[2] H. D. Nelson, “A Finite Rotating Shaft Element Using Timoshenko Beam Theory,” *Journal of Mechanical Design*, vol. 102, no. 4, pp. 793–803, Oct. 1980, doi: 10.1115/1.3254824.

[3] G. Szeidl and L. P. Kiss, *Foundations of Engineering Mechanics Mechanical Vibrations An Introduction*. 2020. [Online]. Available: http://www.springer.com/series/3582

[4] F. F. Ling, *Dynamics of Rotating Systems (Mechanical Engineering Series)*. 2005. doi: https://doi.org/10.1007/0-387-28687-X.

[5] C. T. Loy, K. Y. Lam, and J. N. Reddy, “Vibration of functionally graded cylindrical shells,” *Int J Mech Sci*, vol. 41, no. 3, pp. 309–324, Mar. 1999, doi: 10.1016/S0020-7403(98)00054-X.

[6] J. N. Reddy and C. D. Chin, “Thermomechanical analysis of functionally graded cylinders and plates,” *Journal of Thermal Stresses*, vol. 21, no. 6, pp. 593–626, 1998, doi: 10.1080/01495739808956165.

[7] F. Ebrahimi and A. Jafari, “A Higher-Order Thermomechanical Vibration Analysis of Temperature-Dependent FGM Beams with Porosities,” *Journal of Engineering (United Kingdom)*, vol. 2016, 2016, doi: 10.1155/2016/9561504.

[8] A. Forooghi, S. Rezaey, S. M. Haghighi, and A. M. Zenkour, “Thermal instability analysis of nanoscale FG porous plates embedded on Kerr foundation coupled with fluid flow,” *Eng Comput*, vol. 38, no. S4, pp. 2953–2973, Oct. 2022, doi: 10.1007/s00366-021-01426-3.

[9] X.-H. Dang, V.-L. Nguyen, M.-T. Tran, and B.-P. Nguyen Thi, “Free Vibration Characteristics of Rotating Functionally Graded Porous Circular Cylindrical Shells with Different Boundary Conditions,” *Iranian Journal of Science and Technology, Transactions*

of Mechanical Engineering, vol. 46, no. 1, pp. 167–183, 2022, doi: 10.1007/s40997-020-00413-1.

[10] M. Salehi, R. Gholami, and R. Ansari, "Analytical solution approach for nonlinear vibration of shear deformable imperfect FG-GPLR porous nanocomposite cylindrical shells," *Mechanics Based Design of Structures and Machines*, vol. 51, no. 4, pp. 2177–2199, 2023, doi: 10.1080/15397734.2021.1891096.

[11] K. Gao, W. Gao, B. Wu, D. Wu, and C. Song, "Nonlinear primary resonance of functionally graded porous cylindrical shells using the method of multiple scales," *Thin-Walled Structures*, vol. 125, pp. 281–293, Apr. 2018, doi: 10.1016/j.tws.2017.12.039.

[12] Y. Wang and D. Wu, "Free vibration of functionally graded porous cylindrical shell using a sinusoidal shear deformation theory," *Aerosp Sci Technol*, vol. 66, pp. 83–91, Jul. 2017, doi: 10.1016/j.ast.2017.03.003.

[13] A. R. Ghasemi and M. Meskini, "Free vibration analysis of porous laminated rotating circular cylindrical shells," *JVC/Journal of Vibration and Control*, vol. 25, no. 18, pp. 2494–2508, Sep. 2019, doi: 10.1177/1077546319858227.

[14] Y. P. Chen, M. H. Yao, and W. Zhang, "Nonlinear vibrations of the blade with varying rotating speed," *2011 2nd International Conference on Mechanic Automation and Control Engineering, MACE 2011 - Proceedings*, pp. 1435–1438, 2011, doi: 10.1109/MACE.2011.5987216.

[15] J. Zhao, F. Xie, A. Wang, C. Shuai, J. Tang, and Q. Wang, "A unified solution for the vibration analysis of functionally graded porous (FGP) shallow shells with general boundary conditions," *Compos B Eng*, vol. 156, pp. 406–424, Jan. 2019, doi: 10.1016/j.compositesb.2018.08.115.

[16] H. Li, F. Pang, Y. Ren, X. Miao, and K. Ye, "Free vibration characteristics of functionally graded porous spherical shell with general boundary conditions by using first-order shear deformation theory," *Thin-Walled Structures*, vol. 144, Nov. 2019, doi: 10.1016/j.tws.2019.106331.

[17] H. Li, F. Pang, H. Chen, and Y. Du, “Vibration analysis of functionally graded porous cylindrical shell with arbitrary boundary restraints by using a semi analytical method,” *Compos B Eng*, vol. 164, pp. 249–264, May 2019, doi: 10.1016/j.compositesb.2018.11.046.

[18] H. Wu, J. Yang, and S. Kitipornchai, “Mechanical Analysis of Functionally Graded Porous Structures: A Review,” *International Journal of Structural Stability and Dynamics*, vol. 20, no. 13, Dec. 2020, doi: 10.1142/S0219455420410151.

[19] P. Sathujoda, A. Batchu, B. Obalareddy, G. Canale, A. Maligno, and R. Citarella, “Free vibration analysis of a thermally loaded porous functionally graded rotor–bearing system,” *Applied Sciences (Switzerland)*, vol. 10, no. 22, pp. 1–22, Nov. 2020, doi: 10.3390/app10228197.

[20] Arnab Bose and Prabhakar Sathujoda, “Natural Frequency Analysis of a Porous Functionally Graded Shaft System,” 2020.

[21] Y. Jaiman and P. Sathujoda, “Finite Element based Natural Frequency Analysis of a Porous Functionally Graded Jeffcott Rotor System subjected to Thermal Gradients,” 2021.

[22] V. Vaka, P. Sathujoda, and S. Yelike, “A review on dynamic analysis of porous functionally graded rotor systems,” in *AIP Conference Proceedings*, American Institute of Physics Inc., May 2021. doi: 10.1063/5.0050352.

[23] A. Batchu, B. Obalareddy, and P. Sathujoda, “Modelling of a Porous Functionally Graded Rotor-Bearing System Using Finite Element Method,” in *Advances in Industrial Machines and Mechanisms*, Y. V. D. Rao, C. Amarnath, S. P. Regalla, A. Javed, and K. K. Singh, Eds., Singapore: Springer Singapore, 2021, pp. 273–283.

[24] M. Behar, A. Boukhalfa, and A. L. Aouinat, “Examining the critical speed and electro-mechanical vibration response of a spinning smart single-walled nanotube via nonlocal strain gradient theory,” *Mechanics of Advanced Materials and Structures*, pp. 1–17, 2024, doi: 10.1080/15376494.2024.2341267.

[25] A. L. Aouinat, A. Boukhalfa, and S. A. Belalia, “Analytical Solution Using the State-Space Method for Free Vibration Analysis of Rotating Functionally Graded Nanotubes,” Nov. 2022, doi: 10.1007/s42417-022-00747-x.

[26] H. Assem, A. Hadjoui, and A. Saimi, “Numerical analysis on the dynamics behavior of FGM rotor in thermal environment using h-p finite element method,” *Mechanics Based Design of Structures and Machines*, vol. 50, no. 11, pp. 3925–3948, 2022, doi: 10.1080/15397734.2020.1824791.

[27] H. Assem, A. Hadjoui, and A. Saimi, “Numerical analysis on the dynamics behavior of FGM rotor in thermal environment using h-p finite element method,” *Mechanics Based Design of Structures and Machines*, vol. 50, no. 11, pp. 3925–3948, Nov. 2022, doi: 10.1080/15397734.2020.1824791.

[28] B. Saleh *et al.*, “30 Years of functionally graded materials: An overview of manufacturing methods, Applications and Future Challenges,” *Compos B Eng*, vol. 201, p. 108376, Nov. 2020, doi: 10.1016/j.compositesb.2020.108376.

[29] M. Koizumi, “FGM activities in Japan,” *Compos B Eng*, vol. 28, no. 1–2, pp. 1–4, Jan. 1997, doi: 10.1016/S1359-8368(96)00016-9.

[30] K. LAU, M. LU, H. CHEUNG, F. SHENG, and H. LI, “Thermal and mechanical properties of single-walled carbon nanotube bundle-reinforced epoxy nanocomposites: the role of solvent for nanotube dispersion,” *Compos Sci Technol*, vol. 65, no. 5, pp. 719–725, Apr. 2005, doi: 10.1016/j.compscitech.2004.10.005.

[31] D. Delfosse, “Fundamentals of Functionally Graded Materials,” *Materials Today*, vol. 1, no. 4, p. 18, 1998, doi: 10.1016/S1369-7021(98)80023-0.

[32] V. Birman and L. W. Byrd, “Modeling and Analysis of Functionally Graded Materials and Structures,” *Appl Mech Rev*, vol. 60, no. 5, pp. 195–216, Sep. 2007, doi: 10.1115/1.2777164.

[33] L. J. Gibson and M. F. Ashby, *Cellular Solids*. Cambridge University Press, 1997. doi: 10.1017/CBO9781139878326.

[34] W. S. Sanders and L. J. Gibson, “Mechanics of BCC and FCC hollow-sphere foams,” *Materials Science and Engineering: A*, vol. 352, no. 1–2, pp. 150–161, Jul. 2003, doi: 10.1016/S0921-5093(02)00890-0.

[35] J. Banhart, “Manufacture, characterisation and application of cellular metals and metal foams,” *Prog Mater Sci*, vol. 46, no. 6, pp. 559–632, Jan. 2001, doi: 10.1016/S0079-6425(00)00002-5.

[36] J. S. Rao, *Rotor_Dynamics*. 2011.

[37] G. Genta, *Dynamics of Rotating Systems*. New York, NY: Springer US, 2005. doi: 10.1007/0-387-28687-X.

[38] D. K. Jha, T. Kant, and R. K. Singh, “A critical review of recent research on functionally graded plates,” *Compos Struct*, vol. 96, pp. 833–849, Feb. 2013, doi: 10.1016/j.compstruct.2012.09.001.

[39] K. K. Pradhan and S. Chakraverty, “Free vibration of Euler and Timoshenko functionally graded beams by Rayleigh–Ritz method,” *Compos B Eng*, vol. 51, pp. 175–184, Aug. 2013, doi: 10.1016/j.compositesb.2013.02.027.

[40] D. Chen, K. Gao, J. Yang, and L. Zhang, “Functionally graded porous structures: Analyses, performances, and applications – A Review,” *Thin-Walled Structures*, vol. 191, p. 111046, Oct. 2023, doi: 10.1016/j.tws.2023.111046.

[41] S. W. Yoo, C. M. Lee, and D. H. Kim, “Effect of Functionally Graded Material (FGM) Interlayer in Metal Additive Manufacturing of Inconel-Stainless Bimetallic Structure by Laser Melting Deposition (LMD) and Wire Arc Additive Manufacturing (WAAM),” *Materials 2023, Vol. 16, Page 535*, vol. 16, no. 2, p. 535, Jan. 2023, doi: 10.3390/MA16020535.

[42] C. Veres and M. Tănase, “A Bibliometric Review of 3D-Printed Functionally Graded Materials, Focusing on Mechanical Properties,” *Machines 2025, Vol. 13, Page 232*, vol. 13, no. 3, p. 232, Mar. 2025, doi: 10.3390/MACHINES13030232.

[43] J. Zhu, Z. Lai, Z. Yin, J. Jeon, and S. Lee, “Fabrication of ZrO2–NiCr functionally graded material by powder metallurgy,” *Mater Chem Phys*, vol. 68, no. 1–3, pp. 130–135, Feb. 2001, doi: 10.1016/S0254-0584(00)00355-2.

[44] W. Ge, T. He, M. Wang, and J. Li, “Nano-Grain Ni/ZrO2 Functional Gradient Coating Fabricated by Double Pulses Electrodeposition with Enhanced High Temperature Corrosion Performance,” *Coatings 2020, Vol. 10, Page 332*, vol. 10, no. 4, p. 332, Mar. 2020, doi: 10.3390/COATINGS10040332.

[45] N. Elahi Haghighi and M. J. Hadianfard, “Fabrication of Ni–ZrO2 nanocomposites through a new electroforming bath and Assessment of their morphology, wear, and corrosion resistance,” *Heliyon*, vol. 10, no. 15, Aug. 2024, doi: 10.1016/j.heliyon.2024.e35779.

[46] M. I. A. Latiff, D. M. Nuruzzaman, S. Basri, N. M. Ismail, S. N. S. Jamaludin, and F. F. Kamaruzaman, “Preparation and characterization of 6-layered functionally graded nickel-alumina (Ni-Al2O3) composites,” *IOP Conf Ser Mater Sci Eng*, vol. 342, no. 1, Apr. 2018, doi: 10.1088/1757-899X/342/1/012063.

[47] K. A. Bhaskararao and G. R. Janardhana, “Microstructure, hardness and flexural strength of Ni/Al2O3 FGMs by pressure-less sintering with different cooling rates,” *Boletín de la Sociedad Española de Cerámica y Vidrio*, vol. 60, no. 4, pp. 255–265, Jul. 2021, doi: 10.1016/J.BSECV.2020.03.012.

[48] J. Zygmuntowicz, P. Wiecińska, A. Miazga, K. Konopka, and W. Kaszuwara, “Al2O3/Ni functionally graded materials (FGM) obtained by centrifugal-slip casting method,” *J Therm Anal Calorim*, vol. 130, no. 1, pp. 123–130, Oct. 2017, doi: 10.1007/S10973-017-6232-5.

[49] A. Sotov, A. Kantyukov, A. Popovich, and V. Sufiiarov, “A Review on Additive Manufacturing of Functional Gradient Piezoceramic,” *Micromachines 2022, Vol. 13, Page 1129*, vol. 13, no. 7, p. 1129, Jul. 2022, doi: 10.3390/MI13071129.

[50] B. Parveez, N. A. Jamal, H. Anuar, Y. Ahmad, A. Aabid, and M. Baig, “Microstructure and Mechanical Properties of Metal Foams Fabricated via Melt Foaming and Powder Metallurgy

Technique: A Review," *Materials*, vol. 15, no. 15, p. 5302, Aug. 2022, doi: 10.3390/MA15155302.

[51] B. Kalia, R. Singh, B. S. Pabla, and G. Singh, "On 17-4PH stainless steel dental implant for premolar 4 in canine under compressive loading: effect of solid and octet metastructure," *Open Exploration 2019 1:4*, vol. 1, no. 4, pp. 202–214, Aug. 2024, doi: 10.37349/EBMX.2024.00015.

[52] A. Hassan and I. A. Alnaser, "A Review of Different Manufacturing Methods of Metallic Foams," *ACS Omega*, vol. 9, no. 6, pp. 6280–6295, Feb. 2024, doi: 10.1021/ACSOMEGA.3C08613/ASSET/IMAGES/LARGE/AO3C08613_0016.JPEG.

[53] "Tantalum Metal Foam: An In-Depth Guide." Accessed: Jul. 03, 2025. [Online]. Available: https://www.samaterials.com/tantalum-metal-foam-an-in-depth-guide.html

[54] L. Yin, Y. Nakanishi, A. R. Alao, X. F. Song, J. Abduo, and Y. Zhang, "A review of engineered zirconia surfaces in biomedical applications," *Procedia CIRP*, vol. 65, p. 284, 2017, doi: 10.1016/J.PROCIR.2017.04.057.

[55] "Zirconia Ceramic Foam Filter for Molten Steel Iron Metal Filtration." Accessed: Jul. 03, 2025. [Online]. Available: https://www.chemicalpackings.com/product/zirconia-ceramic-foam-filter.html

[56] "What are Ceramic Foams? Properties, Manufacturing, and Uses." Accessed: Jul. 03, 2025. [Online]. Available: https://www.preciseceramic.com/blog/ceramic-foams-properties-manufacturing-and-uses.html

[57] "High Quality Alumina Ceramic Foam Filters for Foundry - Alumina Ceramic Foam Filters and Ceramic Foam Filters." Accessed: Jul. 03, 2025. [Online]. Available: https://chempacking.en.made-in-china.com/product/PETRyMHJqacb/China-High-Quality-Alumina-Ceramic-Foam-Filters-for-Foundry.html

[58] S. Roedel, J. C. M. Souza, F. S. Silva, J. Mesquita-Guimarães, M. C. Fredel, and B. Henriques, "Optimized route for the production of zirconia structures with controlled

surface porosity for biomedical applications," *Ceram Int*, vol. 44, no. 11, pp. 12496–12503, Aug. 2018, doi: 10.1016/J.CERAMINT.2018.04.042.

[59] S. Ahmad, M. A. Latif, H. Taib, and A. F. Ismail, "Short review: Ceramic foam fabrication techniques for wastewater treatment application," *Adv Mat Res*, vol. 795, pp. 5–8, 2013, doi: 10.4028/WWW.SCIENTIFIC.NET/AMR.795.5.

[60] "Several Production Methods of Alumina and Their Advantages." Accessed: Jul. 03, 2025. [Online]. Available: https://www.preciseceramic.com/blog/several-production-methods-of-alumina-and-their-advantages.html

[61] "Ceramic Foam Market Size, Share, Trends & Forecast Report 2034." Accessed: Jul. 03, 2025. [Online]. Available: https://www.marketresearchfuture.com/reports/ceramic-foam-market-26048

[62] M. N. ; R. U. D. ; Biswas *et al.*, "Chemistry and Physics of Wet Foam Stability for Porous Ceramics: A Review," *Micro 2024, Vol. 4, Pages 552-571*, vol. 4, no. 4, pp. 552–571, Sep. 2024, doi: 10.3390/MICRO4040034.

[63] W. Fu and Y. Li, "Fabrication, Processing, Properties, and Applications of Closed-Cell Aluminum Foams: A Review," *Materials*, vol. 17, no. 3, p. 560, Feb. 2024, doi: 10.3390/MA17030560.

[64] M. L. Jalaluddin *et al.*, "A review of pore-forming agents on the structures, porosities, and mechanical properties of porous ceramics," *AIMS Materials Science 2024 4:634*, vol. 11, no. 4, pp. 634–665, 2024, doi: 10.3934/MATERSCI.2024033.

[65] G. R. Cowper, "The Shear Coefficient in Timoshenko's Beam Theory," *J Appl Mech*, vol. 33, no. 2, pp. 335–340, Jun. 1966, doi: 10.1115/1.3625046.

[66] IRVING H. SHAMES and CLIVE L. DYM, "ENERGY AND FINITE ELEM ENT METHODS IN STRUC TURAL MECHANICS," 1985.

[67] Rajiv Tiwari, *Rotor Systems*. 2018.

[68] J. R. Hutchinson, “Shear Coefficients for Timoshenko Beam Theory,” *J Appl Mech*, vol. 68, no. 1, pp. 87–92, Jan. 2001, doi: 10.1115/1.1349417.

[69] Houmat and A., “a Sector Fourier p - Applied to Free Vibration Analysis of Sectorial Plates,” *JSV*, vol. 243, no. 2, pp. 269–282, May 2001, doi: 10.1006/JSVI.2000.3410.

[70] K. Gao, W. Gao, B. Wu, D. Wu, and C. Song, “Nonlinear primary resonance of functionally graded porous cylindrical shells using the method of multiple scales,” *Thin-Walled Structures*, vol. 125, pp. 281–293, Apr. 2018, doi: 10.1016/j.tws.2017.12.039.

[71] A. Elhannani, K. Refassi, A. Elmeiche, and M. Bouamama, “Vibration analysis of functionally graded tapered rotor shaft system,” *Mechanics and Mechanical Engineering*, vol. 23, no. 1, pp. 241–245, 2019, doi: 10.2478/mme-2019-0032.